FAA WJH Technical Center
00090340

Report No. FAA-RD-76-21

EFFECTS OF SCATTERING BY OBSTACLES IN THE FIELD OF VOR/DVOR

Harry Gruenberg

Kazuhiro Hirasawa

NAFEC
LIBRARY
7 '76

FAA WJH Technical Center
Tech Center Library
Atlantic City, NJ 08405

AVAILABLE IN
ELECTRONIC FORMAT

July 1976

Final Report

Document is available to the public through the
National Technical Information Service,
Springfield, Virginia 22161.

Prepared for

U.S. DEPARTMENT OF TRANSPORTATION
FEDERAL AVIATION ADMINISTRATION
Systems Research & Development Service
Washington, D.C. 20590

NOTICE

This document is disseminated under the sponsorship of the Department of Transportation in the interest of information exchange. The United States Government assumes no liability for its contents or use thereof.

Technical Report Documentation Page

1. Report No.	2. Government Accession No.	3. Recipient's Catalog No.
FAA-RD-76-21		

4. Title and Subtitle	5. Report Date
Effects of Scattering by Obstacles in the Field of VOR/DVOR	July 1976
	6. Performing Organization Code
7. Author(s) Harry Gruenberg, Kazuhiro Hirasawa	8. Performing Organization Report No.
9. Performing Organization Name and Address Electrical and Computer Engineering Department Syracuse University Syracuse, New York 13210	10. Work Unit No. (TRAIS)
	11. Contract or Grant No. DOT-FA73WA-3272
12. Sponsoring Agency Name and Address Department of Transportation Federal Aoiation Administration Systems Research and Development Serviee Washington, D.C. 20590	13. Type of Report and Period Covered Final June 74 - June 75
	14. Sponsoring Agency Code

15. Supplementary Notes

16. Abstract

Theoretical formulas, tables and graphs are presented which summarize the results obtained for the course deviation errors caused by scattering from wires and cylinders in the vicinity of a VOR station.

A summary and an analysis of some experimental results are presented. The experiments were carried out at NAFEC near Atlantic City. On the whole the agreement between theory and experiment is satisfactory.

A listing of modified and simplified computer programs is included.

17. Key Words	18. Distribution Statement
Theoretical analysis of scalloping Scalloping - VOR Scalloping caused by wires Scalloping caused by cylinders	Document is available to the public through the National Technical Information Service, Springfield, Virginia 22151

19. Security Classif. (of this report)	20. Security Classif. (of this page)	21. No. of Pages	22. Price
Unclassified	Unclassified	112	

Form DOT F 1700.7 (8-72) Reproduction of completed page authorized

I. INTRODUCTION

This is the final report concerning work done on Contract No. DOT-FA73WA-3272, "Effects of Scattering by Obstacles in the Field of a VOR" over the period June 18, 1974 through June 18, 1975.

Since the last annual report [1] work has been done in the following areas. First, the theoretical work on straight wires was systamatized and put in tabular and graphical form [2] for possible inclusion in a revised addition of the Siting Handbook. The theoretical results show considerable variations from the empirical data presented in the Handbook to make such a revision desirable.

Secondly, all the moment method programs for wires and small cylinders were revised to give the scalloping envelope directly [3]. These revised computer programs were furnished to the FAA They were constructed and tested by K. Hirasawa. They have the advantage over the originally submitted programs in that they save a good deal of computer time and avoid a "strobscopic effect" when the angular intervals are chosen too large.

Thirdly, a general theory was developed for cylindrical scatterers [4]. While general solutions are presented, they are not yet in a form that is simple enough for inclusion in the Handbook except for relatively short cylinders. Furthermore, the theoretical results are not completely in agreement with results obtained by the moment method for very small cylinders. There are also some discrepancies with the few experimental results available.

Finally, comparisons were made with old experimental results on wire scatterers [3] and new experiments on wires and cylinders carried out at NAFEC at Atlantic City during the period from May to August 1975. The wire experiments reported in [3] and the more recent experiments at NAFEC on wires show that the theory is generally quite accurate in predicting the course scalloping errors. There are some discrepancies for closely-spaced wires probably due to mutual coupling effects. Mutual coupling was neglected in theory and further work along these lines may be useful. The experimental results for cylinders show good agreement with theory in some respects, but also show some discrepancies in other respects. The reasons for these differences have not yet been ironed out and further work in this area is indicated.

This report gives a summary of the straight-wire results [2] in Chapter 2, a summary of the cylinder theory developed so far [4] in Chapter 3, and a summary of the recent experiments at NAFEC in Chapter 4.

It is suggested that further work be undertaken to extend the wire results, to estimate the effects of mutual coupling between wires and the effect of the finite conductivity of the ground. It would also be useful to run off computer calculations to show graphically the effects of all the system parameters on the course deviation error for inclusion in the Handbook. It would also be useful to carry out further experiments on long transmission lines in the vicinity of VOR stations to test the theory in real-life situations.

As mentioned above more work is needed on theory of cylindrical structures so that the results can be reduced to handbook form. Extension of the theory to Doppler VOR's is also important.

II. COURSE DEVIATION FOR WIRES

2-1. Introduction

This chapter gives first a simplified summary of the analytical results for infinite wires discussing the explicit dependence of course deviation errors due to the various system parameters. These results show that in most practical situations, the peak scalloping amplitude in degrees can be expressed in the form $C(h_1/D)\ F(2a)\ h_1^2/D^{3/2}$ where h_1 is the wire height and D the normal distance to the VOR, both expressed in feet. $C(h_1/D)$ is a slowly-varying function of h_1/D which is approximately equal to 20 for $h_1/D < .07$. F(2a) is a slowly-varying function of the wire diameter. It was arbitrarily chosen to be unity for zero gauge wire. It deviates from unity by only ± 30 percent over a range of wire diameters from 0.050 inch to 1.00 inch. These results have been put in tabular form and in the form of a series of curves suitable for inclusion in a future addition of the Handbook.

At the end of the chapter it is shown how one can obtain simple estimates of the scalloping envelope for wires of finite length without resorting to the computer program on file (Appendix I of 1).

Modified computer programs for relatively short wires using the moment method have been given to the FAA in Washington. These are revisions of the original programs allowing direct computation of the course deviation envelope.

The factor F(2a) affects the azimuthal distribution of the scalloping envelope very little. We can therefore set $\phi = 50°$ in Eq. (3) to study the effect of the wire diameter on the scalloping peak. The approximate function

$$F(2a) = \frac{\ln(0.23\lambda_0/a_0)}{\ln(0.23\lambda_0/a)} \tag{5}$$

is plotted in Fig. 3 as a function of the wire diameter and gauge number. It is seen that F(2a) is a very slowly-varying function. It differs from unity by less than ± 29 percent for a range of wire diameters from 0.05 to 1.0 inch.

The factor $G(kh_1\varepsilon)/G(kh_0\varepsilon)$ can be estimated with the use of Fig. 4. In most practical situations this ratio will also be close to unity.

The maximum course deviation (peak scalloping) can most conveniently be written in the form

$$(B-\phi)^{o}_{MAX} = H_{MAX} \frac{h_1^2}{D^{3/2}} \left(\frac{f}{f_0}\right)^{1/2} \frac{G(kh_1\varepsilon)}{G(kh_0\varepsilon)} F(2a) \tag{6}$$

H_{MAX} is a function of h_1/D and h_0. For $h_0 = 16$ ft it can be read off directly from Fig. 2. For other values of h_0 it can be computed from

$$H_{MAX} = 20.3\ G[(kh_0h_1/D)\sin\phi_{MAX}] \cong 20.3\ G[0.56\ h_0(h_1/D)] \tag{7}$$

and Fig. 4. In most practical situations the factor $(f/f_0)^{1/2}$ and all the G factors will be close to unity and hence a good rule-of-thumb, for low values of h_1/D and ε, is

$$(B-\phi)^{o}_{MAX} = C\ F(2a) \frac{h_1^2}{D^{3/2}} \tag{8}$$

if h_1 and D are given in feet. C is essentially the H_{MAX} of Fig. 2. It is close to 20 for $h_1/D < 0.07$. In this range, the maximum course deviation is approximately proportional to the square of the wire height and inversely proportional to the three-halfth power of the normal distance of the wire from the VOR antennas. Furthermore, it is a very slowly-varying function of the wire diameter and almost completely independent of other system parameters.

More accurate results were computed from Eq. (2) assuming $f = f_0 = 115$ MHz, $2a = 2a_0 = 0.325$ inches (zero gauge wire), $h_0 = 16$ feet, and $G(kh_1\varepsilon)/G(kh_0\varepsilon) \doteq 1$. The results are tabulated in Fig. 5 and shown graphically in Figs. 6 and 7. Figure 6 shows the maximum course deviation as a function of wire height with distance as a parameter, Fig. 7 shows the maximum course deviation as a function of distance with wire height as a parameter. It is seen that the curves approach straight lines with slopes +2 and -3/2 as expected. For wire diameters different from zero gauge these results should be multiplied by F(2a) obtained from Fig. 3.

Several corrections may have to be applied to these plotted results. If the carrier frequency differs appreciably from $f_0 = 115$ MHz, a correction factor $(f/f_0)^{1/2}$ should be used. For larger aircraft elevation angles and large disparity between h_0 and h_1, a correction factor

$$G(kh_1\varepsilon)/G(kh_0\varepsilon)$$

may have to be applied. A few VOR stations have values of h_0 that differ significantly from 16 feet. In that case an additional correction factor

$$G(0.56\ h_0h_1/D)/G(9.0\ h_1/D)$$

is needed. This assumes that the maximum remains close to $\phi = 50°$. All G factors can be obtained from Fig. 4.

2-3. Wires of Finite Length

While the results for finite wires were summarized in the final report for the period June 1973 to June 1974, it is useful to have a simple method to obtain approximate results. An exact computer program was given previously.

The following procedure appears to give fairly accurate results and is based on the analytical theory presented in the final report. One first finds the peak scalloping from Eq. (8) or from Figs. 6 or 7 and 3. In most practical situatins $h_1/D < 0.07$ and the constant C in Eq. (8) may be taken to be equal to 20. One can then plot the scalloping envelope for an infinite wire from Fig. 1 by proper renormalization of the peak. The plot should be extended to $\phi = 180°$ by symmetry.

It has been shown that the scalloping envelope for an finite wire differs from that of a wire of infinite length in two respects: There are gradual cut-offs at two critical angles given by

$$\begin{aligned} \cot \phi_{1c} &= \Lambda_1 = \ell_1/D \qquad 0 < \phi_{1c} < \pi \\ \cot \phi_{2c} &= \Lambda_2 = \ell_2/D \qquad 0 < \phi_{2c} < \pi \end{aligned} \tag{9}$$

where ℓ_1 and ℓ_2 denote the position of the end points of the wire (see Fig. 8). At these cut-off points the scalloping amplitude is reduced approximately by a factor two from that of an infinite wire. Secondly, there is an overshoot between these two critical points which ranges from 15 to 30 percent. This is shown in Figs. 9 and 10 for two cases taken from the 1973/74 final report. These figures show the computed envelopes for the finite wires as well as the scalloping envelopes for the corresponding infinite wire at the same normal distance D from the VOR. These

curves also show the critical cut-off angles computed from Eq. (9) and the estimated half deviation at cut-off.

As a further refinement the slope of the scalloping envelope at the cut-off points can be computed from the theoretical expressions. The results are best given in terms of the intercepts Δ_1 and Δ_2 of the slope lines on the ϕ-axis (see Figs. 9 and 10). These are given by

$$|\Delta_1| = \frac{100}{(1 + \Lambda_1^2)^{1/4}(kD)^{1/2}} \text{ degrees}$$
$$|\Delta_2| = \frac{100}{(1 + \Lambda_2^2)^{1/4}(kD)^{1/2}} \text{ degrees} \tag{10}$$

It is seen that these crude estimates agree reasonably well with the computed results and are probably sufficiently accurate for most purposes.

Equation (10) can be derived as follows. In the 1973/74 final report it was shown that near the cut-off points the infinite wire result should be multiplied by a factor of the form

$$|Q| = [(f^2 + g^2)/2]^{1/2} \tag{11}$$

where the functions f and g stand for

$$f = f[(2/\pi)^{1/2}|u|], \qquad g = g[(2/\pi)^{1/2}|u|] \tag{12}$$

and

$$u = (2\Omega)^{1/2}(1 + \Lambda^2)^{1/4}\sin(\delta/2) \tag{13}$$

f and g are related to the Fresnel integrals, $\Omega = kD$, $\Lambda = \ell/D$ where ℓ can stand for ℓ_1 or ℓ_2, and δ is the deviation of ϕ from the critical angle corresponding to ℓ. At the cut-off points $\delta = 0$ and $f = g = 1/2$ and $|Q| = 1/2$ as expected.

The increment Δ is given by the value of $|Q|/(d|Q|/d\delta)$ at $\delta = 0$. Hence

$$\Delta = \frac{f^2 + g^2}{f(df/d\delta) + g(dg/d\delta)} = \frac{1}{(df/d\delta) + (dg/d\delta)} \tag{14}$$

since $f = g = 1/2$ at $\delta = 0$. The derivatives in (14) can be approximated as follows. For small δ, the arguments in f and g reduce to

$$x = (\Omega/\pi)^{1/2}(1 + \Lambda^2)^{1/4}\delta \tag{15}$$

and for small x

$$f(x) = \frac{1 + 0.926x}{2 + 1.792x} \cong \frac{1}{2}\ (1 + 0.030x)$$

$$g(x) = \frac{1}{2 + 4.142x} \cong \frac{1}{2}\ (1 - 2.071x)$$

Hence $df/dx = 0.015$ and $dg/dx = -1.036$ at $x = 0$. Substitution in Eq. (14) leads to

$$|\Delta| = \frac{1}{1.02\ (\Omega/\pi)^{1/2}(1 + \Lambda^2)^{1/4}} \text{ radians}$$

$$= \frac{100}{(\Omega)^{1/2}(1 + \Lambda^2)^{1/4}} \text{ degrees}$$

which is Eq. (10).

K+E 10 X 10 TO ½ INCH 46 1322
7 X 10 INCHES MADE IN U.S.A.
KEUFFEL & ESSER CO.

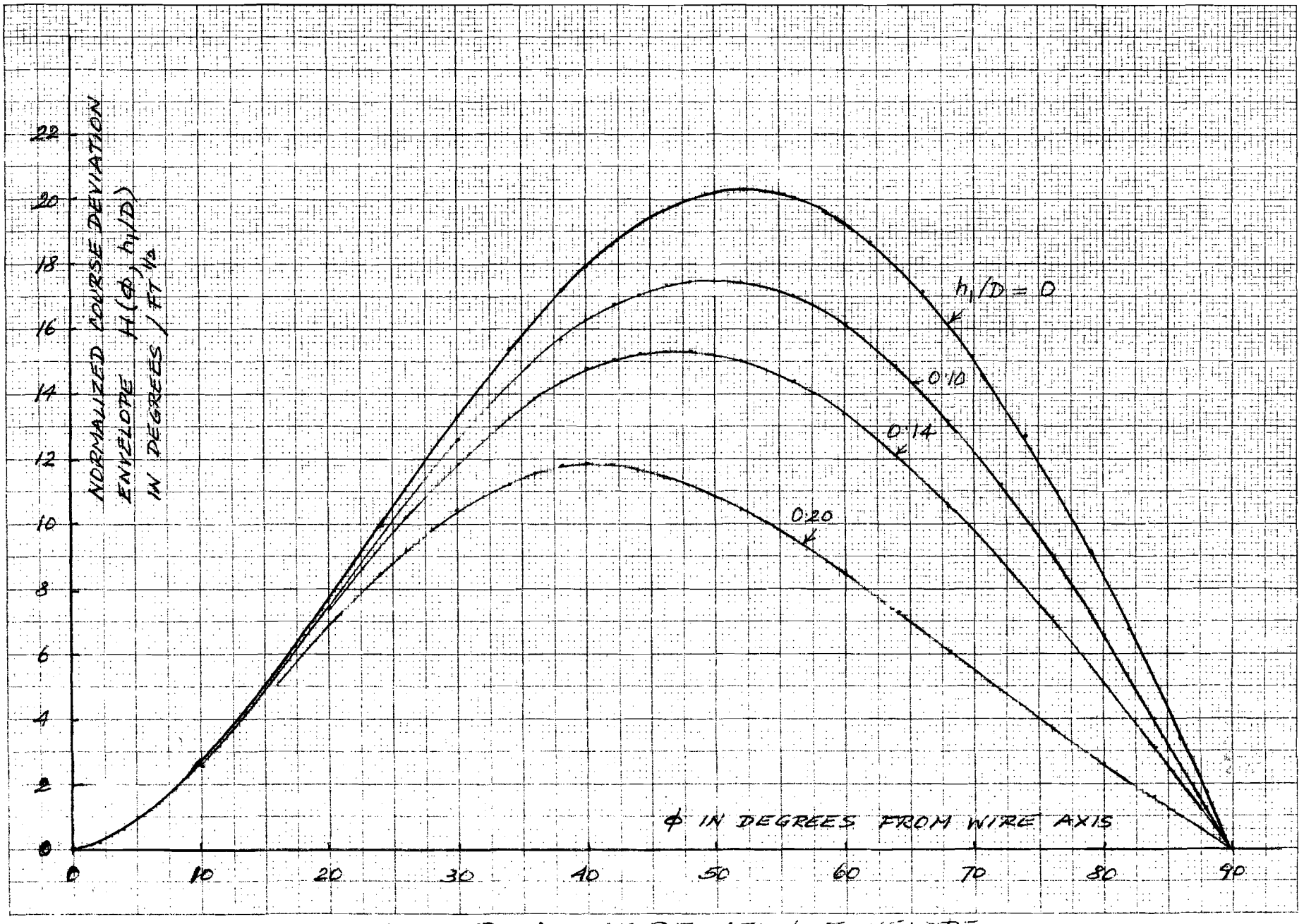

FIG 1. NORMALIZED COURSE DEVIATION ENVELOPE

K+E 10 X 10 TO ½ INCH 46 1322
7 X 10 INCHES MADE IN U.S.A.
KEUFFEL & ESSER CO.

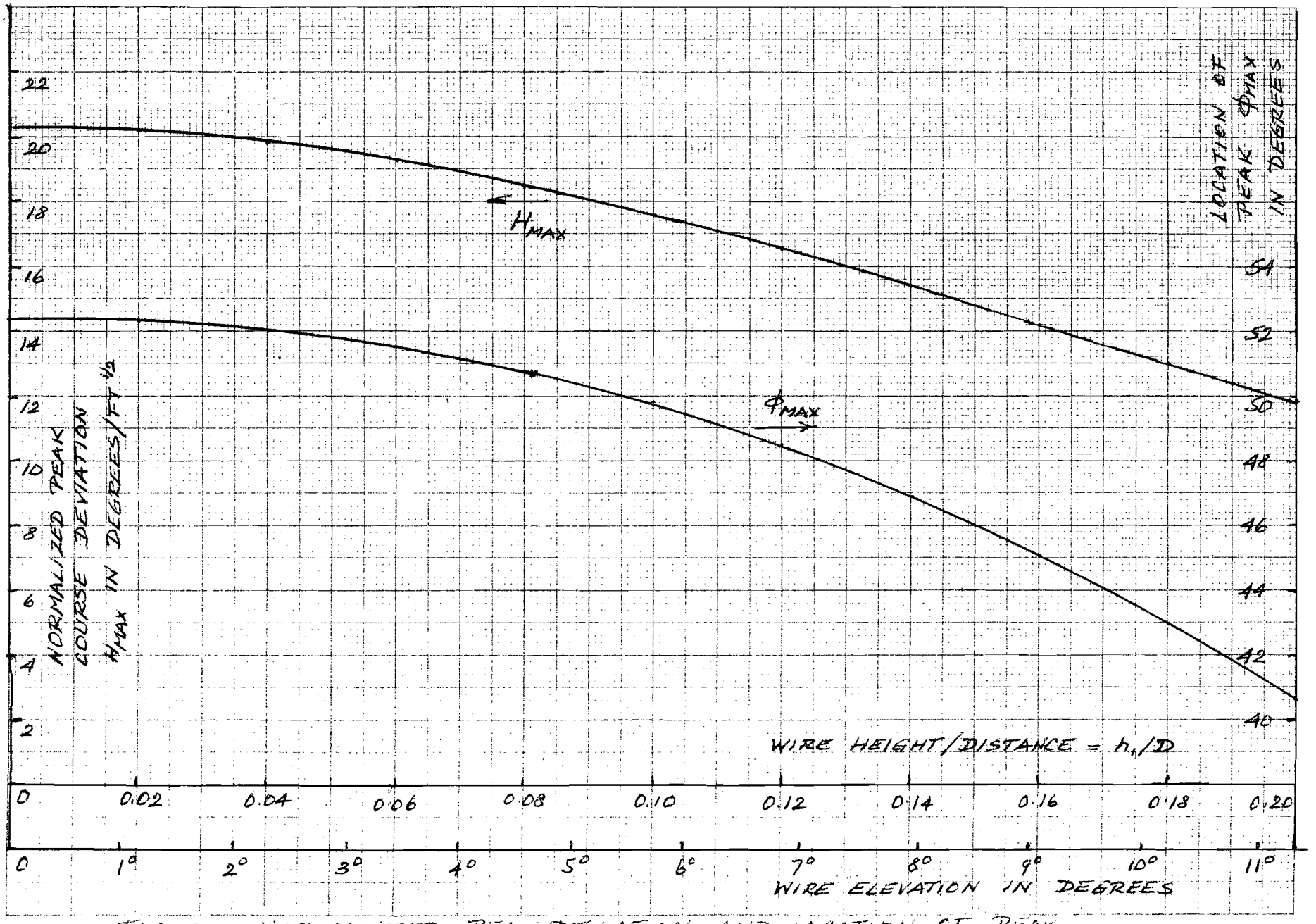

FIG 2. NORMALIZED PEAK DEVIATION AND LOCATION OF PEAK

K+E 10 X 10 TO ½ INCH 46 1322
7 X 10 INCHES MADE IN U.S.A.
KEUFFEL & ESSER CO.

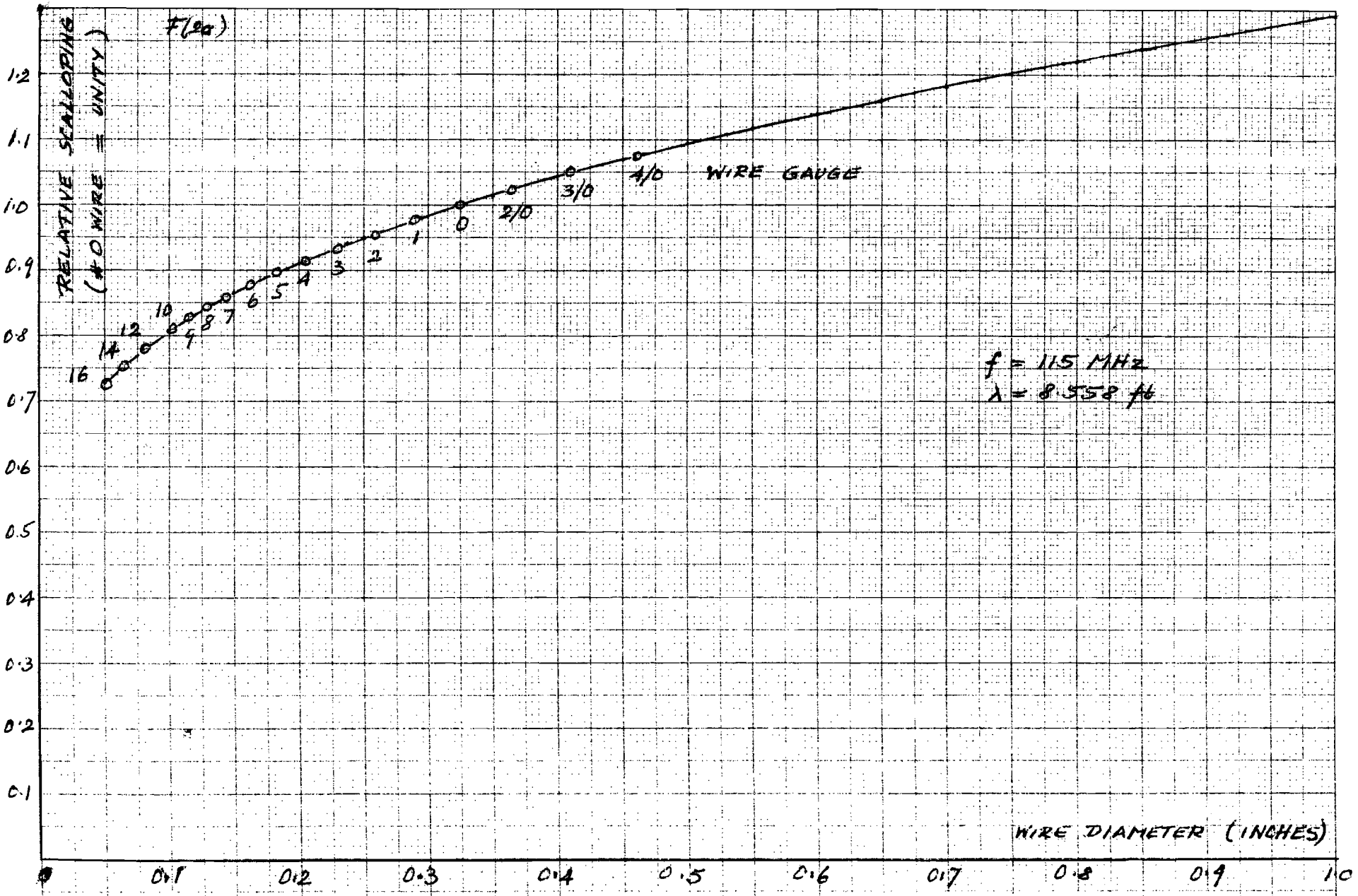

FIG 3. COURSE DEVIATION AS A FUNCTION OF WIRE DIAMETER

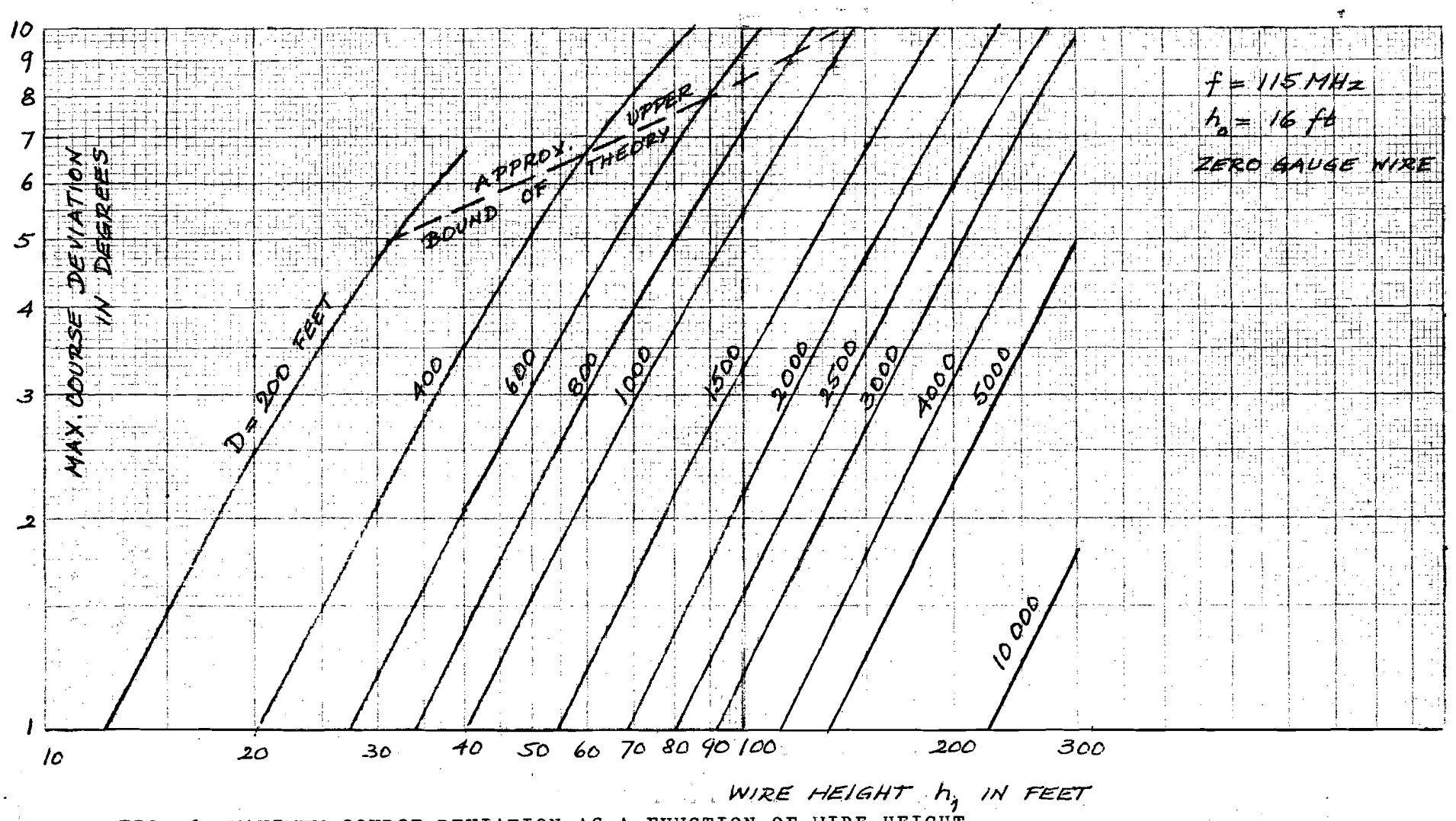

FIG. 6 MAXIMUM COURSE DEVIATION AS A FUNCTION OF WIRE HEIGHT WITH NORMAL DISTANCE TO VOR AS A PARAMETER

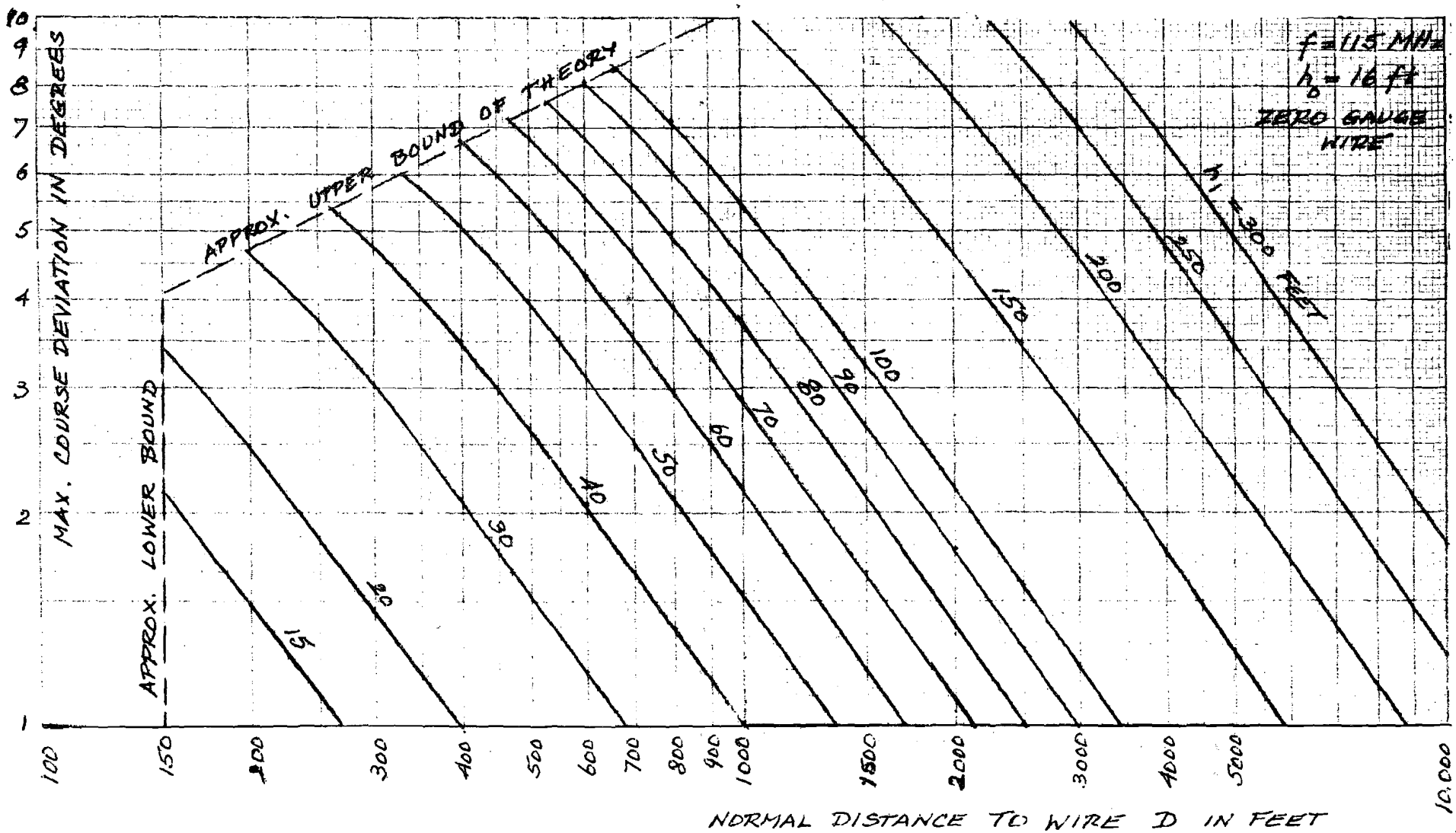

FIG. 7 MAXIMUM COURSE DEVIATION AS A FUNCTION OF DISTANCE FROM VOR WITH WIRE HEIGHT AS PARAMETER

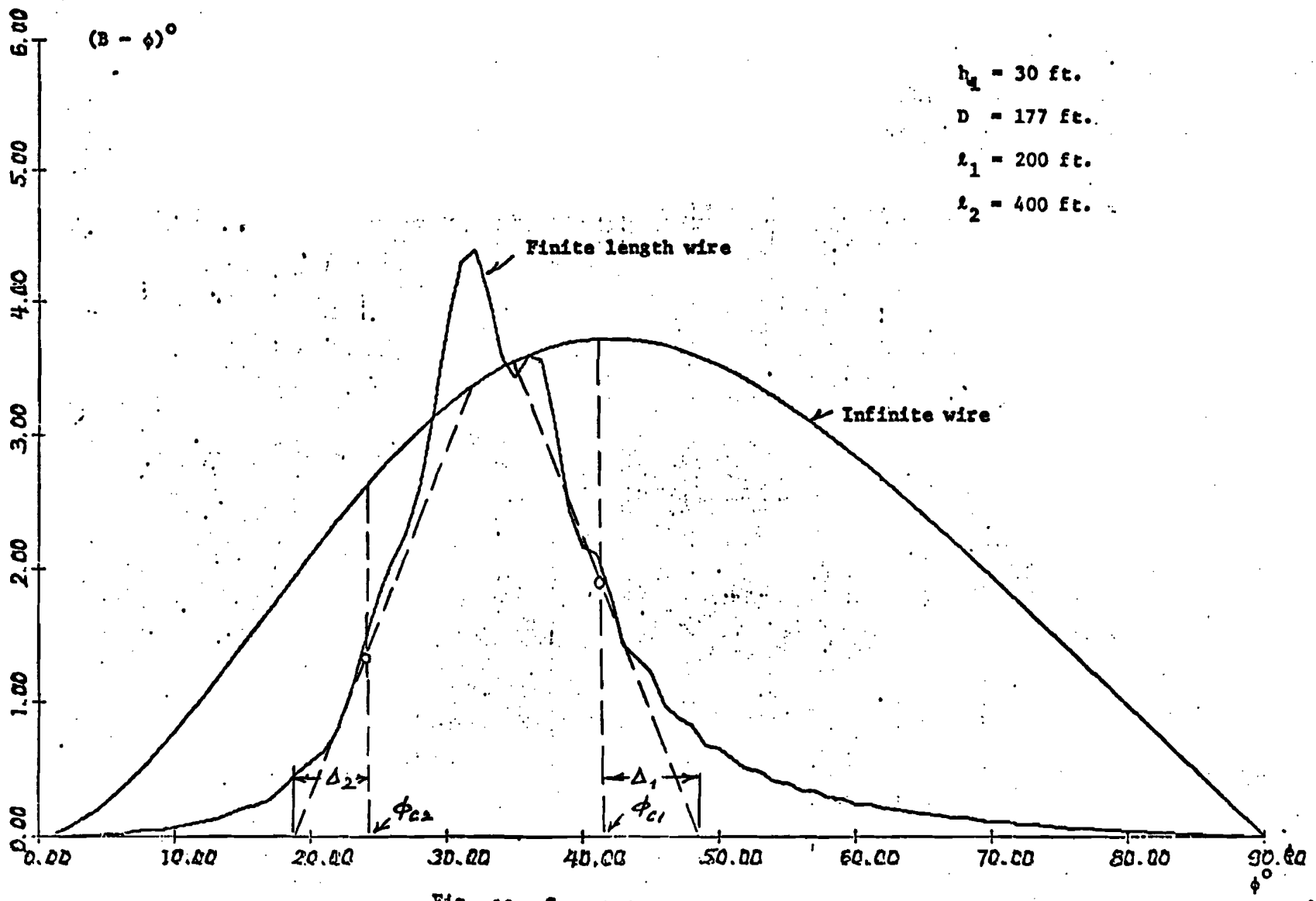

Fig. 10. Computed Course Deviation Envelope

III. SCALLOPING THEORY FOR CYLINDERS

3-1. A General Course Scalloping Formula

If the VOR loops are located at $(0,0,h_o)$ in a rectangular coordinate system with the ground plane at $z=0$ and the aircraft has the spherical coordinates (r,θ,ϕ) then the direct ray at the aircraft has the intensity

$$E_\phi = \frac{K}{r} \exp(-jkr)\ S(\varepsilon)[1 + C(\cos pt \cos\phi + \sin pt \sin\phi)]\cos\varepsilon \qquad (1)$$

Where $\varepsilon = (\pi/2) - \theta$ is the elevation angle of the aircraft and p is the sideband modulation frequency (usually 30 Hz). It is assumed that the vectical radiation pattern $S(\varepsilon)\cos\varepsilon$ is the same for the carrier as for the two sidebands. When the aircraft elevation angle is small we can set $\cos\varepsilon \doteq 1$ and we can neglect the effect of the counterpoise and that of the finite ground conductivity. In that case

$$S(\varepsilon)\cos\varepsilon \doteq \sin(kh_o\varepsilon) \qquad (2)$$

and we can write Eq. (1) approximately as

$$E_\phi = \frac{K}{r} \exp(-jkr)\sin(kh_o\varepsilon)\ [1 + C(\cos pt \cos\phi + \sin pt \sin\phi)] \qquad (3)$$

Here it has been assumed that the two sidebands have horizontal radiation patterns that are exact figure-eights. In the final report for 1974 [1] account was taken of the deviation from a figure-eight pattern due to the loop spacing. This led to a quadrantal error which, to a first approximation, can simply be added to the course error due to scattering from nearby objects. The error introduced by the above simplification is then negligible especially since an effort is always made in practice to compensate for the quadrantal error.

If a scattering object is located near the VOR, the incident field on the point $(r_1,\varepsilon_1,\phi_1)$ of the scatterer will have the same

form as Eq. (3) with r, ε, ϕ replaced by the corresponding subscripted variables. Let us assume that the E_ϕ-components of the scattered fields due to the sidebands can be determined analytically or by the moment method. They can be written in the form

$$E_\phi^s = (KC/r)\ \exp(jkr)\ M_1\ \exp(j\mu_1)\ \cos pt$$

and (4)

$$E_\phi^s = (KC/r)\ \exp(jkr)\ M_2\ \exp(j\mu_2)\ \sin pt$$

for the even and odd sidebands, respectively. The amplitude and phase functions M_i and μ_i $(i=1,2)$ will of course be functions of ϕ and ε. The phase center for these expressions is taken to be the origin of the coordinate system, i.e. the foot of the perpendicular to the ground from the VOR loops.

The total field at the aircraft receiver will be the sum of Eqs. (3) and (4). The scattered field from the carrier can be neglected since the receiver detects only the component of the sidebands in phase with the carrier. Since the scattered carrier signal is small compared to the direct carrier signal, negligible error is introduced when projecting the received sideband signal onto the direct carrier signal instead of the total received carrier. This projection is proportional to

$$\left(\cos\phi + \frac{M_1}{S(\varepsilon)}\cos\mu_1\right)\cos pt + \left(\sin\phi + \frac{M_2}{S(\varepsilon)}\cos\mu_2\right)\sin pt \qquad (5)$$

which can be written in the form $\cos(pt-B)$ where B is determined by

$$\tan B = \frac{\sin\phi + (M_2/S)\cos\mu_2}{\cos\phi + (M_1/S)\cos\mu_1} \qquad (6)$$

In the absence of a scatterer, $M_2 = M_1 = 0$, and B reduces to ϕ. The

receiver measures the phase B of the expression in (5). This differs from the true bearing of the aircraft by the amount

$$B-\phi \cong \tan(B-\phi)=\frac{\tan B - \tan \phi}{1 + \tan B \tan \phi} \tag{7}$$

The replacement of $B-\phi$ by its tangent can be justified as long as the course deviation error is not too high. When Eq. (6) is substituted in (7) we obtain finally

$$B-\phi \cong \frac{1}{S(\varepsilon)} \frac{M_2 \cos \mu_2 \cos \phi - M_1 \cos \mu_1 \sin \phi}{1 + (M_1/S) \cos \mu_1 \cos \phi + (M_2/S) \cos \mu_2 \sin \phi} \tag{8}$$

When the course deviation error is not too large, the terms in M_1 and M_2 in the denominator of Eq. (8) can be neglected with respect to unity. We then get the simpler, but less accurate, result

$$B-\phi \cong \frac{1}{S(\varepsilon)} (M_2 \cos \mu_2 \cos \phi - M_1 \cos \mu_1 \sin \phi) \tag{9}$$

The error introduced in this last step is difficult to estimate in the general case without some knowledge of the functional dependence of M_1 and M_2 on ϕ. It is probably less than 10 percent in most practical situations. The simpler form given by Eq. (9) has the advantage that it can be used to obtain an expression for the scalloping envelope. The advantages of computing the envelope directly, especially in connection with the moment method, have been discussed in the last quarterly report [3].

The factors $\cos \mu_2$ and $\cos \mu_1$ are rapidly oscillating functions. The reason for this is the form of the phase functions of the scattered radiation pattern, μ_1 and μ_2, when they are referred to the origin. For

"lumped" scatterers at $r = D$, $\phi = \phi_o$, with transverse dimensions small compared to D, we have

$$\mu_{1,2} = kD \cos(\phi - \phi_o) + \nu_{1,2} \tag{10}$$

For scattering objected that subtend a large angle at the VOR, such as long horizontal wires, we have more nearly

$$\mu_{1,2} = 2kD \cos(\phi - \phi_o) + \nu_{1,2} \tag{11}$$

In all practical cases kD is very large compared to unity. For scatterers located at distances in excess of 150 feet, we have $kd > 100$. The two terms in Eq. (9) can then be added, for each ϕ, by the phasor addition law giving an envelope function

$$(B-\phi)^{o}_{env} = \frac{180}{\pi S(\varepsilon)} \left[(M_2 \cos\phi)^2 + (M_1 \sin\phi)^2 - 2(M_1 \sin\phi)(M_2 \cos\phi)\cos(\mu_2 - \mu_1)\right]^{1/2} \tag{12}$$

where a factor $(180/\pi)$ has been added to convert from radians to degrees. All that remains now is to determine the magnitude and phase functions, $M_i(\phi,\varepsilon)$ and $\mu_i(\phi,\varepsilon)$, either analytically or by the moment method.

Before we consider special cases and compare with previously obtained results [1] the following comment is in order. Both in the analytical deviations and the moment method programs developed so far, the sideband terms in the VOR radiation pattern were taken to be of the form

$$\cos pt \sin(ks \cos\phi) + \sin pt \sin(ks \sin\phi) \tag{13}$$

to take into account the effect of the finite loop spacing. For $ks < 1$ we have to a good approximation

$$\frac{\sin(ks\cos\phi)}{2J_1(ks)} \cong \cos\phi \quad , \qquad \frac{\sin(ks\sin\phi)}{2J_1(ks)} \cong \sin\phi \tag{14}$$

Hence if M_1 and M_2 are computed on the basis of the incident field in (13) instead of the sideband terms in (3), the above course deviation formulas and the special cases derived below must be divided by $2J_1(ks)$.

For scatterers that subtend a small azimuthal angle at the VOR it is convenient to locate the scatterer at $r=D$ and $\phi=0$ or π. In that case it is easily shown that the scattered radiation due to the odd sideband can be neglected and we get the simpler result

$$(B-\phi)^{o}_{env} = \frac{180}{\pi S(\varepsilon)} \left|M_1(\phi,\varepsilon)\sin\phi\right| \tag{15}$$

This equation is useful, for instance, for scatterers in the form of cylinders with a vertical axis. In the case of circular cylinders of radius a, the restriction for the use of Eq. (15) will be seen to be $a/D \ll 1$, a condition that is usually satisfied in practice.

As another example we consider a horizontal wire of length 2ℓ spaced at a distance h, above the ground. To be specific the wire is located parallel to the x-axis at $y_1 = -D$, $z_1 = h_1$ and the end points are located at $x_1 = \ell_1$ and $x_1 = \ell_2$ with $\ell_2 - \ell_1 = 2\ell$. If the induced currents in the wire due to the two sidebands are given by $I_i(x)$ with $i=1,2$, and the radiation integral is defined as in Appendix A of reference [1].

$$N_i(\phi)\exp j\nu_i(\phi) = \frac{1}{D}\int_{\ell_1}^{\ell_2} I_i(x)\exp(jkx\cos\phi)dx \tag{16}$$

then from Eqs. (30) to (34) of that appendix we get

$$M_i(\phi,\varepsilon) = 60\ kD\ \sin(kh_1\varepsilon)\ N_i(\phi)\ |\sin\phi|$$
$$\mu_i(\phi) = kD\ \sin\phi + \nu_i(\phi) \tag{17}$$

When (16) and (17) as well as (2) are substituted in Eq. (12) one obtains

$$(B-\phi)^{o}_{env} = \frac{10800\ kD}{\pi}\frac{\sin(kh_1\varepsilon)}{\sin(kh_0\varepsilon)}|\sin\phi|[(N_2\cos\phi)^2+(N_1\sin\phi)^2 - 2(N_1\sin\phi)(N_2\cos\phi)\cos(\nu_2-\nu_1)]^{1/2} \tag{18}$$

This result is consistent with Eq. (41a) of Appendix A of [1] if we replace $\omega\mu_o D$ by $\eta_o kD = 120\ \pi kD$, divide by $2J_1(ks)$ as explained above, and combine the two terms in Eq. (41a) as phasors to get the scalloping envelope.

If the wire is symmetrically located with respect to the VOR ($-\ell_1 = \ell_1 = \ell$) and if the wire is long ($2\ell/D >> 1$) the expression in Eq. (18) can be further simplified. The analysis (section 2.2 of Appendix B in reference [1]) shows that in this case

$$\nu_2 = \begin{cases} \nu_1 & \text{for} \quad 0 < |\phi| < \pi/2 \\ \nu_1 + \pi & \text{for} \quad \pi/2 < |\phi| < \pi \end{cases} \tag{19}$$

Hence $\cos\phi\ \cos(\nu_2 - \nu_1) = |\cos\phi|$ and Eq. (18) can be reduced to the form

$$(B-\phi)^{o}_{env} = \frac{10800\ kD}{\pi}\frac{\sin(kh_1\varepsilon)}{\sin(kh_0\varepsilon)}\ |\sin\phi|\ \left|N_2|\cos\phi| - N_1\ \sin\phi\right| \tag{20}$$

When the expressions for N_1 and N_2 derived in the above reference are substituted in Eq. (20) we find as before that there is negligible course deviation error on the side of the wire away from the VOR

($-\pi < \phi < 0$) and the scalloping envelope on the side of the VOR ($0 < \phi < \pi$) is given by Eq. (37) of Appendix B of reference [1] provided that we again divide by $2J_1(ks)$ and also take note of the different wire location (at $y_1 = D$ instead of $y_1 = -D$) by changing ϕ to $-\phi$.

Equation (18) has been successfully used to modify the moment method program for horizontal wires. In a similar way, Eq. (12) has been used to modify the moment method program for arbitrary wires, and Eq. (15) to modify the computer program for vertical cylinders. Equation (15) is also used in the next section to obtain analytical results for circular cylinders.

3-2. Course Deviation Pattern Due to a Circular Cylinder

For analysis purposes it is convenient to locate the cylinder in the azimuthal direction $\phi = 0$ from the VOR at a horizontal distance D. This does not effect the generality of the result but simplifies the analysis and the amount of computations. Scattering has to be computed only for the even sideband (the one that varies as $\cos \phi$) and use can be made of the simplified envelope formula given by Eq. (15).

A plan and elevation view of the configuration is shown in Fig. 11. The cylinder has a diameter 2a and has a length h. The bottom and top surfaces lie in the planes $z = h_1$ and $z = h_2$, respectively, and $h_2 - h_1 = h$.

We shall make the following assumptions:

(1) The cylinder is perfectly conducting. This assumption is reasonably satisfied by many important structures that need to be considered: metal poles, towers, silos, reinforced concrete structures used in atomic power plants, etc.

(2) The radius-to-distance ratio is small ($a/D \ll 1$). This is also usually satisfied in practice.

(3) The distance D itself is large, so that the parameter $kD \gg 1$. This condition is met for the usual VOR frequencies if D is larger than 150 or 200 feet.

(4) The elevation angles to the aircraft and to the highest point on the cylinder are small, perhaps 10 degrees or less. For larger angles corrections due to the counterpoise of the VOR and due to the finite ground conductivity may become important.

(5) The circumferential components of the induced current at each element of the cylindrical surface will be the same as that produced locally on an infinitely long cylinder by a plane wave of the same intensity and phase. This assumption appears reasonable from a geometric optics point of view as long as 2a and h are comparable to the wavelength or larger.

(6) The effect of currents induced on the top and bottom surfaces of the cylinder can be neglected. This is again justified on geometrical optics grounds since these faces are not illuminated. Furthermore these currents are essentially in the y-direction and produce scattered fields in the forward direction near the nulls of the $\sin \phi$ factor in Eq. (15). Another effect of these currents on the flat faces of the cylinder is to generate axial currents on the curved surface. These will produce vertical components in the scattered field which will again not affect the receiver output.

Consider a surface element $a d\psi dz_1$ at the point given by the cylindrical coordinates (a, ψ, z_1) about the axis O'Z'. The rectangular

coordinates in the coordinate system centered at 0 are: $D + a \cos \psi$, $a \sin \psi$, z_1. The length of the distance from 0 to the element is

$$R = [(D + a \cos \psi)^2 + (a \sin \psi)^2 + z_1^2]^{1/2}$$
$$\cong D + a \cos \psi + \frac{a^2 + z_1^2}{2D} \tag{21}$$

The projection of the radius vector $\bar{R}$ to the surface element onto the radius vector $\bar{r}$ to the aircraft is

$$p = \bar{R} \cdot \bar{r}/r = D \sin \theta \cos \phi + a \sin \theta \cos(\psi-\phi) + z_1 \cos \theta$$
$$\cong D \cos \phi + a \cos(\psi-\phi) + z_1 \varepsilon \tag{22}$$

In the last step use was made of assumption (4) which prescribes that $\varepsilon = \pi/2 - \theta << 1$ and hence $\cos \varepsilon \cong 1$, $\sin \varepsilon \cong \varepsilon$.

If we take the direct incident field on the aircraft to be

$$E_\phi^d = \frac{1}{r} \exp(-jkr)\, S(\varepsilon) \begin{cases} \cos \phi & \text{even mode} \\ \sin \phi & \text{odd mode} \end{cases} \tag{23}$$

the incident field at the surface element $a d\psi dz_1$ will be

$$E_\phi^i = \frac{1}{R} \exp(-jkr)\, S(\varepsilon_1) \begin{cases} \cos \phi_1 & \text{even mode} \\ \sin \phi_1 & \text{odd mode} \end{cases} \tag{24}$$

The factors KC cos pt and KC sin pt have been omitted from these expressions since they were seen to have no effect on the final scalloping formula. In Eq. (24) $\varepsilon_1 = z_1/D$ is the elevation angle of the surface element. Because of assumption (4) we can usually write

$$S(\varepsilon) \cong \sin kh_0\varepsilon\ , \quad S(\varepsilon_1) \cong \sin kh_0\varepsilon_1 = \sin(kh_0 z_1/D) \tag{25}$$

From Fig. 1 and assumption (2), $\phi_1 \cong (a/D) \sin \psi << 1$. Hence $\cos \phi_1 \cong 1$ and $\sin \phi_1 \cong (a/D) \sin \psi$. Therefore the odd-mode incident field is negligible with respect to the even-mode field and henceforth will be

omitted from consideration. For the even-mode field we get, using Eq. (22),

$$E_\phi^i = \frac{1}{D} \sin\left(\frac{kh_0 z_1}{D}\right) \exp\left[-jk\left(D + \frac{a^2 + z_1^2}{2D}\right)\right] \exp(-jka \cos\psi) \tag{26}$$

For convenience we write this in the form

$$E_\phi^i = f(z_1) \exp(-jka \cos\psi) \tag{27}$$

Then the incident magnetic field is given by $H_z^i = E_\phi^i/\eta_o$ where η_o is as usual the intrinsic wave impedance $\sqrt{\mu_o/\varepsilon_o}$. By assumption (5) and reference [5] the induced circumferential component of the surface current density is

$$K_\psi = \frac{j2\ f(z_1)}{\pi ka\ \eta_o} \sum_{-\infty}^{\infty} \frac{j^{-n}\ e^{jn\psi}}{H_n^{(2)'}(ka)} \tag{28}$$

The surface current element $K\ ad\psi dz_1$ will produce a scattered field at the aircraft whose ϕ-component is

$$-\frac{j\omega\mu_o}{4\pi r} (K_\psi ad\psi dz_1) \exp[-jk(r-p)] \cos(\psi-\phi)$$

If we substitute for p from Eq. (22) and for K_ψ from Eq. (28) and then add the contribution from the image of the element at $-z_1$ in the proper phase, we obtain

$$d_\phi^2 E^s = \frac{d\psi dz_1}{\pi^2 r} f(z_1) \sin(kz_1\varepsilon) \exp(-jkr) \exp jk[D \cos\phi + a \cos(\psi-\phi)] \cdot$$

$$\cdot \cos(\psi-\phi) \cdot \sum_{-\infty}^{\infty} j^{-n+1} \frac{e^{jn\psi}}{H_n^{(2)'}(ka)} \tag{29}$$

To obtain $M_1 \exp j\mu_1$ we must drop the factor $\exp(-jkr)/r$ (compare Eq. 4)

and integrate over the cylindrical surface. The factor KC cos pt has been dropped previously (Eq. 24).

The ψ-integration can be carried out starting from the integral representation of the Bessel function [6]

$$J_n(z) = \frac{1}{2\pi}\int_{-\pi}^{\pi} \exp[jz\cos(\psi-\phi) + jn(\psi-\phi-\frac{\pi}{2})]d\psi \tag{30}$$

This can be re-written in the form

$$j^{-n}\int_{-\pi}^{\pi} \exp[jz\cos(\psi-\phi) + jn\psi]d\psi = 2\pi J_n(z)\exp(jn\phi)$$

Differentiating both sides with respect to z and setting z = ka yields

$$j^{-n+1}\int_{-\pi}^{\pi} \cos(\psi-\phi)\exp[jka\cos(\psi-\phi) + jn\psi]\,d\psi = 2\pi J_n'(ka)\exp(jn\phi) \tag{31}$$

Comparing with Eq. (29) this is seen to be exactly the integral needed there.

The radiation integral can now be written in the form

$$M_1\exp(j\mu_1) = \frac{2}{\pi k_1 D}\exp[jk(D\cos\phi - D - \frac{a^2}{2D})]\,V(\varepsilon;kD,\ kh_0,\ dh_1,kh_2)H(\phi;ka) \tag{32}$$

and, from Eq. (15), the scalloping envelope

$$(B-\phi)^{o}_{env} = \frac{360|V(\varepsilon)\ H(\phi)\ \sin\phi|}{\pi^2 kD\ \sin(kh_0\varepsilon)} \tag{33}$$

To get the actual course deviation, Eq. (33) must be multiplied by the scalloping factor $\cos(kD\cos\phi + \nu_1)$ where

$$\nu_1 = -\,k(D + \frac{a^2}{2D}) + \text{ang } V(\varepsilon) + \text{ang } H(\phi) \tag{34}$$

Expressing the sine factors in the integrand in terms of exponentials one gets four terms of the form exp $j[+(\varepsilon \pm \varepsilon_o)t - t^2/2\Omega]$. By completing the squares in the exponents, each term can be reduced to the standard form of the Fresnel integral

$$\int_0^x \exp[-j(\pi/2)u^2]du = C(x) - jS(x) \tag{41}$$

After some algebra one finds

$$V(\varepsilon;\Omega,\ p_0,\ p_1,\ p_2) = F(\varepsilon;\Omega,\ p_0,p_2) - F(\varepsilon;\Omega,\ p_0,p_1) \tag{42}$$

where

$$\begin{aligned} &F(\varepsilon;\Omega,\ p_0,x) \\ &= \frac{\sqrt{\pi\Omega}}{4}\{\exp j\,\tfrac{1}{2}\Omega\,(\varepsilon-\varepsilon_o)^2[C(a) - jS(a) - C(b) + jS(b)] \\ &\qquad - \exp j\,\tfrac{1}{2}\Omega\,(\varepsilon+\varepsilon_o)^2[C(c) - jS(c) - C(d) + jS(d)]\} \end{aligned} \tag{43}$$

and

$$\begin{aligned} a &= (\varepsilon-\varepsilon_o)\sqrt{\Omega/\pi} + x/\sqrt{\pi\Omega} \qquad & b &= (\varepsilon-\varepsilon_o)\sqrt{\Omega/\pi} - x/\sqrt{\pi\Omega} \\ c &= (\varepsilon+\varepsilon_o)\sqrt{\Omega/\pi} + x/\sqrt{\pi\Omega} \qquad & d &= (\varepsilon+\varepsilon_o)\sqrt{\Omega/\pi} - x/\sqrt{\pi\Omega} \end{aligned} \tag{44}$$

It is clear from the manner in which the various system parameters are intertwined that the above is not a very useful result. Even though the equations could be easily programmed on a computer, they do not give a good picture of the dependence on individual parameters. Clearly some approximations are needed.

3-3. Summary and Preliminary Discussion

To make the results of the last section more useful they must be simplified and systematized. This has only been possible to a limited extent so far and further work is needed.

We first note that for ka >> 1, the azimuthal dependence of the course deviation pattern is given by $|\sin(\phi/2)|^{1/2}|\sin\phi|$. This expression has maxima at $\pm\phi_o$ where

$$\phi_o = \cos^{-1}(-0.2) = 101.54° \tag{45}$$

The value of the maximum is $\sin\phi_o[\sin(\phi_o/2)]^{1/2} = 0.86233$. It is convenient to normalize with respect to this peak and define

$$f(\phi;ka) = \frac{|H(\phi;ka)\sin\phi|}{(1/2)\sin\phi_o[\pi ka\sin(\phi_o/2)]^{1/2}} = \frac{|H(\phi;ka)\sin\phi|}{0.76422\ (ka)^{1/2}} \tag{46}$$

These normalized scalloping envelopes were computed with the aid of Eqs. (36) and (46). The results are tabulated in Tables 1 to 4 and plotted in Figs. 12 to 21 for values of ka in the range from 0.4 to 8.0. It is seen that there is only one peak in the domain $0 < \phi < 180°$ when $ka < 2.4$. There are two peaks for $2.4 < ka < 4.0$. At ka = 2.6 the two peaks are about equal. One is located at $\phi = 58°$, the other one at $\phi = 120°$. As ka increases, the forward-directed maximum decreases in amplitude but moves closer to the forward scattering direction. This sort of phenomenon has been observed with cylinders of rectangular cross-section. Beyond ka = 4 further ripples appear but they eventually reduce in amplitude and the highest peaks merge near $\phi_o = 101.54°$.

The maxima of $f(\phi;\ ka)$ are plotted versus ka in Fig. 22. The solid line indicates the largest maximum $f_{max}(ka)$, the dashed lines indicate subsidiary maxima. The geometric-optics and long-wavelength limits are indicated by straight lines. It is seen that approximating $f_{max}(ka)$ by its geometric-optics limit (unity) leads to an error of less than 12 percent for ka > 2.

The location of the maxima is indicated in Fig. 23. Again the solid line shows the position of the largest maximum, the dashed lines the position of subsidiary maxima when they occur. At the long-wavelength end (ka << 1) the location of the peak approaches $\phi = 126.38°$ asymptotically. This is the location of the maximum of $|(1 - 2\cos\phi)\sin\phi|$ as expected (see Eq. 38). As ka increases beyond about 5, the largest two peaks merge near $\phi = 101.54°$.

We can summarize the above results by writing the scalloping envelope given in Eq. (33) in the modified form

$$(B-\phi)^{o}_{env} = 27.875\ \frac{(ka)^{1/2}}{kD}\ \frac{|V(\varepsilon;\Omega,\ p_0,p_1,p_2)|}{\sin\ (kh_0\varepsilon)}\ f(\phi;\ ka) \tag{47}$$

For $ka \leq 8$, $f(\phi;\ ka)$ is plotted in Figs. 2 to 11. For ka > 8, $f(\phi;\ ka)$ can be approximated by

$$f(\phi;\ ka) \cong \left|\frac{\sin\ \phi}{\sin\ \phi_o}\right|\ \left|\frac{\sin(\phi/2)}{\sin(\phi_o/2)}\right|^{1/2} = 1.1596\ |\sin\ \phi|\ \sin(\phi/2)|^{1/2} \tag{48}$$

The largest maximum is given by

$$(B-\phi)^{o}_{max} = 27.875\ \frac{(ka)^{1/2}}{kD}\ \frac{|V(\varepsilon;\Omega,\ p_0,p_1,p_2)|}{|\sin(kh_0\varepsilon)|}\ f_{max}(ka) \tag{49}$$

For $ka \leq 8$, $f_{max}(ka)$ can be read off Fig. 22 and the location of the maximum

can be obtained from the solid line in Fig. 23. For ka > 2, $f_{max}(ka) \cong 1$.

For ka < 0.4, the peak course deviation occurs near $\phi = 126°$ and Eqs. (47) and (49) are more conveniently expressed in the approximate forms

$$(B-\phi)^{o}_{env} = \frac{90}{\pi}\frac{(ka)^2}{kD}\frac{|V(\varepsilon;\Omega,\ p_0,p_1,p_2)|}{|\sin(kh_0\varepsilon)|}(1-2\cos\phi)|\sin\phi| \tag{50}$$

$$(B-\phi)^{o}_{max} = 50.426\frac{(ka)^2}{kD}\frac{|V(\varepsilon;\Omega,p_0,p_1,p_2)|}{\sin(kh_0\varepsilon)} \tag{51}$$

There still remains the task of interpreting the integral $V(\varepsilon)$ given by Eq. (37) and its closed form solution given by (42) to (44). While some success towards this goal has been achieved, a good approximate result is, at the moment, only available when the cylinder height is small. This case is important since it allows a direct comparison of the analytical result with the moment method results previously obtained.

To arrive at the approximate result, we re-write Eqs. (43) and (44) in the form

$$F(x) = \frac{\sqrt{\pi\Omega}}{4}\exp[j\ \frac{1}{2}\ \Omega(\varepsilon^2+\varepsilon_o^2)]\{\exp(-jp_0\varepsilon)[E(a)-E(b)]-\exp(jp_0\varepsilon)[E(c)-E(d)]\} \tag{52}$$

$$a = \frac{\varepsilon\Omega - p_0 + x}{\sqrt{\pi\Omega}} \qquad b = \frac{\varepsilon\Omega - p_0 - x}{\sqrt{\pi\Omega}}$$
$$c = \frac{\varepsilon\Omega + p_0 + x}{\sqrt{\pi\Omega}} \qquad d = \frac{\varepsilon\Omega + p_0 - x}{\sqrt{\pi\Omega}} \tag{53}$$

where, for convenience we have written

$$E(x) = C(x) - jS(x) \tag{54}$$

If we write h_2 and h_1 in terms of the mean height $\tilde{h}$ and the cylinder length h, i.e.

$$h_2 = \tilde{h} + h/2 \qquad h_1 = \tilde{h} - h/2 \tag{55}$$

and assume that

$$\frac{kh}{\sqrt{\pi\Omega}} << 1 \tag{56}$$

we can approximate $V(\varepsilon)$ by the Taylor expansion

$$V = F(kh_2) - F(kh_1) = kh\ F'(k\tilde{h}) + \frac{1}{2}\ (kh)^2\ F''(k\tilde{h}) + \ldots \tag{57}$$

Starting from Eq. (52) we find, after some lengthy algebra, that

$$F'(x) = \exp(-j\ \frac{x^2}{2\Omega})\ \sin\ (\varepsilon_o x)\ \sin\ (\varepsilon x) \tag{58}$$

$$F''(x) = \exp(-j\ \frac{x^2}{2\Omega})\{(p_0/\Omega)\cos\ \varepsilon_o x\ \sin\ \varepsilon x + \varepsilon\ \sin\ \varepsilon_o x\cos\ \varepsilon x -$$

$$- j(x/\Omega)\ \sin\ \varepsilon_o x\ \sin\ \varepsilon x\} \tag{59}$$

Substituting (58) and (59) in (57) yields finally:

$$V(\varepsilon) = \exp(-j\frac{k\tilde{h}^2}{2D})\ \{kh\ \sin\ (kh_0\tilde{h}/D)\ \sin(k\tilde{h}\varepsilon) +$$

$$+ \frac{(kh)^2}{2}[\frac{h_0}{D}\ \cos(kh_0\tilde{h}/D)\sin(k\tilde{h}\varepsilon) + \varepsilon\ \sin(kh_0\tilde{h}/D)\cos(k\tilde{h}\varepsilon) -$$

$$- j\ \frac{\tilde{h}}{D}\ \sin(kh_0\tilde{h}/D)\sin(k\tilde{h}\varepsilon)]\} \tag{60}$$

When $kh/\sqrt{\pi\Omega}$ is small enough the second term in the curly bracket could be omitted for crude estimates. We then get approximately

$$|V(\varepsilon)| = kh\ |\sin(kh_0\tilde{h}/D)\ \sin(k\tilde{h}\varepsilon)| \tag{61}$$

This is exactly what one would obtain from the original integral in

Eq. (37) by setting the exponential phase factor in the integrand equal to its value at the average height: $\exp(-j\,\frac{k\tilde{h}^2}{2D})$.

As an example let us consider the small cylinder previously evaluated by the moment method [section 4-2 of reference 1, pp. 39]. The following data are pertinent:

$$f = 115 \text{ MHz}\ ,\quad \lambda = 8.56 \text{ ft},\qquad k = 0.734 \text{ ft}^{-1}$$

$$a = \lambda/4\qquad ,\ ka = \pi/2 = 1.57$$

$$h = 3\lambda/8 = 3.21 \text{ ft},\quad h_1 = 19 \text{ ft},\ h_2 = 22.21 \text{ ft},\ \tilde{h} = 20.6 \text{ ft}$$

$$D = 150 \text{ ft}\ ,\quad h_0 = 16 \text{ ft}$$

$$\varepsilon = 0.0505\ ,\quad \varepsilon_o = h_0/D = 0.1067$$

This makes

$$kh = 2.356 \qquad kh_0 = 11.744 \qquad k\tilde{h} = 15.120$$

$$k\tilde{h}\varepsilon = 0.7636 \qquad \sin(k\tilde{h}\varepsilon) = 0.6915 \qquad \cos(k\tilde{h}\varepsilon) = 0.7224$$

$$k\tilde{h}\varepsilon_o = 1.6134 \qquad \sin(k\tilde{h}\varepsilon_o) = 0.9991 \qquad \cos(k\tilde{h}\varepsilon_o) = -\ 0.0425$$

Hence

$$|V(\varepsilon)| = |1.6278 + [-\ 0.0126 + 0.1012 - j0.2634]| = 1.7365$$

The error in neglecting the second term, i.e. the term in $(kh)^2$, would have been only 6.26%. In other words, Eq. (61) gives a value that is only about 6% lower than Eq. (60). Using this result and Eq. (49) with $f_{max}(1.57) = 1.216$ from Fig. 12 or the corresponding table, we find

$$(B-\phi)^{o}_{max} = 1.20°$$

From Fig. 13 and Table 1 (column for ka = 1.60) the peak course deviation should be close to $\phi = \pm\ 90°$. The shape of scalloping envelope should be

close to that shown in Fig. 3. The wavelength of the scalloping ripples near $\phi = 90°$ should be

$$\Delta\phi = \frac{360}{0.734 \times 150} = 3.27°$$

by Eq. (35).

Comparison with the moment method result [p. 43 of reference 1] shows excellent agreement in most respects. There are 18 half-periods or 9 wavelengths in an interval of about 30° about $\phi = 90°$. This corresponds to a ripple wavelength of about 3.3°. Peak scalloping does occur near $\phi = 90°$ (if allowance is made for the different zero point for the azimuthal angle). The shape of the envelope follows quite closely that in Fig. 3. The only discrepancy appears to be in the absolute value of the peak course deviation: about 1.55° compared to the above theoretical value of 1.20°. Without further study it is difficult to assess what the cause of this discrepancy is. Only three modes were used for the expansion of the azimuthal current distribution in the moment method. It is possible that more modes are required for good accuracy. This question is now being looked into.

Further work is needed to put the general results into more useful forms. It is believed that Eqs. (47) and (49) together with Figs. 22 and 23 and Eqs. (42) to (44) should give good estimates in all practical cases involving vertical cylindrical structures. It would be useful, however, to have simple and good approximations to Eq. (43) for a sufficiently large range of parameters similar to Eq. (61) for short cylinders.

TABLE 1 FOR f(ϕ, ka)

ϕ° ka	0.4	0.8	1.2	1.6	2.0
0.0	0.0000E 00	0.0000E 00	0.0000E 00	0.0000E 00	0.0000E 00
2.5	0.1291E-01	0.3094E-01	0.4121E-01	0.5175E-01	0.6064E-01
5.0	0.2566E-01	0.6152E-01	0.8191E-01	0.1027E 00	0.1202E 00
7.5	0.3810E-01	0.9140E-01	0.1216E 00	0.1521E 00	0.1778E 00
10.0	0.5007E-01	0.1202E 00	0.1598E 00	0.1993E 00	0.2325E 00
12.5	0.6142E-01	0.1477E 00	0.1960E 00	0.2437E 00	0.2836E 00
15.0	0.7202E-01	0.1735E 00	0.2300E 00	0.2848E 00	0.3306E 00
17.5	0.8173E-01	0.1974E 00	0.2613E 00	0.3222E 00	0.3732E 00
20.0	0.9041E-01	0.2190E 00	0.2899E 00	0.3560E 00	0.4115E 00
22.5	0.9796E-01	0.2383E 00	0.3156E 00	0.3860E 00	0.4458E 00
25.0	0.1043E 00	0.2551E 00	0.3384E 00	0.4125E 00	0.4767E 00
27.5	0.1092E 00	0.2691E 00	0.3584E 00	0.4362E 00	0.5051E 00
30.0	0.1128E 00	0.2805E 00	0.3759E 00	0.4577E 00	0.5322E 00
32.5	0.1149E 00	0.2892E 00	0.3914E 00	0.4779E 00	0.5593E 00
35.0	0.1154E 00	0.2952E 00	0.4053E 00	0.4980E 00	0.5875E 00
37.5	0.1144E 00	0.2988E 00	0.4184E 00	0.5190E 00	0.6179E 00
40.0	0.1118E 00	0.3001E 00	0.4313E 00	0.5421E 00	0.6514E 00
42.5	0.1077E 00	0.2996E 00	0.4450E 00	0.5681E 00	0.6881E 00
45.0	0.1021E 00	0.2977E 00	0.4601E 00	0.5979E 00	0.7282E 00
47.5	0.9511E-01	0.2950E 00	0.4775E 00	0.6318E 00	0.7710E 00
50.0	0.8686E-01	0.2923E 00	0.4977E 00	0.6696E 00	0.8158E 00
52.5	0.7763E-01	0.2903E 00	0.5212E 00	0.7112E 00	0.8614E 00
55.0	0.6786E-01	0.2901E 00	0.5480E 00	0.7557E 00	0.9066E 00
57.5	0.5838E-01	0.2924E 00	0.5781E 00	0.8026E 00	0.9502E 00
60.0	0.5062E-01	0.2981E 00	0.6112E 00	0.8507E 00	0.9908E 00
62.5	0.4693E-01	0.3078E 00	0.6469E 00	0.8990E 00	0.1028E 01
65.0	0.4955E-01	0.3218E 00	0.6846E 00	0.9467E 00	0.1059E 01
67.5	0.5865E-01	0.3401E 00	0.7237E 00	0.9927E 00	0.1085E 01
70.0	0.7257E-01	0.3624E 00	0.7635E 00	0.1036E 01	0.1104E 01
72.5	0.8957E-01	0.3882E 00	0.8034E 00	0.1076E 01	0.1116E 01
75.0	0.1085E 00	0.4170E 00	0.8426E 00	0.1112E 01	0.1122E 01
77.5	0.1288E 00	0.4480E 00	0.8805E 00	0.1143E 01	0.1119E 01
80.0	0.1499E 00	0.4806E 00	0.9166E 00	0.1169E 01	0.1110E 01
82.5	0.1714E 00	0.5143E 00	0.9503E 00	0.1189E 01	0.1095E 01
85.0	0.1932E 00	0.5484E 00	0.9812E 00	0.1204E 01	0.1073E 01
87.5	0.2149E 00	0.5824E 00	0.1009E 01	0.1213E 01	0.1046E 01
90.0	0.2365E 00	0.6158E 00	0.1033E 01	0.1216E 01	0.1015E 01
92.5	0.2576E 00	0.6482E 00	0.1053E 01	0.1213E 01	0.9802E 00
95.0	0.2780E 00	0.6792E 00	0.1069E 01	0.1204E 01	0.9434E 00
97.5	0.2978E 00	0.7084E 00	0.1081E 01	0.1190E 01	0.9056E 00
100.0	0.3165E 00	0.7355E 00	0.1088E 01	0.1172E 01	0.8680E 00
102.5	0.3342E 00	0.7602E 00	0.1092E 01	0.1149E 01	0.8319E 00
105.0	0.3505E 00	0.7822E 00	0.1090E 01	0.1122E 01	0.7983E 00
107.5	0.3655E 00	0.8013E 00	0.1085E 01	0.1091E 01	0.7681E 00
110.0	0.3789E 00	0.8174E 00	0.1075E 01	0.1058E 01	0.7421E 00
112.5	0.3907E 00	0.8301E 00	0.1061E 01	0.1022E 01	0.7205E 00
115.0	0.4007E 00	0.8395E 00	0.1044E 01	0.9841E 00	0.7034E 00
117.5	0.4089E 00	0.8454E 00	0.1023E 01	0.9453E 00	0.6906E 00
120.0	0.4151E 00	0.8477E 00	0.9981E 00	0.9057E 00	0.6813E 00
122.5	0.4193E 00	0.8464E 00	0.9703E 00	0.8657E 00	0.6747E 00
125.0	0.4214E 00	0.8414E 00	0.9398E 00	0.8259E 00	0.6699E 00
127.5	0.4214E 00	0.8328E 00	0.9066E 00	0.7864E 00	0.6658E 00
130.0	0.4193E 00	0.8206E 00	0.8712E 00	0.7475E 00	0.6615E 00
132.5	0.4150E 00	0.8047E 00	0.8337E 00	0.7093E 00	0.6560E 00
135.0	0.4086E 00	0.7854E 00	0.7945E 00	0.6720E 00	0.6486E 00
137.5	0.4000E 00	0.7626E 00	0.7538E 00	0.6355E 00	0.6387E 00
140.0	0.3892E 00	0.7366E 00	0.7119E 00	0.5997E 00	0.6259E 00
142.5	0.3764E 00	0.7072E 00	0.6689E 00	0.5645E 00	0.6097E 00
145.0	0.3616E 00	0.6749E 00	0.6252E 00	0.5297E 00	0.5900E 00
147.5	0.3448E 00	0.6396E 00	0.5810E 00	0.4951E 00	0.5666E 00
150.0	0.3262E 00	0.6015E 00	0.5363E 00	0.4604E 00	0.5395E 00
152.5	0.3057E 00	0.5608E 00	0.4913E 00	0.4256E 00	0.5089E 00
155.0	0.2836E 00	0.5177E 00	0.4463E 00	0.3903E 00	0.4748E 00
157.5	0.2599E 00	0.4724E 00	0.4011E 00	0.3544E 00	0.4374E 00
160.0	0.2348E 00	0.4251E 00	0.3561E 00	0.3179E 00	0.3969E 00
162.5	0.2084E 00	0.3760E 00	0.3111E 00	0.2805E 00	0.3536E 00
165.0	0.1808E 00	0.3253E 00	0.2662E 00	0.2424E 00	0.3079E 00
167.5	0.1523E 00	0.2732E 00	0.2215E 00	0.2034E 00	0.2599E 00
170.0	0.1228E 00	0.2200E 00	0.1770E 00	0.1637E 00	0.2102E 00
172.5	0.9273E-01	0.1658E 00	0.1326E 00	0.1234E 00	0.1589E 00
175.0	0.6211E-01	0.1109E 00	0.8834E-01	0.8255E-01	0.1065E 00
177.5	0.3114E-01	0.5557E-01	0.4415E-01	0.4137E-01	0.5348E-01
180.0	0.4485E-06	0.8002E-06	0.6352E-06	0.5957E-06	0.7704E-06

TABLE 2 FOR f(ϕ; ka)

ϕ° ka	2.4	2.8	3.2	3.6	4.0
0.0	0.0000E 00	0.0000E 00	0.0000E 00	0.0000E 00	0.0000E 00
2.5	0.6844E-01	0.7608E-01	0.8264E-01	0.8919E-01	0.9509E-01
5.0	0.1355E 00	0.1504E 00	0.1630E 00	0.1755E 00	0.1867E 00
7.5	0.1999E 00	0.2212E 00	0.2391E 00	0.2565E 00	0.2717E 00
10.0	0.2605E 00	0.2872E 00	0.3092E 00	0.3300E 00	0.3478E 00
12.5	0.3164E 00	0.3474E 00	0.3721E 00	0.3948E 00	0.4135E 00
15.0	0.3672E 00	0.4012E 00	0.4276E 00	0.4506E 00	0.4687E 00
17.5	0.4128E 00	0.4487E 00	0.4758E 00	0.4979E 00	0.5144E 00
20.0	0.4534E 00	0.4906E 00	0.5179E 00	0.5383E 00	0.5523E 00
22.5	0.4898E 00	0.5279E 00	0.5553E 00	0.5737E 00	0.5847E 00
25.0	0.5231E 00	0.5622E 00	0.5900E 00	0.6063E 00	0.6138E 00
27.5	0.5547E 00	0.5952E 00	0.6238E 00	0.6376E 00	0.6407E 00
30.0	0.5862E 00	0.6285E 00	0.6579E 00	0.6686E 00	0.6650E 00
32.5	0.6190E 00	0.6634E 00	0.6929E 00	0.6985E 00	0.6851E 00
35.0	0.6542E 00	0.7003E 00	0.7282E 00	0.7258E 00	0.6980E 00
37.5	0.6923E 00	0.7389E 00	0.7624E 00	0.7479E 00	0.7004E 00
40.0	0.7334E 00	0.7783E 00	0.7933E 00	0.7617E 00	0.6886E 00
42.5	0.7768E 00	0.8169E 00	0.8184E 00	0.7641E 00	0.6600E 00
45.0	0.8215E 00	0.8527E 00	0.8350E 00	0.7527E 00	0.6128E 00
47.5	0.8658E 00	0.8836E 00	0.8410E 00	0.7254E 00	0.5469E 00
50.0	0.9083E 00	0.9075E 00	0.8344E 00	0.6817E 00	0.4645E 00
52.5	0.9471E 00	0.9226E 00	0.8140E 00	0.6222E 00	0.3713E 00
55.0	0.9806E 00	0.9275E 00	0.7796E 00	0.5493E 00	0.2813E 00
57.5	0.1007E 01	0.9213E 00	0.7319E 00	0.4684E 00	0.2288E 00
60.0	0.1026E 01	0.9035E 00	0.6727E 00	0.3894E 00	0.2588E 00
62.5	0.1036E 01	0.8744E 00	0.6055E 00	0.3310E 00	0.3571E 00
65.0	0.1037E 01	0.8350E 00	0.5359E 00	0.3193E 00	0.4820E 00
67.5	0.1028E 01	0.7869E 00	0.4726E 00	0.3661E 00	0.6113E 00
70.0	0.1010E 01	0.7328E 00	0.4279E 00	0.4546E 00	0.7340E 00
72.5	0.9835E 00	0.6762E 00	0.4151E 00	0.5622E 00	0.8434E 00
75.0	0.9492E 00	0.6220E 00	0.4407E 00	0.6741E 00	0.9352E 00
77.5	0.9089E 00	0.5761E 00	0.4988E 00	0.7814E 00	0.1006E 01
80.0	0.8644E 00	0.5452E 00	0.5772E 00	0.8785E 00	0.1055E 01
82.5	0.8180E 00	0.5347E 00	0.6644E 00	0.9617E 00	0.1082E 01
85.0	0.7723E 00	0.5471E 00	0.7524E 00	0.1029E 01	0.1087E 01
87.5	0.7303E 00	0.5802E 00	0.8354E 00	0.1078E 01	0.1073E 01
90.0	0.6949E 00	0.6289E 00	0.9097E 00	0.1109E 01	0.1043E 01
92.5	0.6687E 00	0.6868E 00	0.9729E 00	0.1123E 01	0.1002E 01
95.0	0.6538E 00	0.7484E 00	0.1023E 01	0.1120E 01	0.9535E 00
97.5	0.6507E 00	0.8092E 00	0.1060E 01	0.1103E 01	0.9043E 00
100.0	0.6588E 00	0.8660E 00	0.1084E 01	0.1075E 01	0.8597E 00
102.5	0.6760E 00	0.9163E 00	0.1094E 01	0.1038E 01	0.8249E 00
105.0	0.6998E 00	0.9586E 00	0.1092E 01	0.9951E 00	0.8033E 00
107.5	0.7272E 00	0.9918E 00	0.1079E 01	0.9505E 00	0.7959E 00
110.0	0.7556E 00	0.1015E 01	0.1056E 01	0.9071E 00	0.8012E 00
112.5	0.7826E 00	0.1029E 01	0.1026E 01	0.8679E 00	0.8158E 00
115.0	0.8066E 00	0.1034E 01	0.9900E 00	0.8349E 00	0.8354E 00
117.5	0.8260E 00	0.1029E 01	0.9499E 00	0.8091E 00	0.8557E 00
120.0	0.8401E 00	0.1016E 01	0.9077E 00	0.7906E 00	0.8732E 00
122.5	0.8481E 00	0.9950E 00	0.8650E 00	0.7783E 00	0.8850E 00
125.0	0.8497E 00	0.9678E 00	0.8234E 00	0.7704E 00	0.8896E 00
127.5	0.8450E 00	0.9349E 00	0.7838E 00	0.7646E 00	0.8860E 00
130.0	0.8339E 00	0.8976E 00	0.7470E 00	0.7589E 00	0.8741E 00
132.5	0.8169E 00	0.8567E 00	0.7133E 00	0.7513E 00	0.8542E 00
135.0	0.7943E 00	0.8132E 00	0.6826E 00	0.7403E 00	0.8270E 00
137.5	0.7666E 00	0.7679E 00	0.6543E 00	0.7249E 00	0.7935E 00
140.0	0.7343E 00	0.7217E 00	0.6277E 00	0.7045E 00	0.7549E 00
142.5	0.6982E 00	0.6751E 00	0.6020E 00	0.6792E 00	0.7123E 00
145.0	0.6587E 00	0.6286E 00	0.5764E 00	0.6489E 00	0.6669E 00
147.5	0.6166E 00	0.5825E 00	0.5499E 00	0.6139E 00	0.6196E 00
150.0	0.5722E 00	0.5369E 00	0.5218E 00	0.5750E 00	0.5714E 00
152.5	0.5262E 00	0.4919E 00	0.4917E 00	0.5327E 00	0.5228E 00
155.0	0.4791E 00	0.4474E 00	0.4590E 00	0.4877E 00	0.4744E 00
157.5	0.4312E 00	0.4032E 00	0.4235E 00	0.4407E 00	0.4262E 00
160.0	0.3828E 00	0.3593E 00	0.3853E 00	0.3924E 00	0.3785E 00
162.5	0.3344E 00	0.3153E 00	0.3442E 00	0.3432E 00	0.3312E 00
165.0	0.2859E 00	0.2712E 00	0.3005E 00	0.2937E 00	0.2841E 00
167.5	0.2377E 00	0.2269E 00	0.2543E 00	0.2441E 00	0.2371E 00
170.0	0.1897E 00	0.1821E 00	0.2061E 00	0.1947E 00	0.1900E 00
172.5	0.1420E 00	0.1370E 00	0.1562E 00	0.1456E 00	0.1428E 00
175.0	0.9448E-01	0.9155E-01	0.1049E 00	0.9688E-01	0.9535E-01
177.5	0.4719E-01	0.4584E-01	0.5266E-01	0.4837E-01	0.4772E-01
180.0	0.6788E-06	0.6600E-06	0.7588E-06	0.6957E-06	0.6869E-06

TABLE 3 FOR f(ϕ; ka)

ϕ° ka	4.4	4.8	5.2	5.6	6.0
0.0	0.0000E 00	0.0000E 00	0.0000E 00	0.0000E 00	0.0000E 00
2.5	0.1008E 00	0.1062E 00	0.1113E 00	0.1162E 00	0.1209E 00
5.0	0.1973E 00	0.2073E 00	0.2165E 00	0.2253E 00	0.2334E 00
7.5	0.2858E 00	0.2988E 00	0.3104E 00	0.3211E 00	0.3306E 00
10.0	0.3636E 00	0.3776E 00	0.3894E 00	0.3996E 00	0.4079E 00
12.5	0.4291E 00	0.4421E 00	0.4518E 00	0.4591E 00	0.4636E 00
15.0	0.4824E 00	0.4925E 00	0.4984E 00	0.5006E 00	0.4993E 00
17.5	0.5249E 00	0.5306E 00	0.5312E 00	0.5268E 00	0.5182E 00
20.0	0.5587E 00	0.5591E 00	0.5534E 00	0.5411E 00	0.5238E 00
22.5	0.5866E 00	0.5805E 00	0.5672E 00	0.5455E 00	0.5176E 00
25.0	0.6102E 00	0.5962E 00	0.5734E 00	0.5398E 00	0.4987E 00
27.5	0.6299E 00	0.6054E 00	0.5698E 00	0.5207E 00	0.4615E 00
30.0	0.6443E 00	0.6055E 00	0.5526E 00	0.4835E 00	0.4023E 00
32.5	0.6504E 00	0.5923E 00	0.5170E 00	0.4232E 00	0.3165E 00
35.0	0.6441E 00	0.5615E 00	0.4587E 00	0.3366E 00	0.2026E 00
37.5	0.6215E 00	0.5094E 00	0.3752E 00	0.2231E 00	0.6355E-01
40.0	0.5796E 00	0.4340E 00	0.2668E 00	0.8615E-01	0.9712E-01
42.5	0.5164E 00	0.3360E 00	0.1391E 00	0.7579E-01	0.2658E 00
45.0	0.4325E 00	0.2206E 00	0.6300E-01	0.2416E 00	0.4329E 00
47.5	0.3318E 00	0.1146E 00	0.1987E 00	0.4091E 00	0.5852E 00
50.0	0.2265E 00	0.1463E 00	0.3620E 00	0.5658E 00	0.7104E 00
52.5	0.1615E 00	0.2869E 00	0.5214E 00	0.7008E 00	0.7982E 00
55.0	0.2149E 00	0.4421E 00	0.6658E 00	0.8048E 00	0.8414E 00
57.5	0.3422E 00	0.5919E 00	0.7861E 00	0.8706E 00	0.8374E 00
60.0	0.4863E 00	0.7265E 00	0.8755E 00	0.8946E 00	0.7892E 00
62.5	0.6275E 00	0.8385E 00	0.9293E 00	0.8770E 00	0.7065E 00
65.0	0.7553E 00	0.9226E 00	0.9458E 00	0.8231E 00	0.6090E 00
67.5	0.8662E 00	0.9756E 00	0.9266E 00	0.7437E 00	0.5294E 00
70.0	0.9525E 00	0.9964E 00	0.8769E 00	0.6573E 00	0.5098E 00
72.5	0.1012E 01	0.9864E 00	0.8064E 00	0.5910E 00	0.5686E 00
75.0	0.1045E 01	0.9499E 00	0.7296E 00	0.5744E 00	0.6795E 00
77.5	0.1051E 01	0.8936E 00	0.6662E 00	0.6197E 00	0.8044E 00
80.0	0.1032E 01	0.8277E 00	0.6372E 00	0.7099E 00	0.9170E 00
82.5	0.9941E 00	0.7649E 00	0.6550E 00	0.8172E 00	0.1002E 01
85.0	0.9423E 00	0.7197E 00	0.7141E 00	0.9195E 00	0.1053E 01
87.5	0.8846E 00	0.7043E 00	0.7968E 00	0.1003E 01	0.1067E 01
90.0	0.8303E 00	0.7229E 00	0.8845E 00	0.1059E 01	0.1050E 01
92.5	0.7885E 00	0.7698E 00	0.9635E 00	0.1086E 01	0.1009E 01
95.0	0.7667E 00	0.8332E 00	0.1025E 01	0.1085E 01	0.9552E 00
97.5	0.7680E 00	0.9006E 00	0.1065E 01	0.1060E 01	0.9021E 00
100.0	0.7903E 00	0.9624E 00	0.1081E 01	0.1019E 01	0.8630E 00
102.5	0.8270E 00	0.1012E 01	0.1076E 01	0.9693E 00	0.8465E 00
105.0	0.8702E 00	0.1045E 01	0.1052E 01	0.9216E 00	0.8542E 00
107.5	0.9128E 00	0.1061E 01	0.1016E 01	0.8838E 00	0.8802E 00
110.0	0.9492E 00	0.1060E 01	0.9713E 00	0.8613E 00	0.9145E 00
112.5	0.9756E 00	0.1044E 01	0.9255E 00	0.8552E 00	0.9472E 00
115.0	0.9900E 00	0.1015E 01	0.8839E 00	0.8621E 00	0.9708E 00
117.5	0.9919E 00	0.9779E 00	0.8505E 00	0.8761E 00	0.9810E 00
120.0	0.9816E 00	0.9353E 00	0.8271E 00	0.8906E 00	0.9764E 00
122.5	0.9605E 00	0.8914E 00	0.8133E 00	0.9003E 00	0.9577E 00
125.0	0.9303E 00	0.8490E 00	0.8067E 00	0.9015E 00	0.9273E 00
127.5	0.8931E 00	0.8106E 00	0.8036E 00	0.8925E 00	0.8887E 00
130.0	0.8513E 00	0.7772E 00	0.8004E 00	0.8730E 00	0.8456E 00
132.5	0.8068E 00	0.7488E 00	0.7940E 00	0.8440E 00	0.8015E 00
135.0	0.7617E 00	0.7243E 00	0.7824E 00	0.8074E 00	0.7592E 00
137.5	0.7173E 00	0.7020E 00	0.7642E 00	0.7652E 00	0.7202E 00
140.0	0.6748E 00	0.6800E 00	0.7392E 00	0.7198E 00	0.6849E 00
142.5	0.6345E 00	0.6566E 00	0.7077E 00	0.6732E 00	0.6525E 00
145.0	0.5964E 00	0.6304E 00	0.6706E 00	0.6271E 00	0.6216E 00
147.5	0.5601E 00	0.6006E 00	0.6289E 00	0.5823E 00	0.5904E 00
150.0	0.5250E 00	0.5667E 00	0.5837E 00	0.5393E 00	0.5576E 00
152.5	0.4901E 00	0.5288E 00	0.5363E 00	0.4980E 00	0.5220E 00
155.0	0.4547E 00	0.4872E 00	0.4876E 00	0.4578E 00	0.4831E 00
157.5	0.4180E 00	0.4426E 00	0.4383E 00	0.4180E 00	0.4409E 00
160.0	0.3795E 00	0.3957E 00	0.3890E 00	0.3778E 00	0.3958E 00
162.5	0.3389E 00	0.3471E 00	0.3399E 00	0.3364E 00	0.3484E 00
165.0	0.2960E 00	0.2975E 00	0.2911E 00	0.2934E 00	0.2994E 00
167.5	0.2508E 00	0.2475E 00	0.2426E 00	0.2485E 00	0.2494E 00
170.0	0.2034E 00	0.1975E 00	0.1942E 00	0.2017E 00	0.1992E 00
172.5	0.1543E 00	0.1477E 00	0.1458E 00	0.1530E 00	0.1490E 00
175.0	0.1037E 00	0.9821E-01	0.9729E-01	0.1029E 00	0.9905E-01
177.5	0.5211E-01	0.4902E-01	0.4868E-01	0.5173E-01	0.4943E-01
180.0	0.7510E-06	0.7049E-06	0.7007E-06	0.7456E-06	0.7108E-06

TABLE 4 FOR f(ϕ; ka)

ϕ° ka	6.4	6.8	7.2	7.6	8.0
0.0	0.0000E 00	0.0000E 00	0.0000E 00	0.0000E 00	0.0000E 00
2.5	0.1254E 00	0.1298E 00	0.1339E 00	0.1380E 00	0.1418E 00
5.0	0.2412E 00	0.2484E 00	0.2551E 00	0.2615E 00	0.2674E 00
7.5	0.3392E 00	0.3468E 00	0.3534E 00	0.3592E 00	0.3640E 00
10.0	0.4145E 00	0.4195E 00	0.4228E 00	0.4246E 00	0.4248E 00
12.5	0.4656E 00	0.4652E 00	0.4623E 00	0.4572E 00	0.4500E 00
15.0	0.4944E 00	0.4865E 00	0.4753E 00	0.4612E 00	0.4445E 00
17.5	0.5049E 00	0.4878E 00	0.4669E 00	0.4423E 00	0.4149E 00
20.0	0.5007E 00	0.4727E 00	0.4406E 00	0.4041E 00	0.3648E 00
22.5	0.4826E 00	0.4417E 00	0.3962E 00	0.3461E 00	0.2937E 00
25.0	0.4484E 00	0.3915E 00	0.3300E 00	0.2650E 00	0.2008E 00
27.5	0.3932E 00	0.3173E 00	0.2385E 00	0.1620E 00	0.1060E 00
30.0	0.3120E 00	0.2160E 00	0.1259E 00	0.8472E-01	0.1423E 00
32.5	0.2029E 00	0.9470E-01	0.8484E-01	0.1840E 00	0.2871E 00
35.0	0.7160E-01	0.9613E-01	0.2232E 00	0.3405E 00	0.4386E 00
37.5	0.1024E 00	0.2526E 00	0.3849E 00	0.4903E 00	0.5638E 00
40.0	0.2678E 00	0.4165E 00	0.5330E 00	0.6084E 00	0.6396E 00
42.5	0.4337E 00	0.5638E 00	0.6472E 00	0.6758E 00	0.6503E 00
45.0	0.5829E 00	0.6778E 00	0.7116E 00	0.6801E 00	0.5902E 00
47.5	0.7011E 00	0.7447E 00	0.7163E 00	0.6185E 00	0.4689E 00
50.0	0.7765E 00	0.7565E 00	0.6599E 00	0.5021E 00	0.3242E 00
52.5	0.8017E 00	0.7120E 00	0.5530E 00	0.3666E 00	0.2725E 00
55.0	0.7749E 00	0.6196E 00	0.4258E 00	0.3072E 00	0.4045E 00
57.5	0.7020E 00	0.5022E 00	0.3501E 00	0.4101E 00	0.5956E 00
60.0	0.5987E 00	0.4095E 00	0.4100E 00	0.5875E 00	0.7623E 00
62.5	0.4973E 00	0.4151E 00	0.5641E 00	0.7556E 00	0.8705E 00
65.0	0.4512E 00	0.5279E 00	0.7303E 00	0.8775E 00	0.9069E 00
67.5	0.5016E 00	0.6821E 00	0.8659E 00	0.9371E 00	0.8740E 00
70.0	0.6231E 00	0.8269E 00	0.9506E 00	0.9323E 00	0.7913E 00
72.5	0.7642E 00	0.9363E 00	0.9778E 00	0.8743E 00	0.6978E 00
75.0	0.8906E 00	0.9980E 00	0.9514E 00	0.7889E 00	0.6490E 00
77.5	0.9835E 00	0.1010E 01	0.8863E 00	0.7158E 00	0.6843E 00
80.0	0.1035E 01	0.9777E 00	0.8082E 00	0.6980E 00	0.7855E 00
82.5	0.1043E 01	0.9163E 00	0.7510E 00	0.7503E 00	0.9027E 00
85.0	0.1015E 01	0.8472E 00	0.7443E 00	0.8463E 00	0.9964E 00
87.5	0.9615E 00	0.7964E 00	0.7929E 00	0.9471E 00	0.1046E 01
90.0	0.8992E 00	0.7853E 00	0.8746E 00	0.1024E 01	0.1049E 01
92.5	0.8475E 00	0.8184E 00	0.9597E 00	0.1064E 01	0.1013E 01
95.0	0.8229E 00	0.8811E 00	0.1026E 01	0.1063E 01	0.9567E 00
97.5	0.8325E 00	0.9516E 00	0.1062E 01	0.1031E 01	0.9045E 00
100.0	0.8701E 00	0.1011E 01	0.1065E 01	0.9804E 00	0.8780E 00
102.5	0.9214E 00	0.1049E 01	0.1041E 01	0.9302E 00	0.8860E 00
105.0	0.9715E 00	0.1061E 01	0.9977E 00	0.8967E 00	0.9205E 00
107.5	0.1009E 01	0.1049E 01	0.9491E 00	0.8888E 00	0.9635E 00
110.0	0.1028E 01	0.1017E 01	0.9077E 00	0.9037E 00	0.9979E 00
112.5	0.1027E 01	0.9734E 00	0.8825E 00	0.9302E 00	0.1013E 01
115.0	0.1008E 01	0.9283E 00	0.8758E 00	0.9553E 00	0.1006E 01
117.5	0.9739E 00	0.8893E 00	0.8830E 00	0.9690E 00	0.9798E 00
120.0	0.9317E 00	0.8616E 00	0.8958E 00	0.9663E 00	0.9405E 00
122.5	0.8872E 00	0.8460E 00	0.9057E 00	0.9468E 00	0.8970E 00
125.0	0.8455E 00	0.8394E 00	0.9066E 00	0.9137E 00	0.8572E 00
127.5	0.8102E 00	0.8364E 00	0.8954E 00	0.8720E 00	0.8258E 00
130.0	0.7826E 00	0.8317E 00	0.8721E 00	0.8276E 00	0.8036E 00
132.5	0.7614E 00	0.8210E 00	0.8385E 00	0.7856E 00	0.7875E 00
135.0	0.7441E 00	0.8019E 00	0.7979E 00	0.7487E 00	0.7728E 00
137.5	0.7274E 00	0.7741E 00	0.7538E 00	0.7176E 00	0.7549E 00
140.0	0.7084E 00	0.7384E 00	0.7095E 00	0.6907E 00	0.7307E 00
142.5	0.6851E 00	0.6967E 00	0.6670E 00	0.6654E 00	0.6990E 00
145.0	0.6563E 00	0.6511E 00	0.6272E 00	0.6388E 00	0.6605E 00
147.5	0.6220E 00	0.6037E 00	0.5898E 00	0.6089E 00	0.6166E 00
150.0	0.5825E 00	0.5563E 00	0.5535E 00	0.5744E 00	0.5696E 00
152.5	0.5390E 00	0.5100E 00	0.5170E 00	0.5353E 00	0.5215E 00
155.0	0.4925E 00	0.4652E 00	0.4787E 00	0.4921E 00	0.4737E 00
157.5	0.4441E 00	0.4216E 00	0.4380E 00	0.4458E 00	0.4270E 00
160.0	0.3947E 00	0.3788E 00	0.3944E 00	0.3974E 00	0.3815E 00
162.5	0.3449E 00	0.3358E 00	0.3482E 00	0.3478E 00	0.3367E 00
165.0	0.2953E 00	0.2921E 00	0.3000E 00	0.2979E 00	0.2919E 00
167.5	0.2459E 00	0.2471E 00	0.2504E 00	0.2480E 00	0.2464E 00
170.0	0.1967E 00	0.2005E 00	0.2002E 00	0.1983E 00	0.1997E 00
172.5	0.1475E 00	0.1521E 00	0.1498E 00	0.1487E 00	0.1515E 00
175.0	0.9842E-01	0.1023E 00	0.9961E-01	0.9912E-01	0.1019E 00
177.5	0.4923E-01	0.5146E-01	0.4971E-01	0.4957E-01	0.5126E-01
180.0	0.7066E-06	0.7418E-06	0.7147E-06	0.7134E-06	0.7390E-06

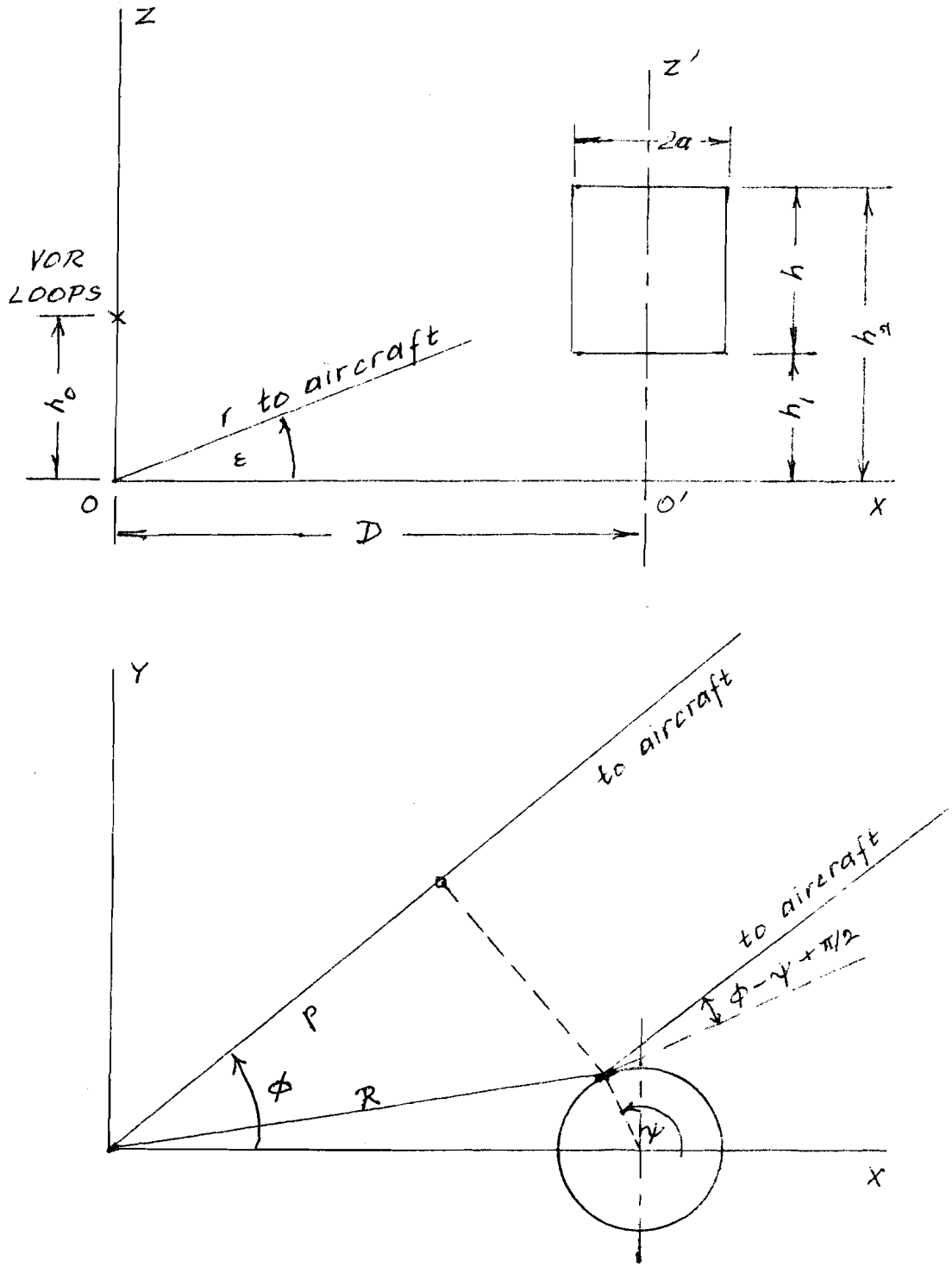

FIG. 11 ELEVATION AND PLAN VIEW

K+E 10 X 10 TO ½ INCH 7 X 10 INCHES
KEUFFEL & ESSER CO. MADE IN U.S.A.

46 1322

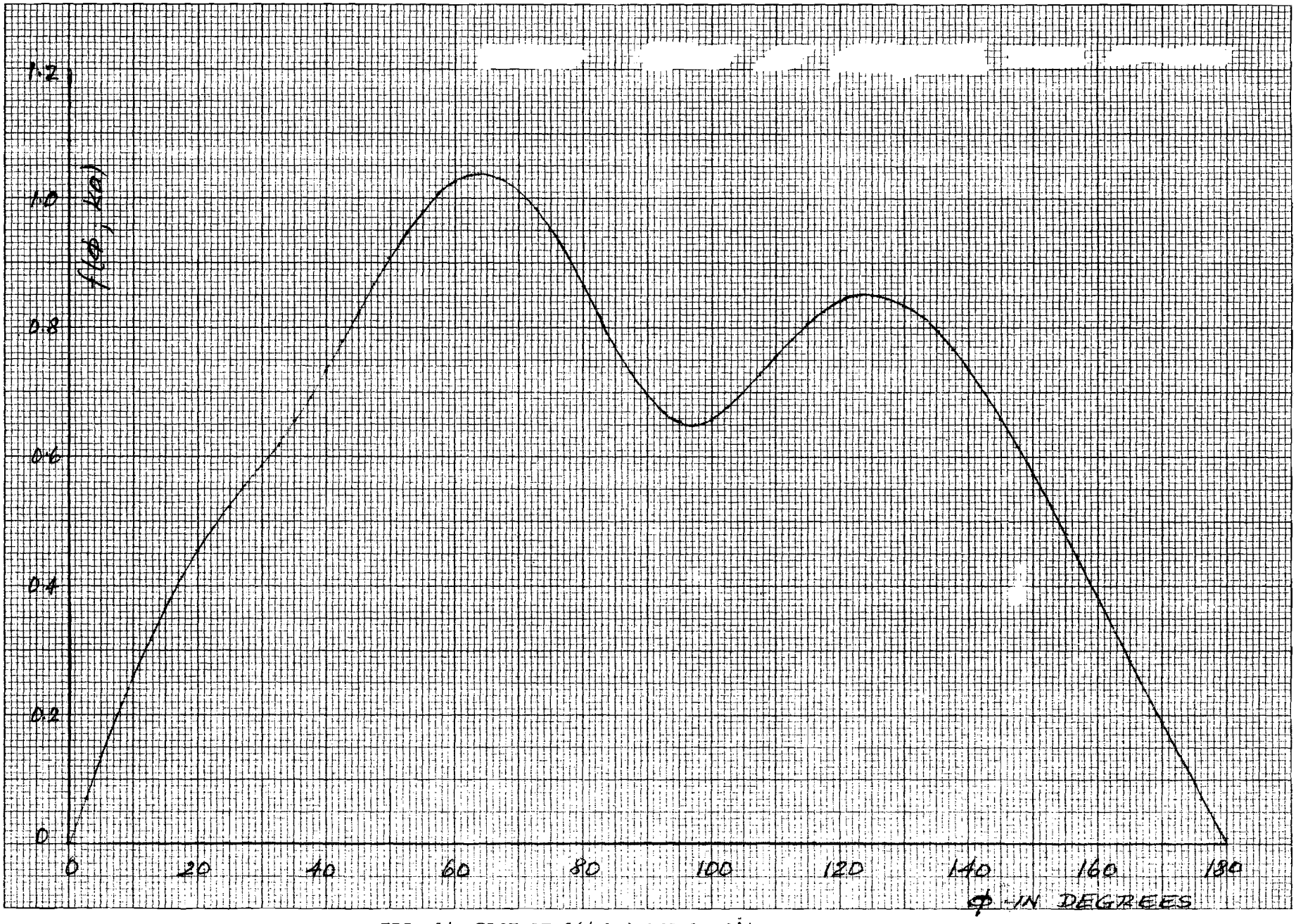

FIG. 14 PLOT OF $f(\phi;ka)$ FOR $ka=2.4$

K+E 10 X 10 TO ½ INCH 7 X 10 INCHES
KEUFFEL & ESSER CO. MADE IN U.S.A.
46 1322

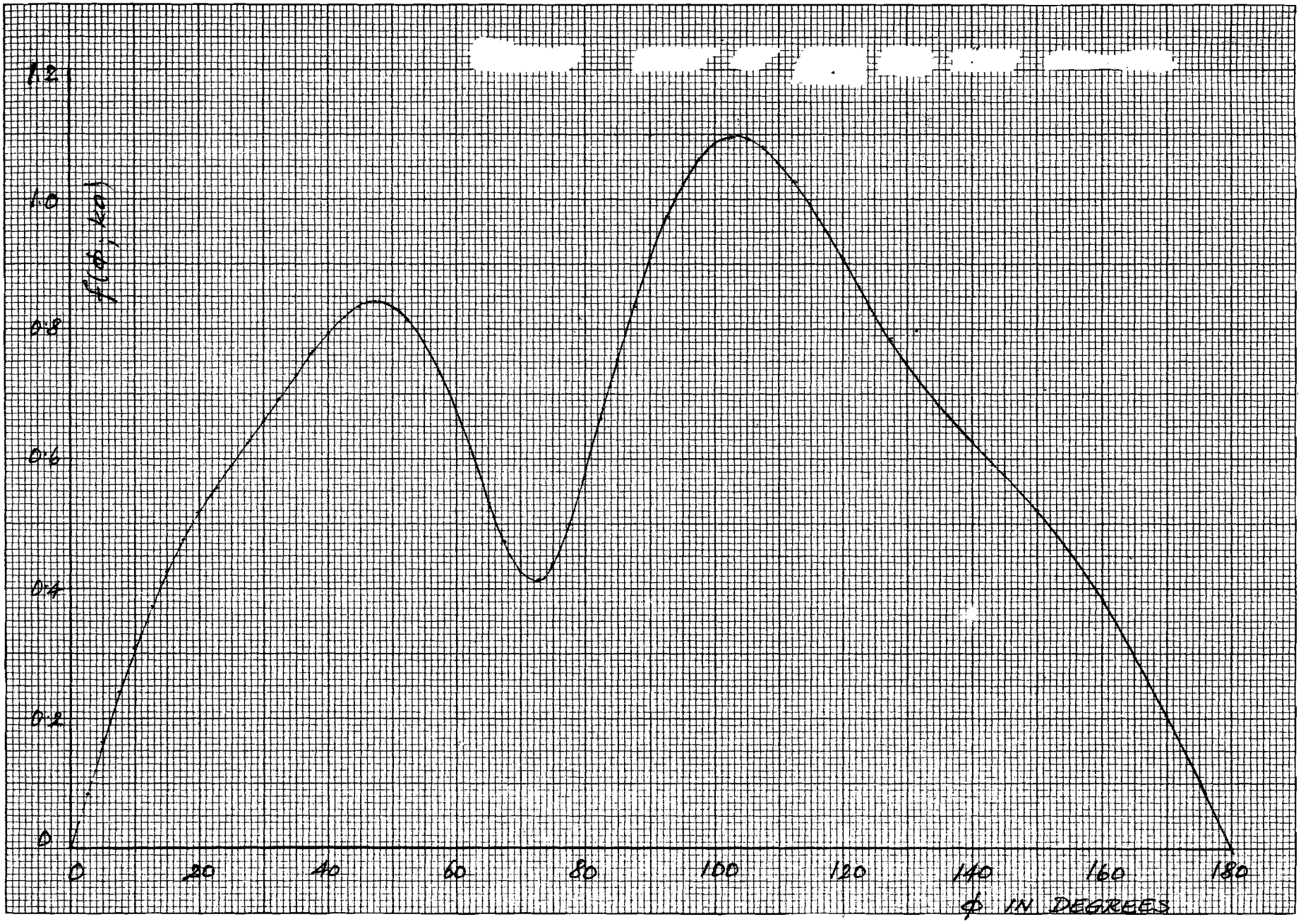

FIG. 15 PLOT OF $f(\phi;ka)$ FOR ka=3.2

K+E 10 X 10 TO ½ INCH 7 X 10 INCHES
KEUFFEL & ESSER CO. MADE IN U.S.A.

46 1322

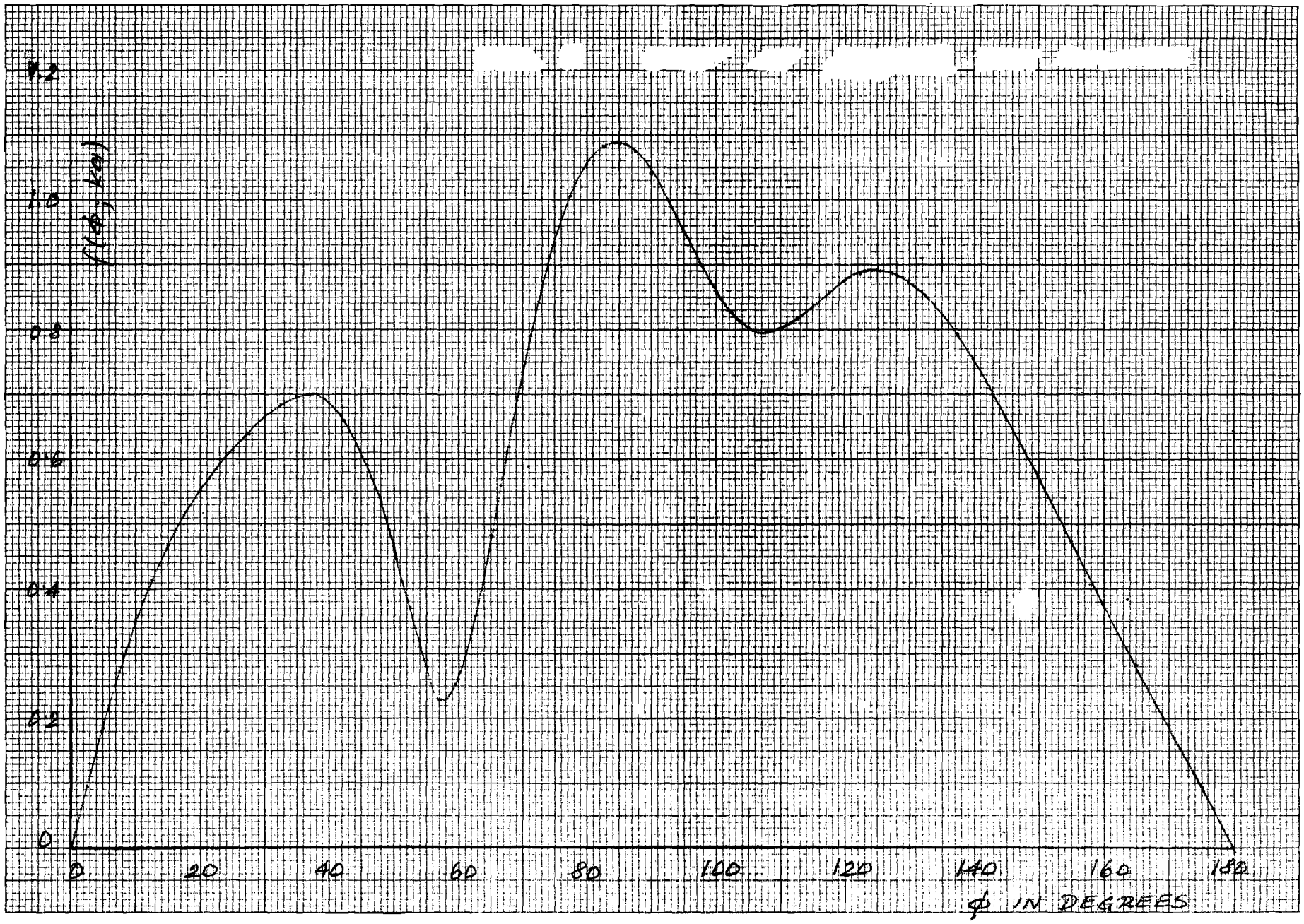

FIG. 16 PLOT OF f(φ;ka) FOR ka=4.0

K+E 10 X 10 TO ½ INCH 7 X 10 INCHES
KEUFFEL & ESSER CO. MADE IN U.S.A.

46 1322

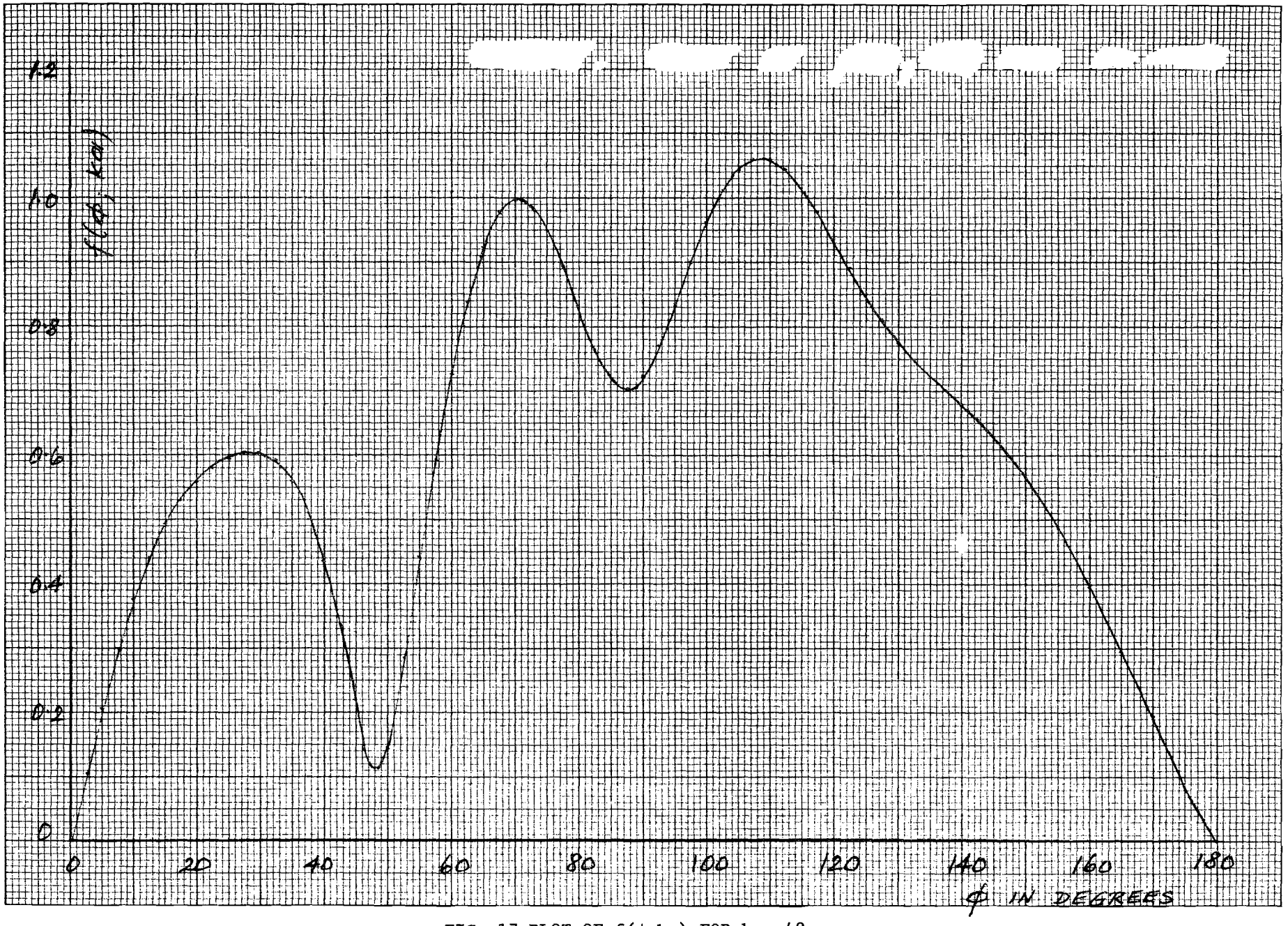

FIG. 17 PLOT OF f(φ;ka) FOR ka= 48

K+E 10 X 10 TO ½ INCH 7 X 10 INCHES
KEUFFEL & ESSER CO. MADE IN U.S.A.

46 1322

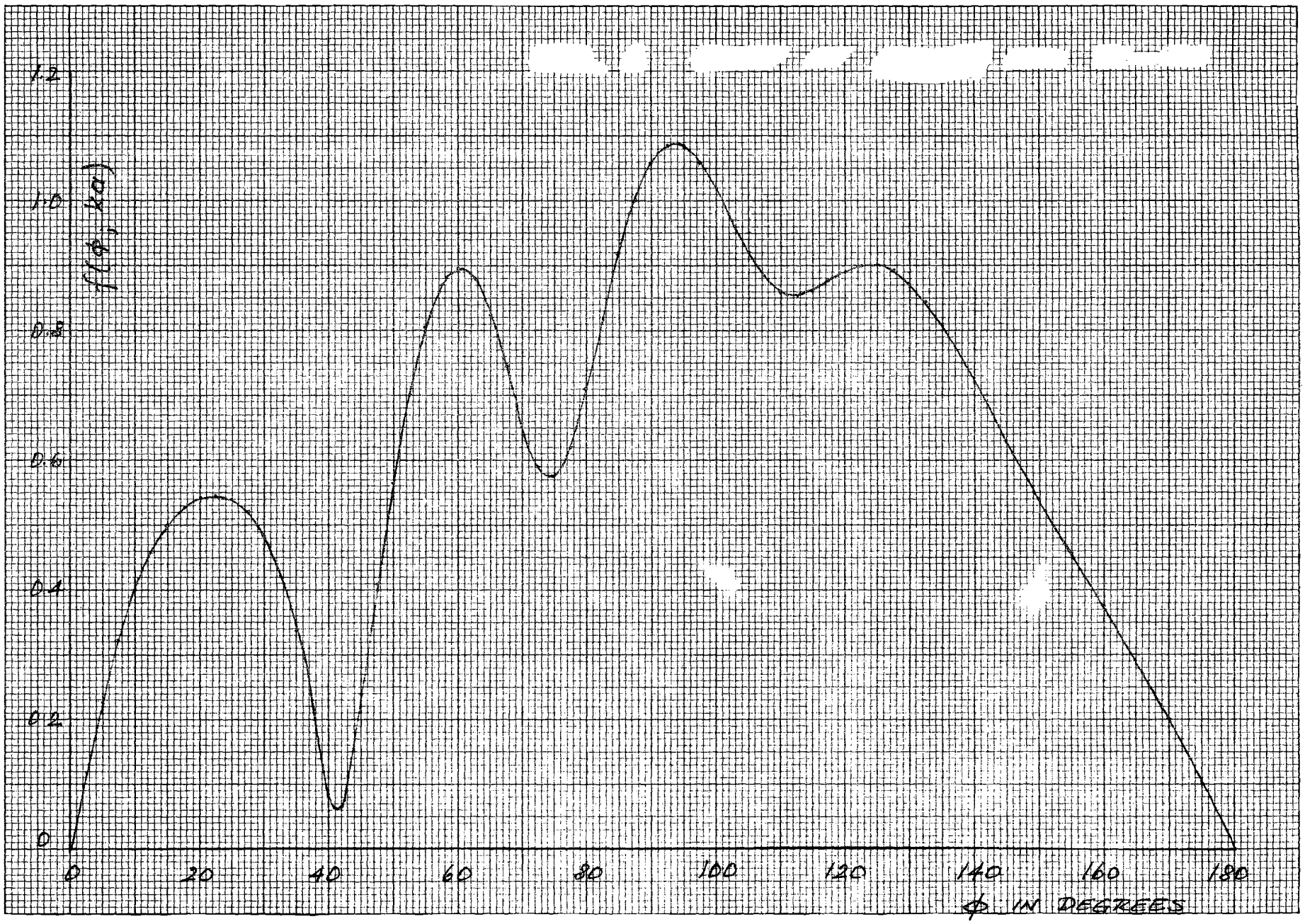

FIG. 18 PLOT OF f(ϕ;ka) FOR ka=5.6

K•Σ 10 X 10 TO ½ INCH 7 X 10 INCHES
KEUFFEL & ESSER CO. MADE IN U.S.A.

46 1322

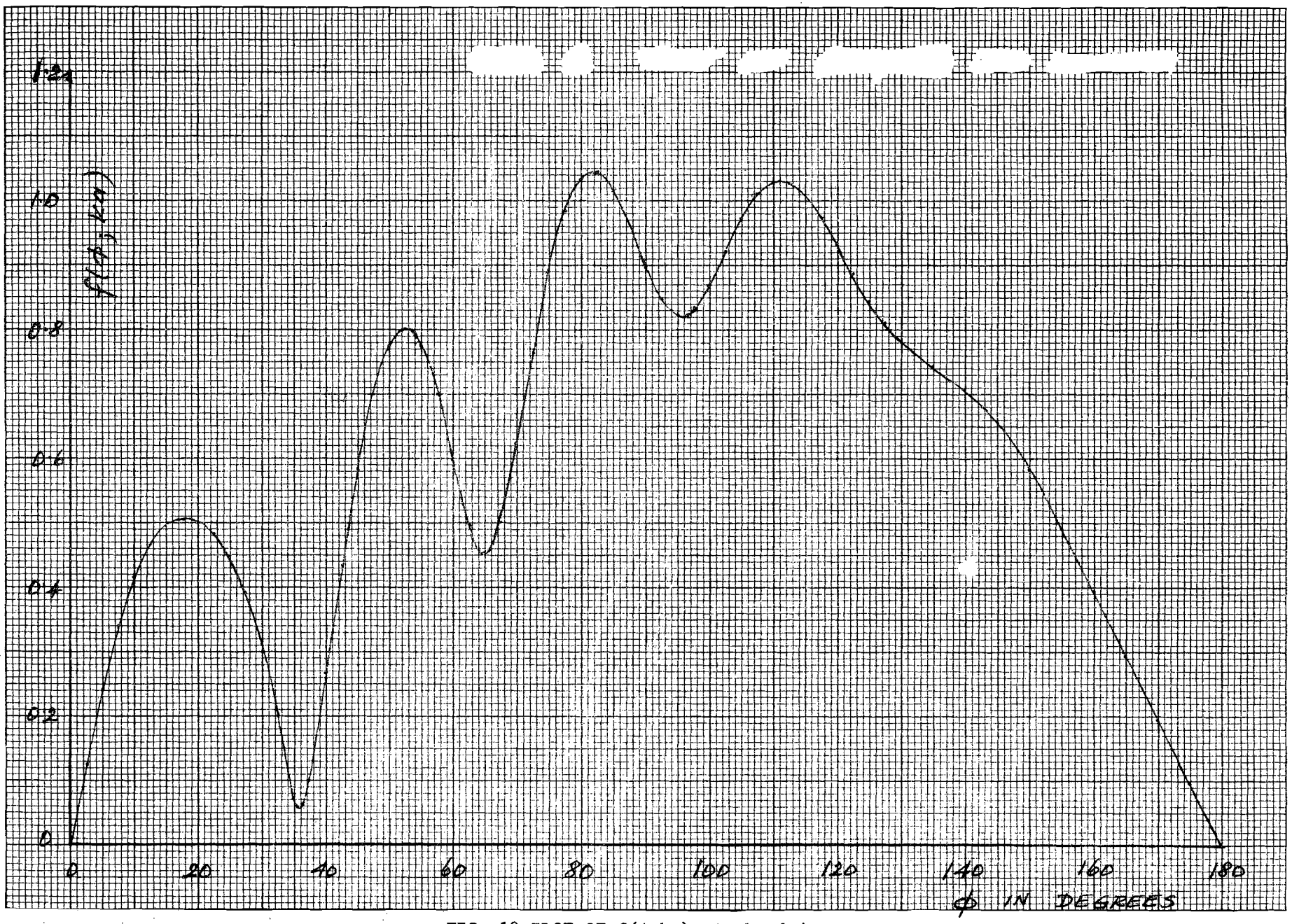

FIG. 19 PLOT OF f(ϕ;ka) FOR ka=6.4

R*E KEUFFEL & ESSER CO. MADE IN U.S.A. 46 1322

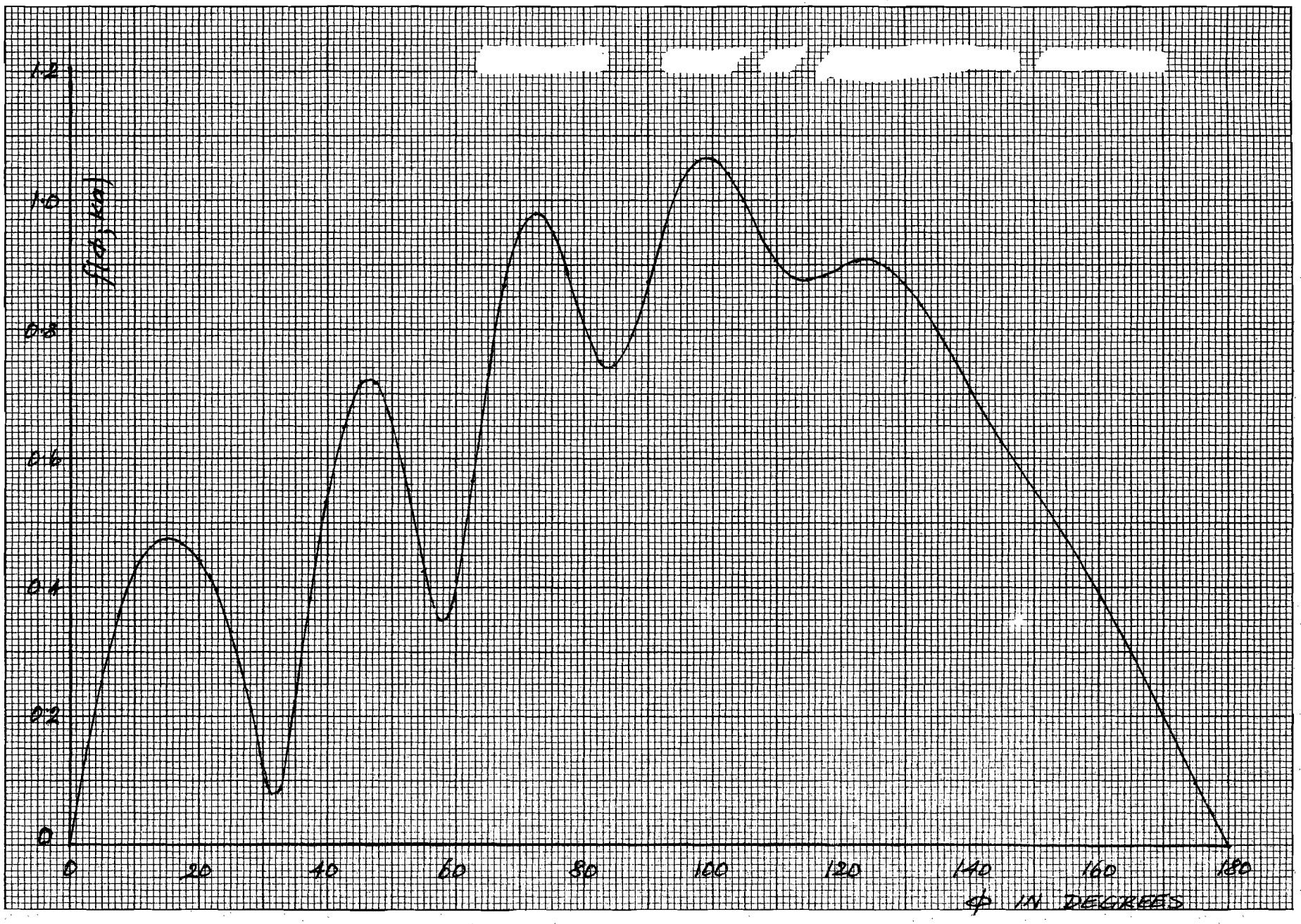

FIG. 20 PLOT OF f(φ;ka) FOR ka=7.2

K+E 10 X 10 TO ½ INCH 7 X 10 INCHES
KEUFFEL & ESSER CO. MADE IN U.S.A.

46 1322

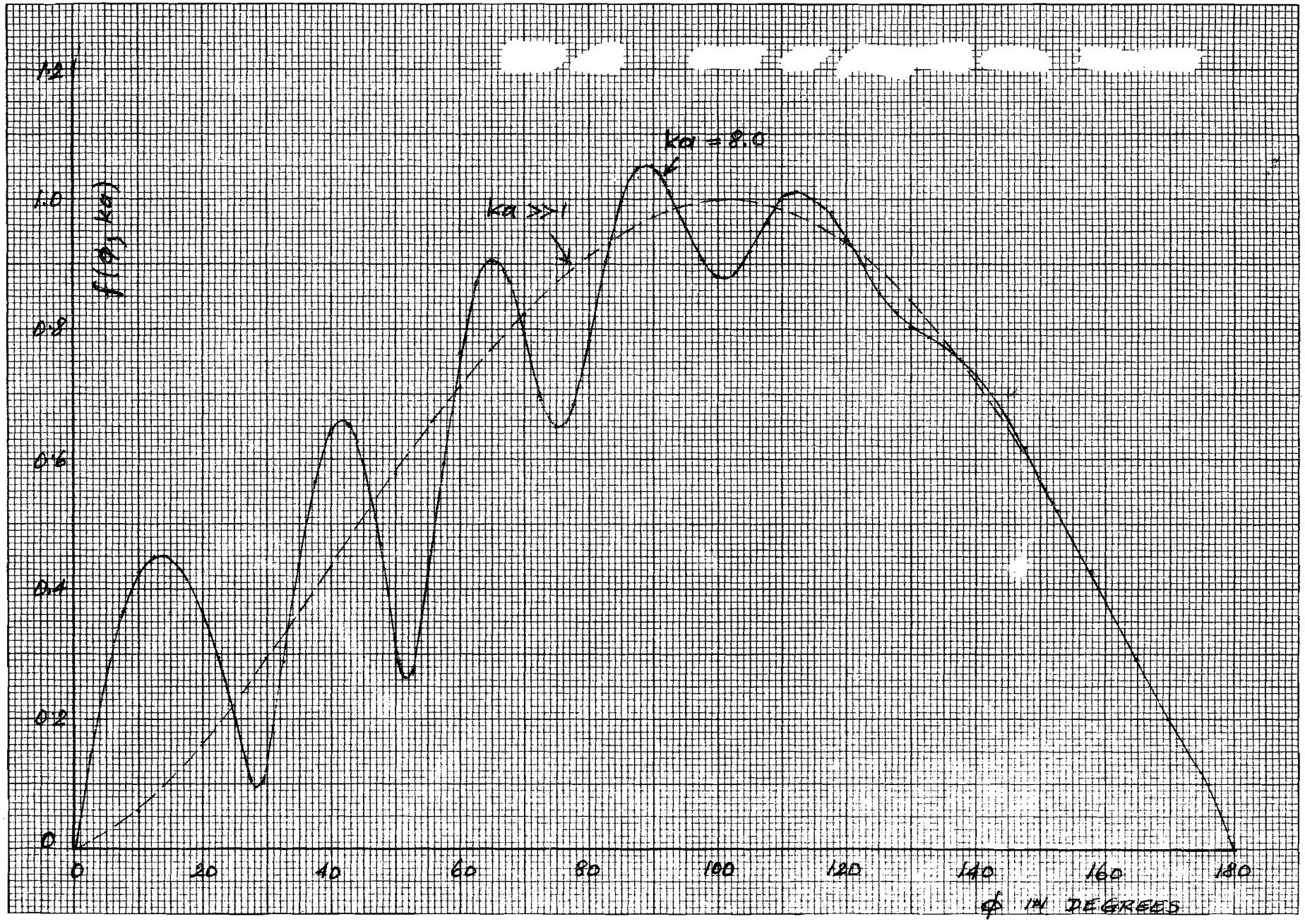

FIG. 21 PLOT OF f(ϕ;ka) FOR ka=8.0

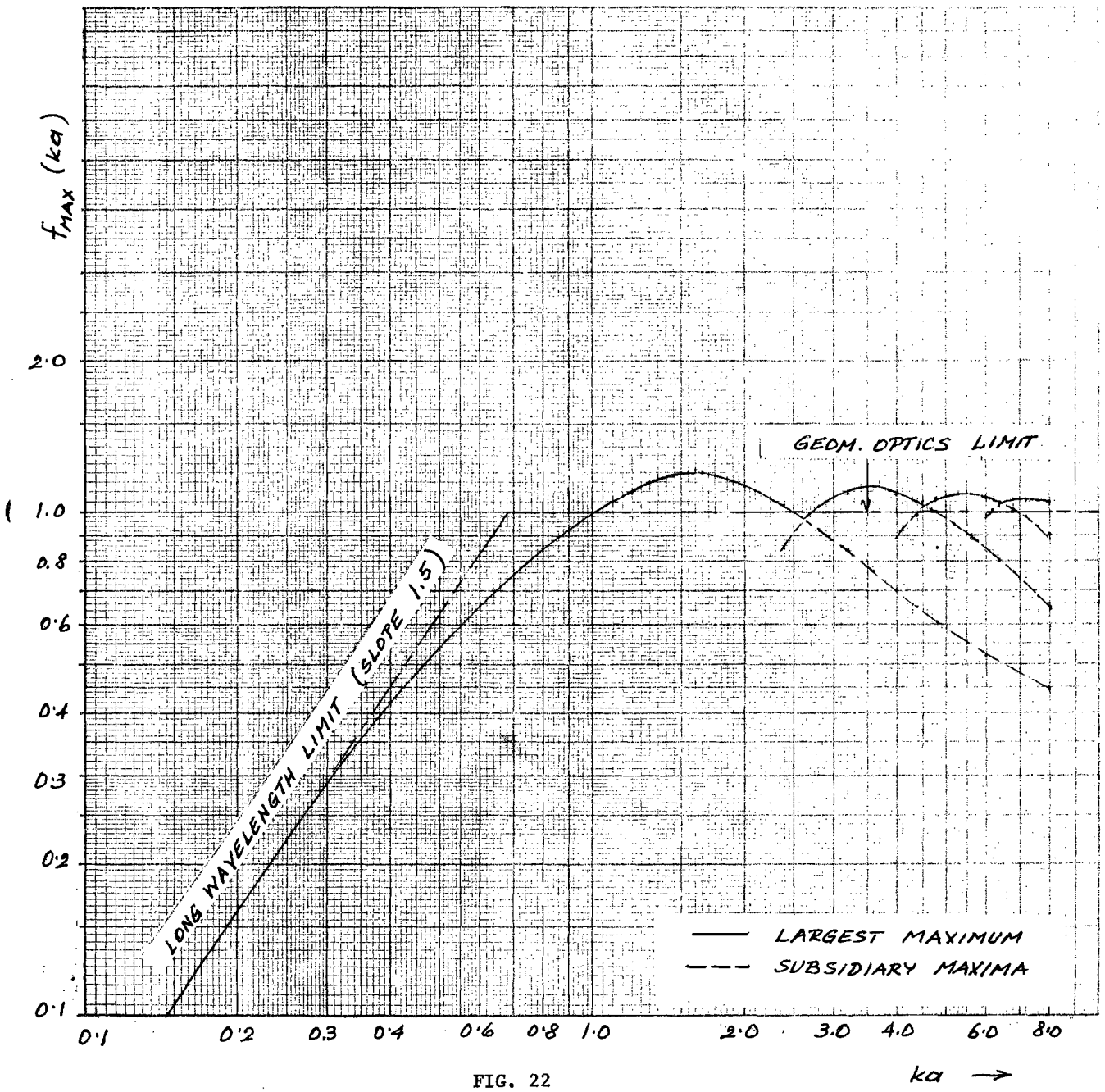

FIG. 22

PLOT OF f_{MAX}(ka)

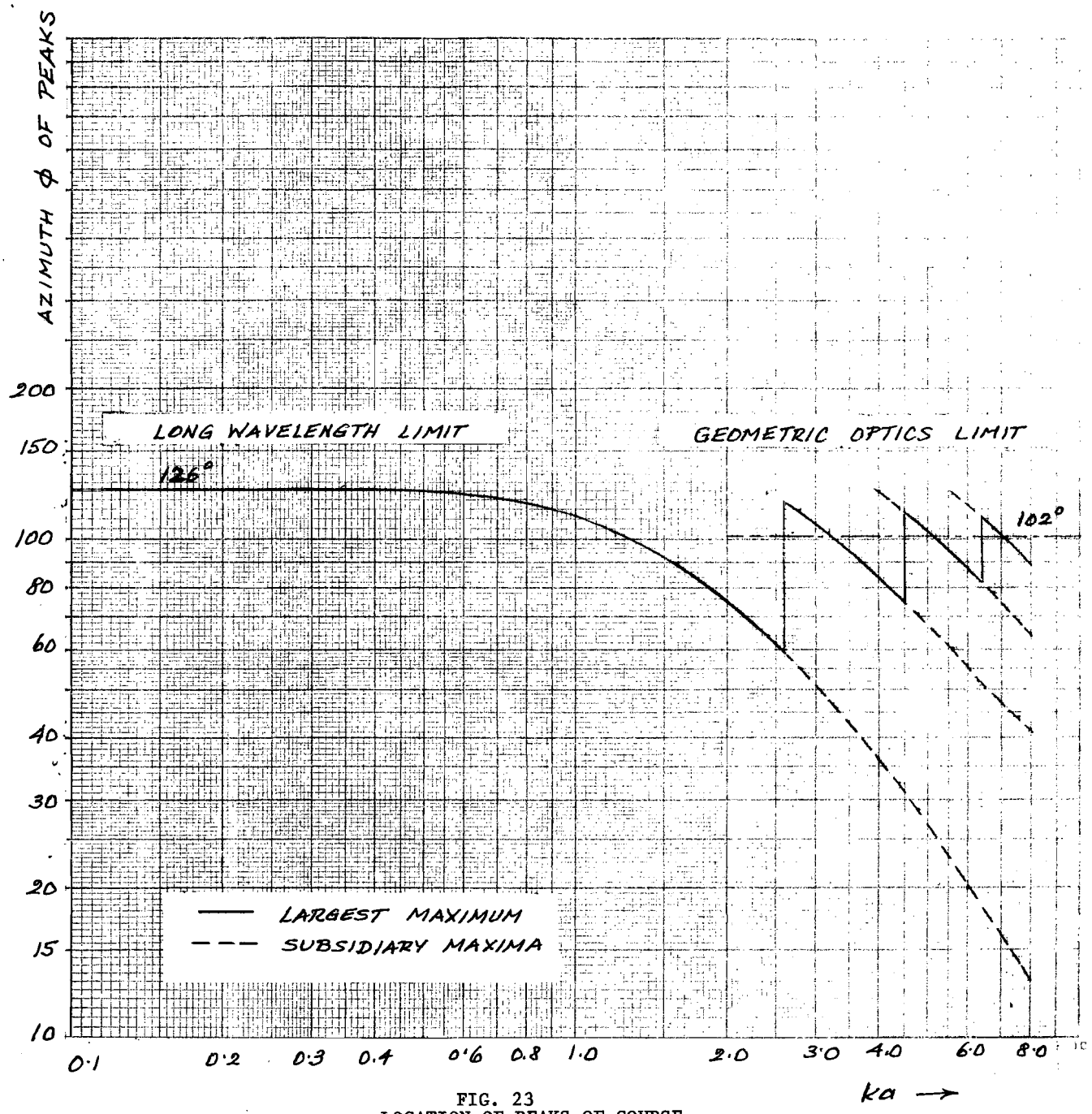

FIG. 23
LOCATION OF PEAKS OF COURSE
DEVIATION ENVELOPE

IV. EXPERIMENTAL RESULTS

4-1. Experiments with Wires

Analysis of old experiments were reported on both in last year's Final Report [1] and also in an Interim Engineering Report [3] and comparisons were made with theory. Unfortunately, not all important parameters were recorded in these experiments which date back twenty years or more. In some cases it was possible to ascertain what these parameters were by talking to the original experimenters. In other cases, reasonable estimates were possible. On the whole these experiments show good agreement with the theory developed under this contract over the last two years.

Nevertheless, it was decided to carry out some new experiments with straight wires and one bent-wire configuration to check theoretical predictions that previously had not been carefully tested. The experiments were performed by E. Lind at NAFEC near Atlantic City, N.J. during June and July 1975. The procedure followed was essentially that described in reference [7] except that peak course deviation errors were not averaged over 10-degree intervals. The test site is not ideal. While the ground is cleared of all trees and underbrush to a radius of 500 feet from the VOR and is essentially free of trees up to a radius of 1000 feet, there are a number of scattering objects at distances varying between 1000 feet and 2500 feet and beyond. There are power and telephone lines as close as 1000 feet to the VOR site and radar stations and other structures about 2000 feet away. These produce background scalloping errors which are as high as $\pm$ 1 degree in some azimuthal directions. To minimize errors due to this "background noise," the following precautions were taken:

1. The test scatterers were placed close enough to the VOR and high enough above ground to produce maximum course deviation errors of at least $\pm$ 3 degrees. By placing the scatterers close to the VOR the scalloping frequency was kept low, about 0.06 Hz or less, so that the aircraft receivers were working near peak sensitivity.

2. The scatterers were placed at such azimuthal positions to make the maximum course deviation errors fall in angular sectors where the background errors were small or non-existent.

3. The aircraft was made to circle the VOR site at a comparatively large radius, about 25 nautical miles. Since the aircraft speed was of the order of 190 knots this made the scalloping frequency of the more distant background scatterers high enough (0.6 Hz and more) to cut down the background errors. The half-amplitude points of the aircraft receivers used were near 0.35 Hz.

The aircraft was directed into circular orbits by radar control from the ground. Tests were conducted at aircraft altitudes of 1500, 3000 and 6000 feet. Since the results of the experiments did not change appreciably with altitude only the results for 3000 feet are reported here. It should be noted in passing that this observation in itself confirms one of the predictions of the theory for low aircraft elevation angles.

Signals from the VOR were recorded continuously and simultaneously by two receivers (Bendix and Collins) in the aircraft. The two receivers had nearly the same frequency characteristics. They were calibrated on the ground before each flight. While their outputs during flight tests were nearly identical in most cases they occasionally showed differences as high as one degree. In these cases the average was recorded. It is

believed that in most cases the measured peak deviation errors are accurate to about $\pm$ 10 percent.

In all wire experiments, number 6 copper wires (0.162 inch diameter) were used. They were kept from sagging and held in a horizontal position by rope supports. In experiments with two wires, the wires were kept at the desired separation by wooden spacers. They were stretched between two cross bars and could be moved up and down the supporting poles by pulleys. The nominal plan view of the pole locations is shown in Fig. 24. Single and double wire experiments were carried out with the wire(s) stretched between poles P1 and P2. The perpendicular distance from the VOR antenna to the wire axis was nominally 200 feet. A survey after the poles were installed showed that this distance was actually a little large so a value of D = 205 feet is used in computations. With this value of D, the angle ϕ measured from the wire axis is related to the magnetic azimuth by

$$\phi = 124° - \text{azimuth angle}.$$

Experiment 1:

This involved a single wire between poles P1 and P2 at a height of 28.5 feet above the ground. The ground level at the location of the poles was found to be 2.7 feet below the ground level at the VOR site. In the theoretical formulas a wire height of $h_1 = 28.5 - 2.7 = 25.8$ feet was therefore used. For an infinitely long wire at this height and at a normal distance of D = 205 feet from the VOR we get a peak course deviation error of 3.65° both from Fig. 6 and by interpolation in the table of Fig. 5. Since these charts are prepared for zero gauge wires, we

obtain a correction factor 0.88 for No. 6 wire from Fig. 3. A further small correction is needed since the VOR frequency in the experiments was 109 MHz rather than the 115 MHz used in obtaining the charts. This leads to a corrected peak error for an infinite wire of

$$3.65 \times 0.88 \times (109/115)^{1/2} = 3.13°$$

The same result can also be obtained by the use of Eq. (6) of Chapter II. For $h_1/D = 25.8/205 = 0.126$ one obtains from Fig. 2 that $H_{max} = 16.2$ and the peak should occur at $\phi = \phi_{max} = 48°$. The correction factor for the wire diameter is again $F(2a) = 0.88$. The correction factor $G(kh_1\varepsilon)/G(kh_0\varepsilon)$ can be obtained from Fig. 4. Using $k = 0.696\ ft^{-1}$, $h_1 = 25.8$, $h_0 = 16$ and ε = aircraft altitude/aircraft range we get 0.993, 0.990 and 0.95, respectively, for aircraft altitudes of 1500, 3000 and 6000 feet respectively. Hence:

$$(B-\phi)^{o}_{max} = H_{max} \frac{h_1^2}{D^{3/2}} \left(\frac{f}{f_0}\right)^{1/2} \frac{G(kh_1\varepsilon)}{G(kh_0\varepsilon)} F(2a)$$

$$= 16.2 \frac{25.8^2}{205^{3/2}} \left(\frac{109}{115}\right)^{1/2} \times 0.99 \times 0.88 = 3.12°$$

To this we must still apply a receiver reduction factor based on the scalloping frequency. This factor is about 0.966 for a receiver half width of 3.35 Hz, an aircraft speed of 190 knots at a range of 25 nautical miles. Hence the expected peak errors for an infinite wire would be 3.0° at azimuthal angles of $\phi = \pm 48°$ and $\pm 132°$.

For the 100-foot wire we expect the scalloping envelope to be confined between the critical angles of 38.6° and 53.8° (as well as between -38.6° and -53.8°). Hence we can only expect two maxima near

$$360 \frac{h_1}{D} \frac{\Delta h}{\lambda} = 5 \ \Delta h \text{ degrees}$$

This is equal to 5, 10 and 15 degrees, respectively, for the three spacings leading to array factors of 1.996, 1.985 and 1.966. Using the theoretical single-wire result from the first experiment these lead to expected peak scalloping values of 7.47, 7.42 and 7.35 degrees, respectively. The experimental results are 4.6, 4.8 and 5.5 degrees, down 38, 35 and 25 percent from the expected values. This seems to indicate that mutual effects are of some importance, especially for small spacings, if precise predictions are needed. For crude estimates this refinement may not be required.

As far as the shape of the scalloping error envelope is concerned the theory predicts that the envelope should be the same as that for a single wire with peaks at $\phi = \pm 46.4°$. The experiments confirm this. The scalloping ripple spacing is also the same as that for a single wire.

Experiment 3

This involved two parallel No. 6 gauge wires stretched between poles P1 and P2, both at the same height of 25.8 feet with horizontal spacings of 31 and 43 inches, respectively. The purpose was to check cancellation effects predicted by the theory. If d is the horizontal spacing between the two wires and mutual effects can be neglected the theory predicts that the course deviation envelope for the double wire can be obtained from that of the single wire by multiplication by the array factor

$$2\left|\cos\left[\frac{1}{2} kd(1 + \sin \phi)\right]\right|$$

The result of multiplying the theoretical single-wire curve by this factor is shown in Fig. 26 for two wire spacings. Experimental points are also shown.

The experimental results show a rather wide scatter and the detailed agreement with theory is not too good. However some basic predictions of the theory are verified: For the 31-inch spacing the scalloping error is substantially reduced with about zero error in the azimuthal range near $\phi = 48°$. The measured course deviation errors on either side of $\phi = 48°$ exceeds the theoretical prediction by about 0.6°. This discrepance is not much larger than the expected measurement error.

For the 43-inch spacing, both theory and experiment predict a peak error near $\phi = 47°$. However the theoretical prediction for the peak error is 4° while the experiments give about 2°. As in experiment 2, these amplitude discrepancies may be due to mutual coupling effects.

Experiment 4

In this case one No. 6 gauge wire was stretched between the three poles P1, P2, and P3 to form an equilateral triangle. All wires were at an effective height of 25.8 feet above the ground plane at the VOR site. In this case there is very little mutual coupling between the wires. Furthermore, each side of the triangle produces course errors in a different and very narrow azimuthal sector. Hence the scalloping pattern can be computed by considering each side separately.

The wire between P1 and P2 has already been discussed in connection with experiment 1. It should give rise to a course deviation error in the narrow sector between $\phi = 38°$ and $\phi = 54°$ with a peak of 3.74° near $\phi = 46°$. Two consecutive aircraft runs at 3000 feet altitude do indeed give peak errors of 3.4° and 3.6°, respectively, near $\phi = 47°$.

To obtain a theoretical estimate for the wire between P2 and P3 we must first determine the perpendicular distance from the VOR and the new

lateral offsets for the wire ends. By simple geometrical considerations from Fig. 24 (with D corrected to 205 ft) one obtains:

$$D' = 319 \text{ ft}, \ \ell_1' = 52.5 \text{ ft}, \ \ \ell_2' = 152.5 \text{ ft}$$

Let us first estimate the peak course error we could expect from a wire of infinite length at a perpendicular distance of 319 ft from the VOR and a height of 25.8 ft. By interpolation from Fig. 7 we get about 2° for zero gauge wire. With the correction factor of 0.88 from Fig. 3 for No. 6 wire this reduces to about 1.8°. A more accurate result can be obtained using Eq. (6) of Chapter II. From Fig. 2 we find for $h_1/D = 25.8/319 = 0.081$ that $H_{max} = 18.4$ and $\phi_{max} = 50.8°$. Hence an infinite wire would give a static peak error of

$$(B-\phi)^{o}_{max} = 18.4 \frac{25.8^2}{319^{3/2}} \times \left(\frac{109}{11.5}\right)^{1/2} \times 0.88 = 1.82°$$

near $\phi' = 51°$.

To obtain an estimate for the finite wire we compute the critical angles

$$\phi'_{c1} = \cot^{-1}\left(\frac{52.5}{319}\right) = 80.6°, \ \phi'_{c2} = \cot^{-1}\left(\frac{152.5}{319}\right) = 64.4°$$

We therefore should expect a peak error near $\phi' = 72.5°$. At this point the infinite-wire error pattern is down from its peak. The reduction can be estimated from the $h_1/D = 0.10$ curve of Fig. 1. At $\phi = 72.5°$ the error is down to 60 percent of the peak value. However, we also know that the finite wire usually has about a 30% overshoot compared to the infinite wire. Furthermore, there will be a small reduction because of the receiver response introducing another factor of about 0.96. Taking all these factors into consideration we obtain for the peak error

$$1.82 \times 0.60 \times 1.20 \times 0.98 = 1.28°$$

Essentially the same result is obtained directly from both computer programs for wires: based on the analytical formula and based on the moment method. To compare with experiment we still have to relate ϕ' to ϕ and the magnetic aximuth. From Fig. 24 we see that $\phi = 240 - \phi'$. Hence the course deviation error should have a peak of 1.28° at $\phi = 167.5°$ and should fall off to about half this value near $\phi = 159.4°$ and $\phi = 175.6°$. The experiments show a peak of 1.3° at $\phi = 167°$ in excellent agreement with theory.

The third side of the wire, P1 to P3, is almost radially out from the VOR. The perpendicular distance of this side from the VOR is too small to expect an accurate prediction from the analytical formulas. However, this is not serious because the course error produced by this side will be small anyway. It should occur in a narrow azimuthal sector with a maximum at $\phi = 1675 + 120 = 287.5°$. The experiments do show a peak error of about 0.7° in the azimuthal range from $\phi = 285°$ to $\phi = 295°$.

In summary we can say that there is excellent agreement between theory and experiment.

4-2. Experiments with Cylinders

These experiments involved a cylindrical scatterer of 9 feet diameter and a height of 9 feet. The cylinder surface was wire mesh. No mesh was put on the top and bottom surfaces. This was an oversight that was not discovered until after the completion of the tests. The moment-method calculations assumed conducting surfaces on top and bottom as well on the curved sides.

The cylinder was located with its axis 150 feet from the VOR and at an azimuth of 240°. Measurements were made with the mean height of the cylinder at 20 and 30 feet, respectively. Aircraft range, altitude and speed were the same as for the previous experiments.

In the notation of Fig. 11 we have

$2a = 9$ ft, $h = 9$ ft, $D = 150$ ft

For $\tilde{h} = 30$ ft, we have $h_1 = 25.5$ ft, $h_2 = 34.5$ ft

for $\tilde{h} = 20$ ft, we have $h_1 = 15.5$ ft, $h_2 = 24.5$ ft

Since the pattern is symmetrical about the line from the VOR to the cylinder axis, the angle ϕ is measured from azimuth 240° and theoretical results are only computed for the interval (0, 180°). Theoretical results were computed for mean cylinder heights of 15.5, 20, 25.5 and 30 feet both by the moment method and the theoretical formulas in Chapter III (Eqs. 51 and 61). Both methods were corrected for the effect of scalloping frequency.

Figures 27 and 28 show the moment-method results for the two cylinder heights used in the experiments. They show peaks at $\phi = 46°$ and $\phi = 118°$ (and, of course, at -46° and -118°). The theoretical formulas predict approximately the same double-peaked pattern with peak locations at $\phi = \pm 48°$ and $\pm 103°$ from Fig. 23 for ka = 3.13. Figure 15 shows a theoretical pattern for ka = 3.2 which is not too far off.

The experimental results show quite a bit of scatter but they show the same even symmetry and the general shape predicted by theory with peaks at approximately $\pm 50°$ and $\pm 110°$. Because the peaks are relatively broad this can be considered in good agreement with theory. The amplitudes of the peaks are of the same order of magnitude as those predicted by theory, but the agreement is not as good as in the case of wire scatterers. Table 5 gives a summary of the theoretical and measured amplitudes.

Table 5. Peak Course Deviation Errors in Degrees

Mean Cylinder Height	Moment Method		Formula		Measurements	
	$\phi = 46°$	$\phi = 118°$	$\phi = 48°$	$\phi = 103°$	$\phi = 50°$	$\phi = 110°$
30 ft	3.38	4.38	3.37	4.28	3.0	3.0
25.5 ft	2.72	3.48	3.25	4.13	not measured	
20 ft	1.87	2.36	2.85	3.62	3.0	3.0
15.5 ft	1.23	1.52	2.10	2.65	not measured	

From the table we come to the following conclusions:

(a) Both the moment-method and the analytical theory predict the general shape of the course deviation pattern and the location of the peaks correctly.

(b) The moment-method and the analytical formula predict that the second peak should be about 24 to 30 percent higher than the first peak with some dependence on the cylinder height. The experimental data appear to give approximately equal peaks.

(c) For a mean cylinder height of 30 feet, the peak course deviations computed from the moment method and the analytical formula are in excellent agreement but the measured peak values are too low by comparison: 11 and 30 percent down, respectively.

(d) The theoretical formula and the moment method give a somewhat different dependence on the mean height of the cylinder. This discrepancy has not yet been resolved. The experimental result at a mean height of 20 feet seem to favor the theoretical formula but the agreement is not perfect: about 5 and 20 percent errors for the two peaks.

There is a further point of close agreement between theory and experiment. Theory predicts a minimum scalloping ripple wavelength of

4. It is recommended that experiments be conducted with cylinders of larger diameters, heights, and with a greater variation in the other parameters: distanced from a VOR, mean height above ground, etc.

5. It is recommended that further theoretical work be done to examine the assumptions used in the deviation of the formulas and to put the results for cylinders of arbitrary height and diameter into a simplified tabulated and graphical form for inclusion in a future edition of the Siting Handbook.

6. It is recommeded that the unfinished work on scatters in the form of towers with rectangular cross sections, hangars, and other buildings be completed.

7. It is recommended that the remaining programs for Doppler VOR be completed.

8. Method of determining the combination of two reflected signals from two separated scatteres of different parameters and effect on course errors.

9. Work on scatterers to include double sideband DVOR.

10. Use of scale models for tests in lieu of flight tests where applicable.

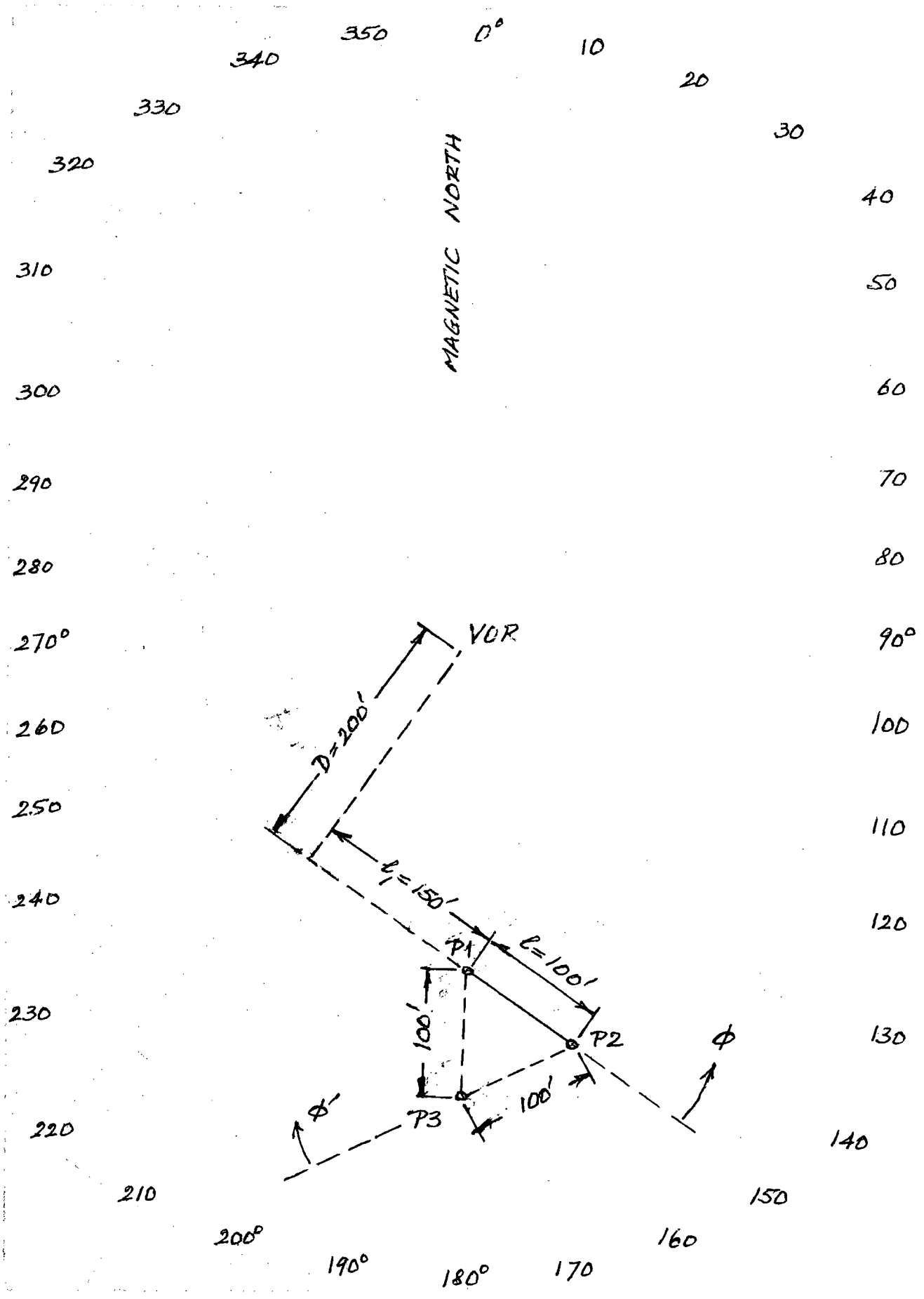

FIG. 24 PLAN VIEW OF EXPERIMENT

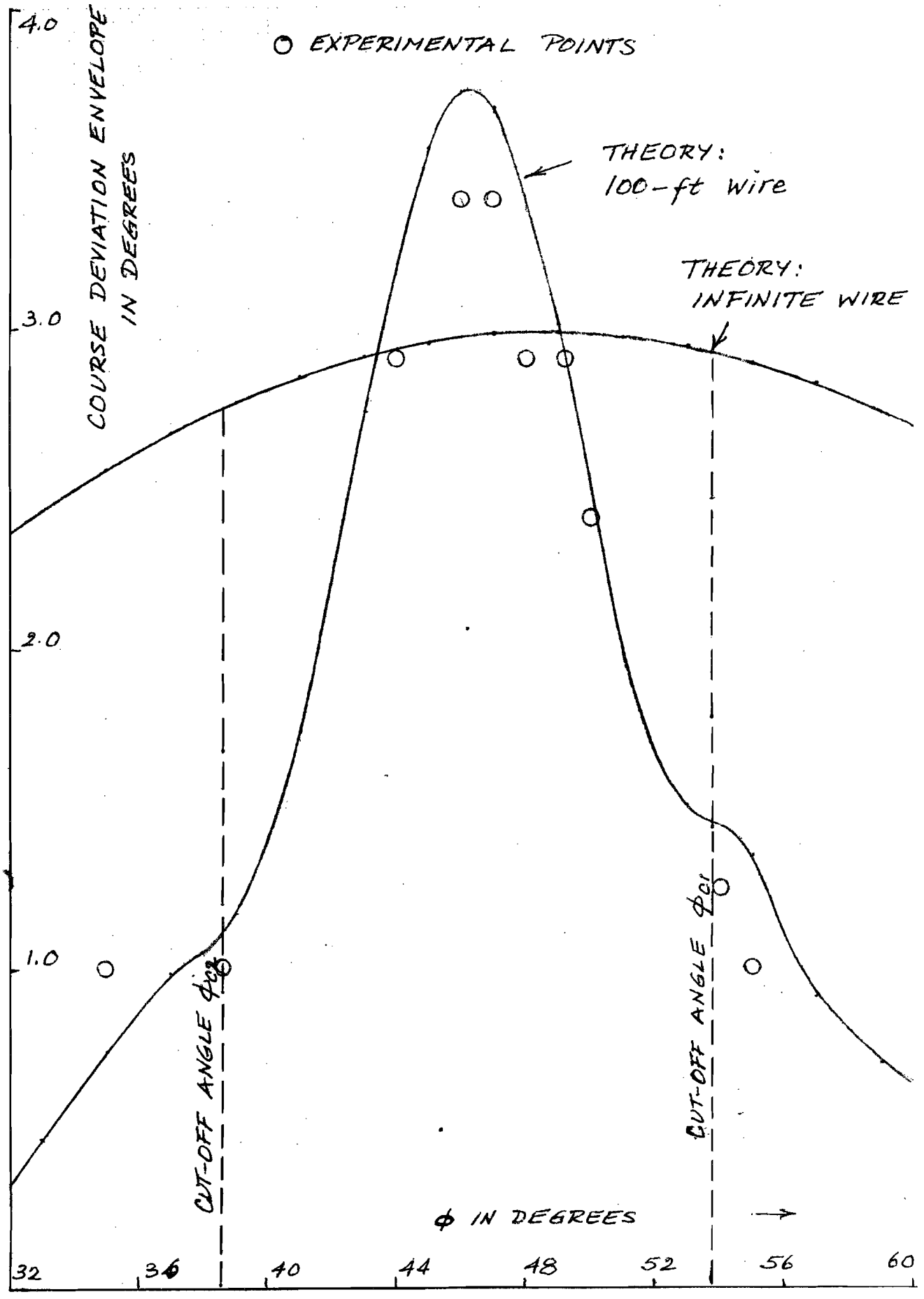

FIG. 25 SINGLE-WIRE EXPERIMENT

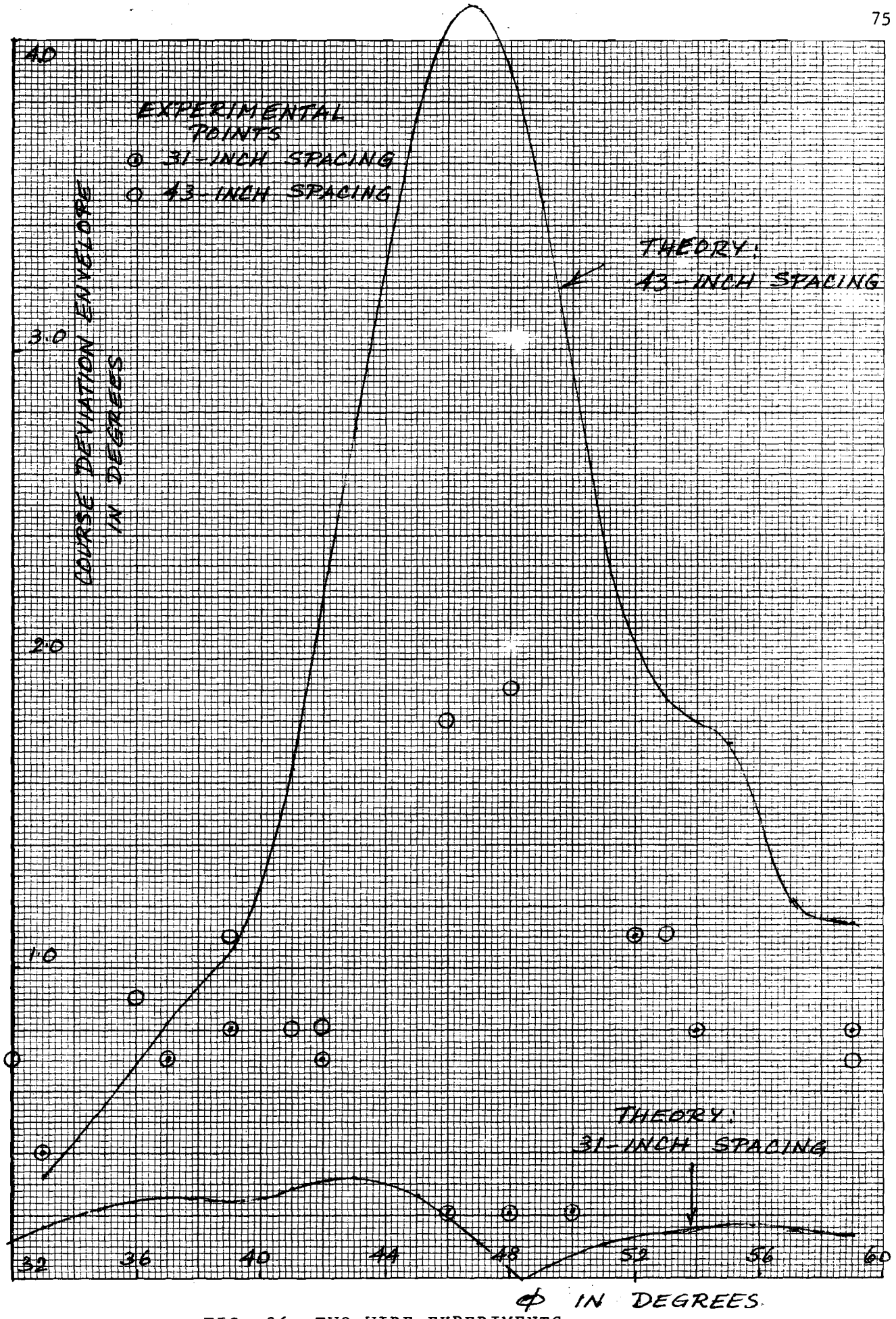

FIG. 26 TWO-WIRE EXPERIMENTS

46 1322
K+E 10 X 10 TO ½ INCH 7 X 10 INCHES KEUFFEL & ESSER CO. MADE IN U.S.A.

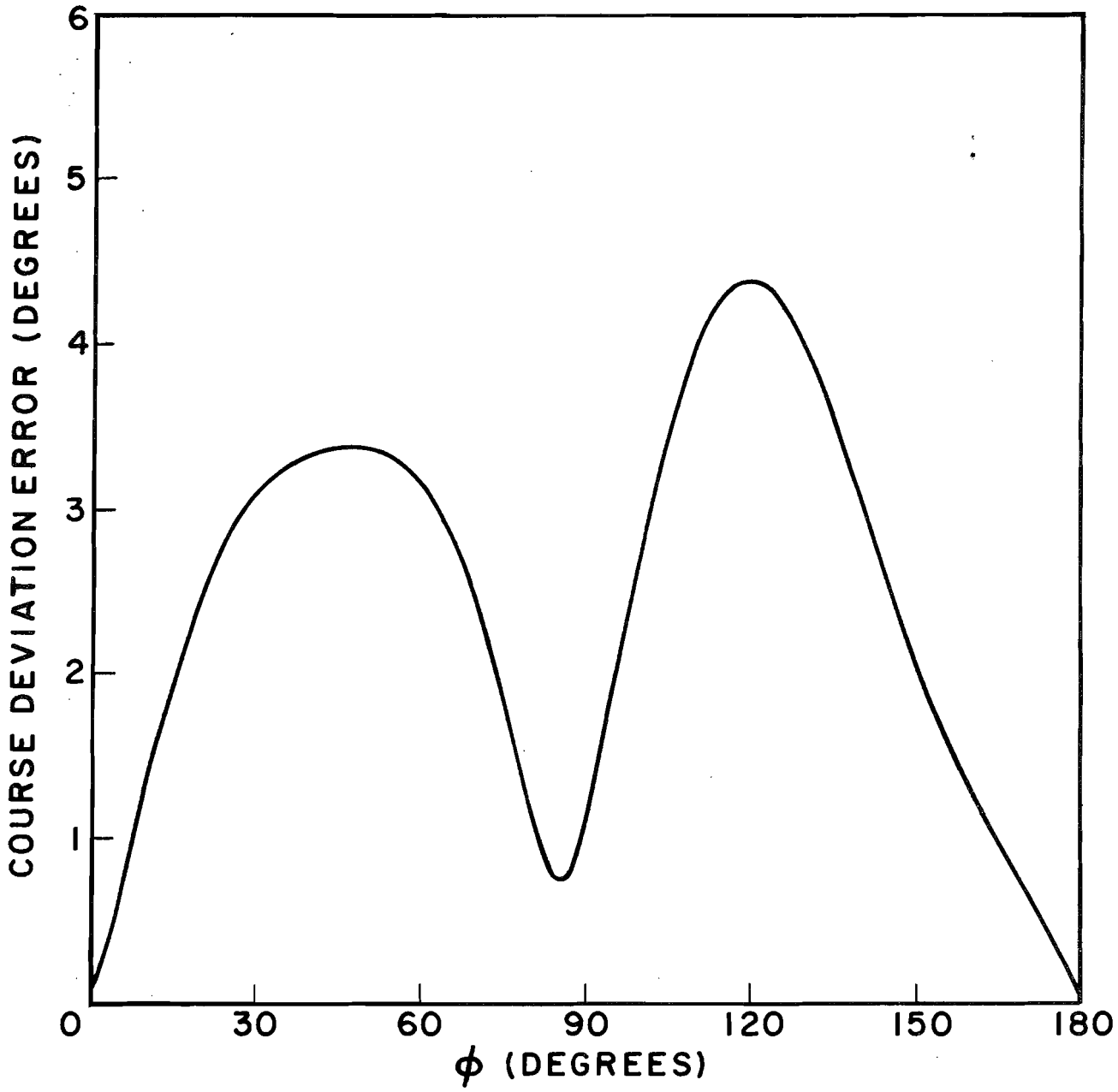

Fig. 27. Course Deviation Envelope for Cylinder Mean Height 30 feet.

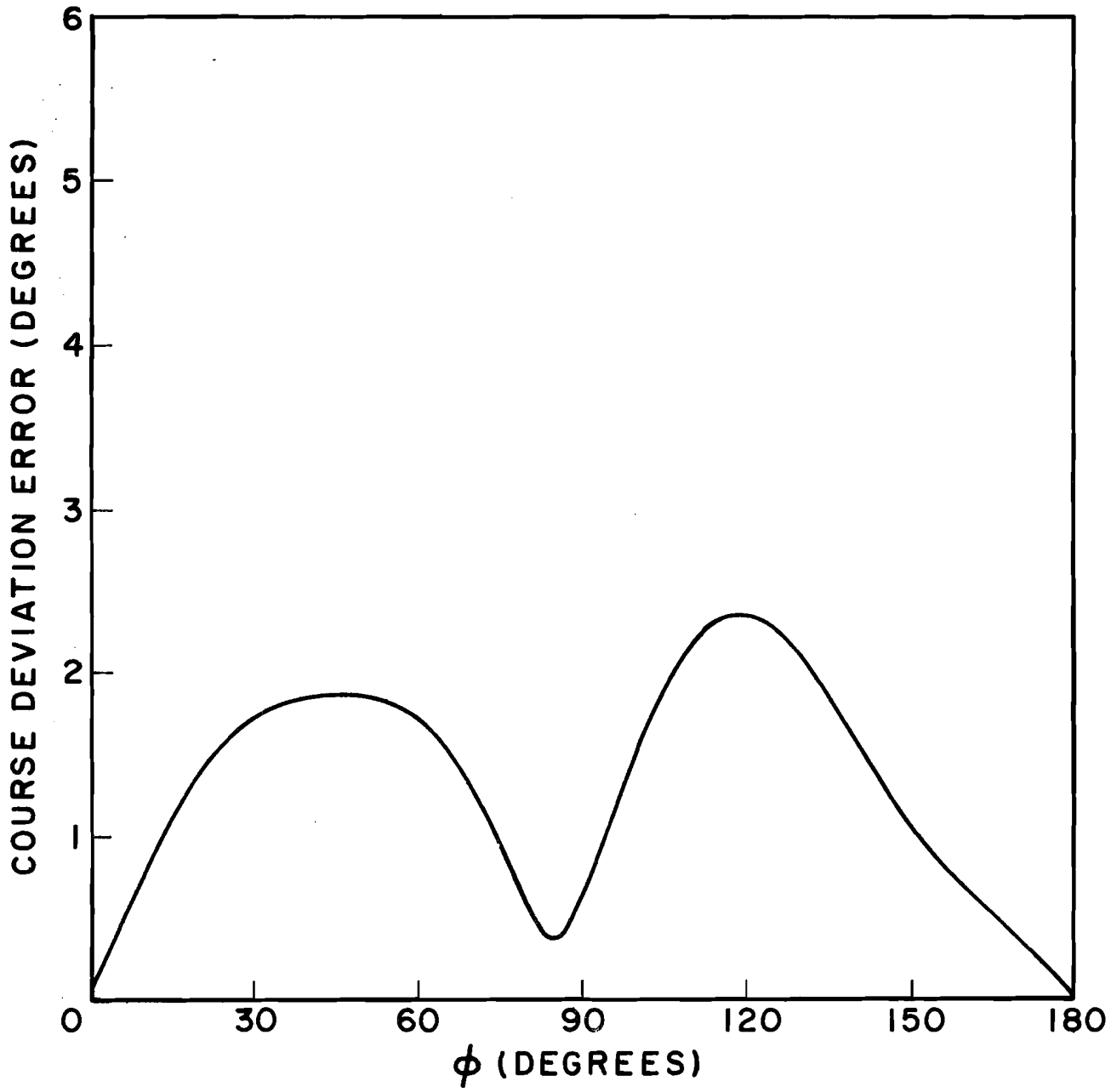

Fig. 28. Course Deviation Envelope for Cylinder Mean Height 20 feet.

APPENDIX A

This appendix gives a listing of a program for calculating course scalloping envelopes for thin-wire obstacles in the field of a conventional VOR. This program is a modification of the moment method program of Appendix D in the 1974 Final Report [1]. It should be used for comparatively short wires only. Compared to the old program, the listing here reduces the amount of computation and gives the scalloping envelope directly. In this manner a good picture of the course error curve is obtained even when comparatively large azimuthal increments are used.

Corrections for the presence of the counterpoise have also been included. This requires an additional card 6 with three inputs:

H = height of counterpoise above the ground in feet

SH = height of VOR loops above the counterpoise in feet

R = radius of the counterpoise in feet

The old card 7 remains card 7 and the old card 6 becomes card 8.

```
C     SUBROUTINE CALZ FOR PARALLEL WIRES OR A STRAIGHT WIRE
      SUBROUTINE CALZ(N,N1)
      COMPLEX          PSI(1120),U,U1,U2,U3,U4,U5,U6,Z( 79, 79)
      COMMON XX(280),XY(280),XZ(280),TX(280),TY(280),TZ(280),AL(280)
      COMMON T(560),TP(560),BK,RAD2(10),L(5),LR(10)
      COMMON /COB/Z
      DIMENSION DC(1120)
      U=(0.,1.)
      PI=3.141593
      ETA=376.7307
      C1=.125/PI
      C2=.25/PI
      J1=1
      J2=-2
      DO 1 J=1,N
      IF(L(J1)-J) 3,4,3
    4 J2=J2+2
      J1=J1+1
    3 J3=(J-1)*4
      J4=J3+1
      J5=J4+1
      J6=J5+1
      J7=J6+1
      K4=J2+1
      K5=K4+1
      K6=K5+1
      K7=K6+1
      S1=AL(K4)+AL(K5)
      S2=AL(K6)+AL(K7)
      T(J4)=AL(K4)*.5*AL(K4)/S1
      T(J5)=AL(K5)*(AL(K4)+.5*AL(K5))/S1
      T(J6)=AL(K6)*(AL(K7)+.5*AL(K6))/S2
      T(J7)=AL(K7)*.5*AL(K7)/S2
      TP(J4)=AL(K4)/S1
      TP(J5)=AL(K5)/S1
      TP(J6)=-AL(K6)/S2
      TP(J7)=-AL(K7)/S2
      J2=J2+2
    1 CONTINUE
      U3=U*BK*ETA
      U4=-U/BK*ETA
      BK2=BK*BK/2.
      BK3=BK2*BK/3.
      NO=1
      NW=J1-1
      DO 10 NS=1,NW
      L8=L(NS)
      N3=2*(L8+NS-2)
      DO 15 K=1 ,4
      N7=N3+K
      IF(N7-LR(NO)) 5,6,5
    6 AA=RAD2(NO)
      NO=NO+1
    5 CONTINUE
      K1=(K-1)*N1
      DO 16 NF= 1,N1
      N8=NF+K1
      S1=XX(N7)-XX(NF)
      S2=XY(N7)-XY(NF)
      S3=XZ(N7)-XZ(NF)
```

```
      R2=S1*S1+S2*S2+S3*S3+AA
      R=SQRT(R2)
      RT=ABS(S1*TX(N7)+S2*TY(N7)+S3*TZ(N7))
      RT2=RT*RT
      RH=(R2-RT2)
      ALP=.5*AL(N7)
      AR=ALP/R
      S1=BK*R
      U2=COS(S1)-U*SIN(S1)
      IF(AR-.1) 22,22,21
   21 U2=U2*C1/ALP
      S1=RT-ALP
      S2=RT+ALP
      S3=SQRT(S1*S1+RH)
      S4=SQRT(S2*S2+RH)
      IF(S1) 18,18,19
   18 AI1=ALOG((S2+S4)*(-S1+S3)/RH)
      GO TO 20
   19 AI1=ALOG((S2+S4)/(S1+S3))
   20 AI2=AL(N7)
      AI3=(S2*S4-S1*S3+RH*AI1)/2.
      AI4=AI2*(RH+ALP*ALP/3.+RT2)
      S3=AI1*R
      S1=AI1-BK2*(AI3-R*(2.*AI2-S3))
      S2=-BK*(AI2-S3)+BK3*(AI4-3.*AI3*R+R2*(3.*AI2-S3))
      GO TO 28
   22 U2=U2*C2/R
      BA=BK*ALP
      BA2=BA*BA
      AR2=AR*AR
      AR3=AR2*AR
      ZR=RT/R
      ZR2=ZR*ZR
      ZR3=ZR2*ZR
      ZR4=ZR3*ZR
      H1=(3.-30.*ZR2+35.*ZR4)*AR3/40.
      A1=AR*(-1.+3.*ZR2)/6.+(3.-30.*ZR2+35.*ZR4)*AR3/40.
      A0=1.+AR*A1
      A2=-ZR2/6.-AR2*(1.-12.*ZR2+15.*ZR4)/40.
      A3=AR*(3.*ZR2-5.*ZR4)/60.
      A4=ZR4/120.
      S1=A0+BA2*(A2+BA2*A4)
      S2=BA*(A1+BA2*A3)
   28 PSI(N8)=U2*(S1+U*S2)
      DC(N8)=TX(NF)*TX(N7)+TY(NF)*TY(N7)+TZ(NF)*TZ(N7)
   16 CONTINUE
   15 CONTINUE
      J3=(L8-1)*4
      J7=-2
      J9=1
      DO 25 NF=1,N
      J1=(NF-1)*4
      IF(L(J9)-NF) 26,27,26
   27 J9=J9+1
      J7=J7+2
   26 U5=0.
      U6=0.
      J5=0
      DO 23 JS=1,4
      J4=J3+JS
```

```
      J8=J5+J7
      DO 24 JF=1,4
      J6=J8+JF
      J2=J1+JF
      U5=T(J2)*T(J4)*DC(J6)*PSI(J6)+U5
      U6=TP(J2)*TP(J4)*PSI(J6)+U6
   24 CONTINUE
      J5=J5+N1
   23 CONTINUE
      Z(L8,NF)=U5*U3+U6*U4
      Z(NF,L8)=Z(L8,NF)
   30 J7=J7+2
   25 CONTINUE
   10 CONTINUE
      DO 65 I=1,NW
      L8=L(I)
      L7=I+1
      IF(L7.GT.NW) GO TO 50
      L6=L(L7)
      GO TO 55
   50 L6=N+1
   55 L5=L6-1
      DO 65 J=1,NW
      M8=L(J)
      M7=J+1
      IF(M7.GT.NW) GO TO 58
      M6=L(M7)
      GO TO 57
   58 M6=N+1
   57 M5=M6-1
      DO 65 K=L8,L5
      K1=K+1
      DO 60 M=M8,M5
      M1=M+1
      IF(M1.GT.M5.OR.K1.GT.L5) GO TO 60
      Z(K1,M1)=Z(K,M)
   60 CONTINUE
   65 CONTINUE
      RETURN
      END
C     SUBROUTINE ROW FOR WIRES PAPALLEL TO THE GROUNDPLANE (VOR)
      SUBROUTINE ROW(N,CT,ST,CP,SP,SX,E,III)
      COMPLEX C(3,139),E,U,U1,U2,U3,U4,U5,SX
      COMMON XX(280),XY(280),XZ(280),TX(280),TY(280),TZ(280),AL(280)
      COMMON T(560),TP(560),BK,RAD2(10),L(5),LR(10) /C04/C
      DIMENSION BKR(280),DP(280),BK5(5)
      U=(0.,1.)
      BK1=BK*ST*CP
      BK2=BK*ST*SP
      BK3=BK*CT
      N2=1
      N3=-2
      DO 1 NS=1,N
      IF (L(N2)-NS) 2,3,2
    3 KK=1
      N3=N3+2
      N2=N2+1
      BK5(N2)=BK3*XZ(NS)
      GO TO 4
    2 KK=3
```

```
    4 DO 5 K=KK,4
      N7=N3+K
      BKR(N7)=XX(N7)*BK1+XY(N7)*BK2
      DP(N7)=-TX(N7)*SP+TY(N7)*CP
    5 CONTINUE
      N3=N3+2
    1 CONTINUE
      N2=1
      N3=-2
      U3=0.
      U4=0.
      DO 6 NS=1,N
      IF (L(N2)-NS) 7,8,7
    8 N3=N3+2
      N2=N2+1
    7 J1=(NS-1)*4
      U1=0.
      U2=0.
      DO 9 JS=1,4
      J2=J1+JS
      J3=N3+JS
      S1=BKR(J3)
      U5=T(J2)*(COS(S1)+U*SIN(S1))
      U2=U2+U5*DP(J3)
    9 CONTINUE
      BK4=BK5(N2)
      U4=U4+U2*C(III,NS)*SIN(BK4)
      N3=N3+2
    6 CONTINUE
      E= SX*U4*            2.*U
      RETURN
      END
      SUBROUTINE LINEQ(N)
      SUBROUTINE INCF(BK,CT,SCP,ST,SSP,EX,EI,III,H,SH,R)
      COMPLEX  EX,EI(3),U1,SB
      U1=(0.,1.)
      SI=1.
      CI=1.
      CALL CTP(H,SH,CT,R,SB,BK)
      IF(III-2) 10,20,30
   10 EI(III)=-EX*SB*ST*CI
      GO TO 50
   20 EI(III)=EX*ST*SB*SSP*SI
      GO TO 50
   30 EI(III)=EX*ST*SB*SCP*SI
   50 RETURN
      END
      FUNCTION F(X)
      F=(1.+.926*X)/(2.+(1.792+3.104*X)*X)
      RETURN
      END
      FUNCTION G(X)
      G=1./(2.+(4.142+(3.492+6.670*X)*X)*X)
      RETURN
      END
      FUNCTION C(X)
      A=3.141593*X*X*.5
      C    =.5+F(X)*SIN(A)-G(X)*COS(A)
      RETURN
      END
```

```
      FUNCTION S(X)
      A=3.141593*X*X*.5
      S    =.5-F(X)*COS(A)-G(X)*SIN(A)
      RETURN
      END
      SUBROUTINE CTP(H,SH,E,R,SS,BK)
      COMPLEX SS,U,D
      U=(0.,1.)
      PI=3.141593
      AK=BK*.3048
      HO=SH+H
      R1=R*R+SH*SH
      RO=SQRT(R1)
      ANG=SH/R
      ALP=ATAN(ANG)
      A=AK*RO/PI
      SA=SQRT(A)
      PO=2.*SA*SIN(ALP*.5)
      D=2.*C(PO)+SH/H-U*(2.*S(PO)+SH/H)
    5 AL1=(ALP+E)*.5
      AL2=(ALP-E)*.5
      P1=2.*SA*SIN(AL1)
      P2=2.*SA*SIN(AL2)
      X=AK*H*SIN(E)
      Y=AK*SH*SIN(E)
      SX=SIN(X)
      SY=SIN(Y)
      SI=SX/X
      SJ=SY/Y
      CX=COS(X)
      CY=COS(Y)
      IF(P2) 30,35,35
   30 P2=-P2
      SP=-S(P2)
      CP=-C(P2)
      GO TO 38
   35 SP=S(P2)
      CP=C(P2)
   38 SS=COS(E)/D*(SH/H*SJ*CX+(C(P1)+CP    )*SI*CY+(S(P1)-SP    )*SI*SY-
     1U*(SH*SJ*CX/H+(S(P1)+SP    )*SI*CY-(C(P1)-CP)*SI*SY))*AK*HO*SIN(E)
      RETURN
      END
      COMPLEX Z( 79, 79),U
      COMMON /COB/Z
      U=(0.,1.)
      DO 400 I=1,N
      DO 400 J=I,N
      IF(I.EQ.1) GO TO 405
      IX=I-1
      DO 410 K=1,IX
  410 Z(I,J)=Z(I,J)-Z(I,K)*Z(K,J)
  405 CONTINUE
      IF(I.EQ.J) GO TO 400
      Z(J,I)=Z(I,J)
      A=REAL(Z(I,I))
      B=AIMAG(Z(I,I))
      ZM=A*A+B*B
      Z(I,J)=(Z(I,J)*(A-U*B))/ZM
  400 CONTINUE
      RETURN
```

```
      END
      COMPLEX EX,U2,SX,U(139),C(3,139),EI(3),UV(4),U1,EJ(3),EK(3),
     1Z( 79 ,79)
      COMMON XX(280),XY(280),XZ(280),TX(280),TY(280),TZ(280),AL(280)
      COMMON T(560),TP(560),BK,RAD2(10),L(5),LR(10) /COA/C
      COMMON /COB/Z
      DIMENSION PX(281),PY(281),PZ(281),LL(5),RAD(10),ER(721),ES(721)
      READ (1,101)          NW,NP,NR,FRM
  101 FORMAT (3I4,F7.2)
      WRITE (3,102) NW,NP,NR,FRM
  102 FORMAT('0 NW   NP   NR    FRM(MHZ)'/3I4,F10.2)
      ETA=376.7307
      BK=6.283184*FRM/300.
      DO 50 I=1,NP
      AI=I
      PX(I)=-200.*.3048
      PY(I)=(AI-1.)*.3048/160.*100.+150.*.3048
   50 PZ(I)=30.*.3048
      WRITE (3,104) (PX(I),I=1,NP)
      WRITE (3,105) (PY(I),I=1,NP)
      WRITE (3,106) (PZ(I),I=1,NP)
  104 FORMAT ('0PX'/(1X,10F10.4))
  105 FORMAT ('0PY'/(1X,10F10.4))
  106 FORMAT ('0PZ'/(1X,10F10.4))
      READ (1,107) (LL(I),I=1,NW)
  107 FORMAT (20I4)
      WRITE (3,108) (LL(I),I=1,NW)
  108 FORMAT ('0LL'/(1X,10I4))
      READ (1,107) (LR(I),I=1,NR)
      WRITE (3,103) (LR(I),I=1,NR)
  103 FORMAT ('0LR'/(1X,10I4))
      LR(NR+1)=410
      LL(NW+1)=410
      READ (1,109) (RAD(I),I=1,NR)
  109 FORMAT (5E14.7)
      WRITE (3,110)(RAD(I),I=1,NR)
  110 FORMAT ('0RAD'/(1X,8E14.7))
      READ(1,125) HS,DIT
  125 FORMAT(F10.1,F10.2)
      WRITE(3,121) HS,DIT
  121 FORMAT('0HEIGHT:',F7.1 ,' FEET,    DISTANCE:',F6.2 ,' MILE')
      READ(1,140) H,SH,R
  140 FORMAT(3F10.2)
      WRITE(3,145) H,SH,R
  145 FORMAT(' H=',F7.2,' SH=',F7.2,' R=',F7.2,' IN FEET')
      DO 46 I=1,NR
      RAD2(I)=RAD(I)*RAD(I)
   46 CONTINUE
      J1=1
      J2=2
      N1=0
      DO 2 J=1,NP
      IF (LL(J1)-J) 3,4,3
    4 J2=J2-1
      L(J1)=J2
      J1=J1+1
      GO TO 2
    3 N1=N1+1
      J3=J-1
      IF((N1/2*2-N1).EQ.0)  J2=J2+1
```

```
      XX(N1)=.5*(PX(J)+PX(J3))
      XY(N1)=.5*(PY(J)+PY(J3))
      XZ(N1)=.5*(PZ(J)+PZ(J3))
      S1=PX(J)-PX(J3)
      S2=PY(J)-PY(J3)
      S3=PZ(J)-PZ(J3)
      S4=SQRT(S1*S1+S2*S2+S3*S3)
      TX(N1)=S1/S4
      TY(N1)=S2/S4
      TZ(N1)=S3/S4
      AL(N1)=S4
    2 CONTINUE
      L(J1)=J2
      N=J2-2
      CALL CALZ (N,N1)
      READ (1,107) NL
      IF (NL) 42,42,41
   41 WRITE (3,118) NL
  118 FORMAT ('ONL'/I3/'OLP                    LOAD')
      DO 43 I=1,NL
      READ (1,119) LP,ZL
  119 FORMAT (I4,2E13.6)
      WRITE (3,120) LP,ZL
  120 FORMAT (I4,5X,2E13.6)
      Z(LP,LP)=Z(LP,LP)+ZL
   43 CONTINUE
   42 CALL LINEQ(N)
      U1=(0.,1.)
      S=16.*.0254
      DO 26 III=2,3
      J1=1
      J2=-2
      DO 27 J=1,N
      IF (L(J1)-J) 29,28,29
   28 J2=J2+2
      J1=J1+1
      KK=1
      GO TO 30
   29 UV(1)=UV(3)
      UV(2)=UV(4)
      KK=3
   30 DO 31 M=KK,4
      J3=J2+M
      AX=XZ(J3)
      BB=XX(J3)*XX(J3)+XY(J3)*XY(J3)
      BD=SQRT(BB)
      DD=SQRT(AX**2+BB)
      CT=AX/DD
      ST=BD/DD
      SP=XY(J3)/BD
      CP=XX(J3)/BD
      XDP=-TX(J3)*SP+TY(J3)*CP
      R=SQRT(BB+AX*AX)
      SPT=BK*S*SP*ST
      CPT=BK*S*CP*ST
      SSP=SIN(SPT)
      SCP=SIN(CPT)
      SU=-BK*R
      EX=(COS(SU)+U1*SIN(SU))/R
      CALL INCF(BK,CT,SSP,ST,SCP,EX,EI,III,H,SH,R)
```

```
      UV(M)=-XDP*EI(IIT)
   31 CONTINUE
      J3=(J-1)*4
      J4=J3+1
      J5=J4+1
      J6=J5+1
      J7=J6+1
      U(J)=T(J4)*UV(1)+T(J5)*UV(2)+T(J6)*UV(3)+T(J7)*UV(4)
      J2=J2+2
   27 CONTINUE
      DO 415 I=1,N
      IF(I.EQ.1) GO TO 420
      IX=I-1
      DO 425 J=1,IX
  425 U(I)=U(I)-Z(I,J)*U(J)
  420 CONTINUE
      A=REAL(Z(I,I))
      B=AIMAG(Z(I,I))
      ZM=A*A+B*B
  415 U(I)=(U(I)*(A-U1*B))/ZM
      DO 430 I=2,N
      II=N+1-I
      IY=II+1
      DO 430 J=IY,N
  430 U(II)=U(II)-Z(II,J)*U(J)
      DO 9 I=1,N
      C(III,I)=U(I)
    9 CONTINUE
   26 CONTINUE
      DIS=DIT*1609.344
      HT=HS*.3048
      TH=ATAN2(DIS,HT)
      THE=TH*57.29578
      SX= .0795774    *ETA*BK*U1
      CT=COS(TH)
      ST=SIN(TH)
    1 READ(1,137,END=500) SPH,EPH,AINC
  137 FORMAT(3F10.2)
      WRITE(3,138) SPH,EPH,AINC
  138 FORMAT('0START PHI=',F7.2,' END PHI=',F7.2,' INCREMENT=',F7.2,
     1'    (DEGREE)')
      IF(AINC.LE.0.) GO TO 450
      WRITE(3,600)
  600 FORMAT('0     PHI        ERROR        (DEGREE)')
      PHI=SPH
      IQ=0
      HH=(H+SH)*.3048
      A=BK*(3.141593*.5-TH)
      S2=SIN(A*HH)
   90 PH=PHI*.0174533
      SP=SIN(PH)
      CP=COS(PH)
      DO 96 III=2,3
      CALL POW(N,CT,ST,SP,CP,SX,U2,III)
      EI(III)=U2
   96 CONTINUE
      E1=REAL(EI(2))
      E2=AIMAG(EI(2))
      E3=REAL(EI(3))
      E4=AIMAG(EI(3))
```

```
      EK2=SQRT(E1*E1+E2*E2)
      EK3=SQRT(E3*E3+E4*E4)
      E5=EK2*CP
      E6=EK3*SP
      EP1=0.
      IF(EK2.EQ.0.) GO TO 32
      EP1=ATAN2(E2,E1)
   32 EP2=0.
      IF(EK3.EQ.0.) GO TO 33
      EP2=ATAN2(E4,E3)
   33 EE=E5*E5+E6*E6-2.*EK2*EK3*CP*SP*COS(EP1-EP2)
      EW=SQRT(EE)
      ER2=90.*EW/(3.141593*ABS(S2)*.433)
      ER2=ABS(ER2)
      IF(ER2.LT.-270.) ER2=ER2+360.
      IF(ER2.GT.270.) ER2=ER2-360.
      IF(ER2.GE.-270..AND.ER2.LT.-90.) ER2=ER2+180.
      IF(ER2.LE.270..AND.ER2.GT.90.) ER2=ER2-180.
      WRITE(3,98) PHI,ER2
   98 FORMAT(F9.2,F10.3)
      IQ=IQ+1
      ES(IQ)=PHI
      ER(IQ)=ER2
      PHI=PHI+AINC
      IF(PHI.LE.EPH.AND.PHI.GT.SPH) GO TO 90
      PUNCH 400,IQ,(ES(I),I=1,IQ)
      PUNCH 410,(ER(I),I=1,IQ)
  400 FORMAT(I5,(10F7.2))
  410 FORMAT(10F8.3)
      GO TO 1
  450 WRITE(3,460)
  460 FORMAT('0**ERROR** THE INCREMENT OF PHI IS NOT POSITIVE')
  500 STOP
      END
 1 161   1 115.
 1  22  43  64
 1
 .00206
3000.       25.
 12.        4.        26.
 0
 0.       360.        2.
```

```
C     SUBROUTINE CALZ FOR ARBITRARY WIRES
      SUBROUTINE CALZ(N,N1)
      COMPLEX          PSI( 400),U,U1,U2,U3,U4,U5,U6,Z(40,40)
      COMMON XX(280),XY(280),XZ(280),TX(280),TY(280),TZ(280),AL(280)
      COMMON T(560),TP(560),BK,RAD2(10),L(5),LR(10)
      COMMON /COB/Z
      DIMENSION DC(400)
      U=(0.,1.)
      PI=3.141593
      ETA=376.7307
      C1=.125/PI
      C2=.25/PI
      J1=1
      J2=-2
      DO 1 J=1,N
      IF(L(J1)-J) 3,4,3
    4 J2=J2+2
      J1=J1+1
    3 J3=(J-1)*4
      J4=J3+1
      J5=J4+1
      J6=J5+1
      J7=J6+1
      K4=J2+1
      K5=K4+1
      K6=K5+1
      K7=K6+1
      S1=AL(K4)+AL(K5)
      S2=AL(K6)+AL(K7)
      T(J4)=AL(K4)*.5*AL(K4)/S1
      T(J5)=AL(K5)*(AL(K4)+.5*AL(K5))/S1
      T(J6)=AL(K6)*(AL(K7)+.5*AL(K6))/S2
      T(J7)=AL(K7)*.5*AL(K7)/S2
      TP(J4)=AL(K4)/S1
      TP(J5)=AL(K5)/S1
      TP(J6)=-AL(K6)/S2
      TP(J7)=-AL(K7)/S2
      J2=J2+2
    1 CONTINUE
      U3=U*BK*ETA
      U4=-U/BK*ETA
      BK2=BK*BK/2.
      BK3=BK2*BK/3.
      N9=0
      N2=1
      N3=1
      N3=-2
      DO 10 NS=1,N
      IF(L(N2)-NS) 12,11,12
   11 KK=1
      N3=N3+2
      N2=N2+1
      GO TO 13
   12 KK=3
      DO 14 NF=1,N1
      N4=NF+N1
      N5=N4+N1
      N6=N5+N1
      DC(NF)=DC(N5)
      DC(N4)=DC(N6)
```

```
      PSI(NF)=PSI(N5)
      PSI(N4)=PSI(N6)
   14 CONTINUE
   13 CONTINUE
      DO 15 K=KK,4
      N7=N3+K
      IF(N7-LR(NO)) 5,6,5
    6 AA=RAD2(NO)
      NO=NO+1
    5 CONTINUE
      K1=(K-1)*N1
      NX=(NS-1)*2+1
      DO 16 NF=NX,N1
      N8=NF+K1
      S1=XX(N7)-XX(NF)
      S2=XY(N7)-XY(NF)
      S3=XZ(N7)-XZ(NF)
      R2=S1*S1+S2*S2+S3*S3+AA
      R=SQRT(R2)
      RT=ABS(S1*TX(N7)+S2*TY(N7)+S3*TZ(N7))
      RT2=RT*RT
      RH=(R2-RT2)
      ALP=.5*AL(N7)
      AR=ALP/R
      S1=BK*R
      U2=COS(S1)-U*SIN(S1)
      IF(AR-.1) 22,22,21
   21 U2=U2*C1/ALP
      S1=RT-ALP
      S2=RT+ALP
      S3=SQRT(S1*S1+RH)
      S4=SQRT(S2*S2+RH)
      IF(S1) 18,18,19
   18 AI1=ALOG((S2+S4)*(-S1+S3)/RH)
      GO TO 20
   19 AI1=ALOG((S2+S4)/(S1+S3))
   20 AI2=AL(N7)
      AI3=(S2*S4-S1*S3+RH*AI1)/2.
      AI4=AI2*(RH+ALP*ALP/3.+RT2)
      S3=AI1*R
      S1=AI1-BK2*(AI3-R*(2.*AI2-S3))
      S2=-BK*(AI2-S3)+BK3*(AI4-3.*AI3*R+R2*(3.*AI2-S3))
      GO TO 28
   22 U2=U2*C2/R
      BA=BK*ALP
      BA2=BA*BA
      AR2=AR*AR
      AR3=AR2*AR
      ZR=RT/R
      ZR2=ZR*ZR
      ZR3=ZR2*ZR
      ZR4=ZR3*ZR
      H1=(3.-30.*ZR2+35.*ZR4)*AR3/40.
      A1=AR*(-1.+3.*ZR2)/6.+(3.-30.*ZR2+35.*ZR4)*AR3/40.
      A0=1.+AR*A1
      A2=-ZR2/6.-AR2*(1.-12.*ZR2+15.*ZR4)/40.
      A3=AR*(3.*ZR2-5.*ZR4)/60.
      A4=ZR4/120.
      S1=A0+BA2*(A2+BA2*A4)
      S2=BA*(A1+BA2*A3)
```

```
   28 PSI(N8)=U2*(S1+U*S2)
      DC(N8)=TX(NF)*TX(N7)+TY(NF)*TY(N7)+TZ(NF)*TZ(N7)
   16 CONTINUE
   15 CONTINUE
      N3=N3+2
      J3=(NS-1)*4
      J7=-2
      J9=1
      DO 25 NF=1,N
      J1=(NF-1)*4
      IF(L(J9)-NF) 26,27,26
   27 J9=J9+1
      J7=J7+2
   26 N9=N9+1
      IF(NS.GT.NF) GO TO 30
      U5=0.
      U6=0.
      J5=0
      DO 23 JS=1,4
      J4=J3+JS
      J8=J5+J7
      DO 24 JF=1,4
      J6=J8+JF
      J2=J1+JF
      U5=T(J2)*T(J4)*DC(J6)*PSI(J6)+U5
      U6=TP(J2)*TP(J4)*PSI(J6)+U6
   24 CONTINUE
      J5=J5+N1
   23 CONTINUE
      NX=N9-N*(NS-1)
      Z(NS,NX)=U5*U3+U6*U4
      Z(NX,NS)=Z(NS,NX)
   30 J7=J7+2
   25 CONTINUE
   10 CONTINUE
      RETURN
      END
C     SUBROUTINE ROW FOR ARBITRARY WIRES (V O R)
      SUBROUTINE ROW(N,CT,ST,CP,SP,SX,E,III)
      COMPLEX C(3,139),E,U,U1,U2,U3,U4,U5,SX
      COMMON XX(280),XY(280),XZ(280),TX(280),TY(280),TZ(280),AL(280)
      COMMON T(560),TP(560),BK,RAD2(10),L(5),LR(10) /COA/C
      DIMENSION BKR(202),DP(202),BKZ(202)
      U=(0.,1.)
      BK1=BK*ST*CP
      BK2=BK*ST*SP
      BK3=BK*CT
      N2=1
      N3=-2
      DO 1 NS=1,N
      IF (L(N2)-NS) 2,3,2
    3 KK=1
      N3=N3+2
      N2=N2+1
      GO TO 4
    2 KK=3
    4 DO 5 K=KK,4
      N7=N3+K
      BKR(N7)=XX(N7)*BK1+XY(N7)*BK2
      DP(N7)=-TX(N7)*SP+TY(N7)*CP
```

```
      BKZ(N7)=XZ(N7)*BK3
    5 CONTINUE
      N3=N3+2
    1 CONTINUE
      N2=1
      N3=-2
      U3=0.
      U4=0.
      DO 6 NS=1,N
      IF (L(N2)-NS) 7,8,7
    8 N3=N3+2
      N2=N2+1
    7 J1=(NS-1)*4
      U1=0.
      U2=0.
      DO 9 JS=1,4
      J2=J1+JS
      J3=N3+JS
      S1=BKR(J3)
      S2=BKZ(J3)
      U5=T(J2)*(COS(S1)+U*SIN(S1))*U*SIN(S2)*2.
      U2=U2+U5*DP(J3)
    9 CONTINUE
      U4=U4+U2*C(III,NS)
      N3=N3+2
    6 CONTINUE
      E=SX*U4
      RETURN
      END
```

APPENDIX B

The following program replaces that in Appendix F of the 1974 Final Report [1]. The program computes the scalloping due to metallic scatterers in the form of bodies of revolution with vertical axes. The modifications are the same as those listed in Appendix A: The scalloping envelope is computed directly and the effect of the counterpoise has been included.

The first part of the program is unchanged. In the second part of the program a new input card has to be placed between the second and third data card. This new card must give the values of H, SH, and R as in Appendix A.

```
      BODY-OF-REVOLUTION (AXIS Z-AXIS)
      SUBROUTINE INVOLT(V1,II,LL,HH,SH,RR)
      COMPLEX V1(  40),A5,A6,U,CS,A(40),SB
      COMMON U,R(42),ZS(42),SV(42),CV(42),BK,NP,NN,T(80),TR(80)
     1,ST(42),CT(42),RO(42),BD
      DIMENSION BJ(126),ALP(40),FK(20)
      S=16.*.0254
      KG=NP-1
      NM=KG/2-1
      ANN=-NN*(-1)**LL
      M2=NN+2
      A5=3.141593*U**NN
      MX=2
      IF(II.EQ.1) MX=1
      DO 100 J=1,NM
      J1=J+NM
      V1(J)=0.
      V1(J1)=0.
  100 CONTINUE
      DO 156 M=1,MX
      FK(1)=1.
      DO 153 J=1,M2
      J1=J+1
      B=J
      FK(J1)=FK(J)*B
  153 CONTINUE
      DO 302 J=1,KG
      CX=CT(J)
      CALL CTP(HH,SH,CX,RR,SB,BK)
      IF(II-2) 50,60,65
   50 X=BK*R(J)*ST(J)
      A1=BK*RO(J)
      CS=COS(A1)-U*SIN(A1)
      A(J)=CS*ST(J)*SB      /RO(J)
      GO TO 80
   60 ALP(J)=0.
      X=BK*R(J)*ST(J)
      A1=BK*(RO(J)-S*ST(J)*(-1.)**M)
      GO TO 70
   65 B1=S*ST(J)*(-1.)**M/RO(J)
      A1=BK*RO(J)
      SQ=1.+B1*B1
      X=BK*R(J)*SQRT(SQ)*ST(J)
      ALP(J)=ATAN2(B1,1.)
   70 CS=COS(A1)-U*SIN(A1)
      A(J)= CS*ST(J)*SB      *.5*U/RO(J)
   80 J1=J
      I1=NN
      IF(I1) 303,304,303
  304 I1=I1+1
      J1=J1+KG
  303 DO 305 JJ=I1,M2
      IF(X-1.E-5) 1,1,2
    1 IF(JJ-1) 3,3,4
    3 BJ(J1)=1.
      GO TO 306
    4 BJ(J1)=0.
      GO TO 306
    2 RH=X/2.
      RH2=RH*RH
```

```
      RH3=RH**(JJ-1)
      BJ(J1)=RH3/FK(JJ)
      SS=BJ(J1)
    8 SST=SS*1.E-7
      DO 155 K=1,20
      B=K
      C=K+JJ-1
      SS=-SS*RH2/(B*C)
      BJ(J1)=BJ(J1)+SS
      IF(ABS(SS)-SST) 306,306,155
  155 CONTINUE
      STOP
  306 J1=J1+KG
  305 CONTINUE
  302 CONTINUE
      IF(NN) 307,308,307
  308 DO 309 J=1,KG
      J1=J+2*KG
      BJ(J)=-BJ(J1)
  309 CONTINUE
  307 DO 300 J=1,NM
      J1=J+NM
      DO 301 I=1,4
      I1=2*(J-1)+I
      I4=4*(J-1)+I
      I2=I1+KG
      I3=I2+KG
      BJ1= BJ(I3)+BJ(I1)
      BJ2= BJ(I3)-BJ(I1)
      IF(II-2) 90,95,95
   90 V1(    J)=     A5*A(I1)*BJ1*T(I4)*SV(I1)*(-1.)**LL+V1(J)
      V1(    J1)=U*A5*A(I1)*BJ2*TR(I4)+V1(J1)
      GO TO 301
   95 ALN=ALP(I1)*ANN
      SA= SIN(ALP(I1))
      CA=COS(ALP(I1))
      A6=A5*A(I1)*(COS(ALN)+U*SIN(ALN))
      V1(J)=V1(J)-A6*SV(I1)*(CA*BJ1+U*SA*BJ2)*T(I4)*(-1.)**M*(-1.)**LL
      V1(    J1)=V1(    J1)-A6*(U*CA*BJ2-SA*BJ1)*TR(I4)*(-1.)**M
  301 CONTINUE
  300 CONTINUE
  156 CONTINUE
      RETURN
      END
      SUBROUTINE PLANE(VVR,THR,PHR,II)
      COMPLEX VVR(40),A5,U
      COMMON U,R(42),ZS(42),SV(42),CV(42),BK,NP,NN,T(80),TR(80)
     1,ST(42),CT(42),RO(42),BD
      DIMENSION BJ(126),FK(20)
      PHS=-3.141593*.5
      KG=NP-1
      NM=KG/2-1
      ANN=-NN*(-1)**II
      M2=NN+2
      A5=2.*3.141593*U**(NN+1)
      FK(1)=1.
      DO 153 J=1,M2
      J1=J+1
      FK(J1)=FK(J)*J
  153 CONTINUE
```

```
      CS=COS(THR)
      SN=SIN(THR)
      BL=BK*BD*COS(PHR-PHS)*SN
      PH=(1.570796-PHR)*ANN+BL
      A5=A5*(COS(PH)+U*SIN(PH))
      BCS=BK*CS
      DO 302 J=1,KG
      X=R(J)*BK*SN
      J1=J
      I1=NN
      IF(I1) 303,304,303
  304 I1=I1+1
      J1=J1+KG
  303 DO 305 JJ=I1,M2
      IF(X-1.E-5) 1,1,2
    1 IF(JJ-1) 3,3,4
    3 BJ(J1)=1.
      GO TO 306
    4 BJ(J1)=0.
      GO TO 306
    2 RH=X/2.
      RH2=RH*RH
      RH3=RH**(JJ-1)
      BJ(J1)=RH3/FK(JJ)
      SS=BJ(J1)
    8 SST=SS*1.E-7
      DO 155 K=1,20
      A=K
      B=K+JJ-1
      SS=-SS*RH2/(A*B)
      BJ(J1)=BJ(J1)+SS
      IF(ABS(SS)-SST) 306,306,155
  155 CONTINUE
      STOP
  306 J1=J1+KG
  305 CONTINUE
  302 CONTINUE
      IF(NN) 307,308,307
  308 DO 309 J=1,KG
      J1=J+2*KG
      BJ(J)=-BJ(J1)
  309 CONTINUE
  307 DO 300 J=1,NM
      J1=J+NM
      VVR(J )=0.
      VVR(J1)=0.
      DO 300 I=1,4
      I1=2*(J-1)+I
      I4=4*(J-1)+I
      I2=I1+KG
      I3=I2+KG
      A6=ZS(I1)*BCS
      BJ1=(BJ(I3)+BJ(I1))*.5
      BJ2=(BJ(I3)-BJ(I1))*.5
      VVR(J )=VVR(J )+A5*SV(I1)*BJ1*U*T(I4)*(-1.)**II*2.*U*SIN(A6)
      VVR(J1)=VVR(J1)+A5*BJ2*TR(I4)*U*2.*SIN(A6)
  300 CONTINUE
      RETURN
      END
      FUNCTION F(X)
```

```
H(J3)
H(J5)
DH(J2)/2./DEL1
(DH(J2)+DH(J3)/2.)/DEL1
(DH(J5)+DH(J4)/2.)/DEL2
DH(J5)/2./DEL2


344

HT)
78
  *ETA*BK*U

3*.5-TH)


J=1
Y(I),I=1,NZ)
)
NN,(Y(I),I=1,NZ)
 ',I2,'  ADMITTANCE'/(6E13.5))

1,III,II,HH,SH,RR)

M2
=0.

D.II.EQ.2) KK=2
D.II.EQ.2) LL=2

2

=TX(III,KM,JX)-Y(J1)*V1(I)*(-1.)**KK-Y(J2)*V1(I2)*


PHI       ERROR       (DEGREE)')
```

```
120 PHR=PHI*.0174533
    SP=SIN(PHR)
    CP=COS(PHR)
    SPT=BK*S*SP*SW
    CPT=BK*S*CP*SW
    SSP=SIN(SPT)
    SCP=SIN(CPT)
    BB=ATAN2(SSP,SCP)*57.29578
    IF(BB.LT.-180.) BB=BB+360.
    IF(BB.GT.180.) BB=BB-360.
    DO 96 III=2,3
    EI(III)=0.
    DO 80 KM=1,NX
    NN=KM-1
    KJ=2
    IF(NN.EQ.0) KJ=1
    DO 80 II=1,KJ
    CALL PLANE(VVR,TH ,PHR,II)
    DO 10 I=1,NM2
    IK=(II-1)*NM2+I
    EI(III)=EI(III)+VVR(I)*TX(III,KM,IK)
 10 CONTINUE
 80 CONTINUE
    EI(III)=-SX*EI(III)
 96 CONTINUE
    E1=REAL(EI(2))
    E2=AIMAG(EI(2))
    E3=REAL(EI(3))
    E4=AIMAG(EI(3))
    EK2=SQRT(E1*E1+E2*E2)
    EK3=SQRT(E3*E3+E4*E4)
    E5=EK2*CP
    E6=EK3*SP
    EP1=0.
    IF(EK2.EQ.0.) GO TO 32
    EP1=ATAN2(E2,E1)
 32 EP2=0.
    IF(EK3.EQ.0.) GO TO 33
    EP2=ATAN2(E4,E3)
 33 EE=E5*E5+E6*E6-2.*EK2*EK3*CP*SP*COS(EP1-EP2)
    EW=SQRT(EE)
    ER2=90.*EW/(3.141593*ABS(S2)*.433)
    ER2=ABS(ER2)
    IF(ER2.LT.-270.) ER2=ER2+360.
    IF(ER2.GT.270.) ER2=ER2-360.
    IF(ER2.GE.-270..AND.ER2.LT.-90.) ER2=ER2+180.
    IF(ER2.LE.270..AND.ER2.GT.90.) ER2=ER2-180.
    PHX=PHI+90.
    WRITE(3,98) PHX,ER2
 98 FORMAT(F9.2,F10.3)
    IQ=IQ+1
    ES(IQ)=PHX
    ER(IQ)=ER2
    PHI=PHI+AINC
    IF(PHI.LE.EPH-90..AND.PHI.GT.SPH-90.) GO TO 120
    PUNCH 400,IQ,(ES(I),I=1,IQ)
    PUNCH 410,(ER(I),I=1,IQ)
400 FORMAT(I5,(10F7.2))
410 FORMAT(10F8.3)
    GO TO 50
```

```
450 WRITE(3,460)
460 FORMAT(' **ERROR** THE INCREMENT OF PHI IS NOT POSITIVE')
 52 STOP
    END
  3    15    115.
-150.        19.
 12.          4.          26.
     0    .0625    .1250    .1875    .25        .25      .25      .25      .25      .25
   .25    .1875    .125     .0625        0
     0        0        0        0        0    .0625    .1250    .1875     .25     .3125
  .375     .375     .375     .375     .375
4000.        15.
 70.         110.         2.
0.76889E-05  0.47562E-03  0.39739E-04  0.18705E-03  0.42698E-04  0.89675E-04
0.22172E-04  0.92420E-05 -0.89255E-06  0.10011E-04 -0.17332E-05  0.10644E-04
0.0          0.0          0.0          0.0          0.0          0.0
0.0          0.0          0.0          0.0          0.0          0.0
0.35615E-04  0.17492E-03  0.21103E-03  0.16409E-02  0.29598E-03  0.23331E-03
0.21354E-03 -0.46017E-04  0.54772E-04 -0.63478E-04 -0.61901E-06  0.10912E-04
0.0          0.0          0.0          0.0          0.0          0.0
0.0          0.0          0.0          0.0          0.0          0.0
0.41939E-04  0.89683E-04  0.30181E-03  0.23686E-03  0.53270E-03  0.13030E-02
0.49138E-03  0.67699E-04  0.21539E-03 -0.51436E-04  0.22107E-04  0.10446E-04
0.0          0.0          0.0          0.0          0.0          0.0
0.0          0.0          0.0          0.0          0.0          0.0
0.22107E-04  0.10446E-04  0.21539E-03 -0.51437E-04  0.49138E-03  0.67699E-04
0.53270E-03  0.13030E-02  0.30181E-03  0.23686E-03  0.41939E-04  0.89684E-04
0.0          0.0          0.0          0.0          0.0          0.0
0.0          0.0          0.0          0.0          0.0          0.0
-0.61927E-06  0.10912E-04  0.54773E-04 -0.63477E-04  0.21354E-03 -0.46015E-04
0.29598E-03  0.23331E-03  0.21102E-03  0.16409E-02  0.35614E-04  0.17492E-03
0.0          0.0          0.0          0.0          0.0          0.0
0.0          0.0          0.0          0.0          0.0          0.0
-0.17332E-05  0.10644E-04 -0.89229E-06  0.10012E-04  0.22171E-04  0.92428E-05
0.42697E-04  0.89676E-04  0.39737E-04  0.18704E-03  0.76885E-05  0.47562E-03
0.0          0.0          0.0          0.0          0.0          0.0
0.0          0.0          0.0          0.0          0.0          0.0
0.0          0.0          0.0          0.0          0.0          0.0
0.0          0.0          0.0          0.0          0.0          0.0
0.16819E-05 -0.35521E-02  0.97344E-05  0.27216E-02 -0.28945E-05 -0.80816E-03
-0.86931E-05  0.41908E-03 -0.69734E-05 -0.13969E-03  0.13166E-06  0.43699E-04
0.0          0.0          0.0          0.0          0.0          0.0
0.0          0.0          0.0          0.0          0.0          0.0
0.10275E-04  0.27424E-02  0.41372E-03 -0.66313E-02  0.16977E-03  0.48094E-02
0.13498E-03 -0.18425E-02  0.32121E-04  0.61056E-03 -0.74822E-05 -0.14386E-03
0.0          0.0          0.0          0.0          0.0          0.0
0.0          0.0          0.0          0.0          0.0          0.0
-0.44856E-05 -0.83651E-03  0.16741E-03  0.48455E-02  0.17120E-03 -0.86207E-02
0.12665E-03  0.55671E-02  0.13414E-03 -0.18608E-02 -0.61417E-05  0.43764E-03
0.0          0.0          0.0          0.0          0.0          0.0
0.0          0.0          0.0          0.0          0.0          0.0
-0.61387E-05  0.43764E-03  0.13414E-03 -0.18609E-02  0.12665E-03  0.55671E-02
0.17120E-03 -0.86207E-02  0.16741E-03  0.48455E-02 -0.44854E-05 -0.83650E-03
0.0          0.0          0.0          0.0          0.0          0.0
0.0          0.0          0.0          0.0          0.0          0.0
-0.74860E-05 -0.14386E-03  0.32122E-04  0.61056E-03  0.13498E-03 -0.18425E-02
0.16976E-03  0.48094E-02  0.41372E-03 -0.66313E-02  0.10277E-04  0.27424E-02
0.0          0.0          0.0          0.0          0.0          0.0
0.0          0.0          0.0          0.0          0.0          0.0
0.13275E-06  0.43699E-04 -0.69724E-05 -0.13969E-03 -0.86961E-05  0.41908E-03
```

-0.28904E-05	-0.80816E-03	0.97322E-05	0.27216E-02	0.16818E-05	-0.35521E-02
0.97603E-04	-0.15106E-03	0.72309E-04	-0.44178E-03	-0.28353E-04	-0.13459E-03
-0.57258E-04	-0.21157E-03	-0.29188E-04	-0.48494E-04	0.69987E-05	-0.59956E-04
0.53110E-03	0.10255E-03	-0.17296E-02	0.18694E-03	0.51347E-03	0.49105E-04
-0.51268E-03	0.24150E-05	0.22668E-03	0.10376E-05	-0.50148E-04	-0.72410E-05
0.71358E-04	-0.44592E-03	0.13299E-03	0.58539E-03	0.14592E-03	-0.26219E-03
0.10360E-03	-0.87910E-04	0.66464E-05	-0.18900E-03	-0.28524E-04	-0.47637E-04
0.41103E-03	0.75482E-04	0.35869E-03	0.16622E-03	-0.15637E-02	0.62677E-05
0.37480E-03	0.63873E-04	-0.23876E-03	0.57136E-04	-0.59821E-04	0.29723E-04
-0.29065E-04	-0.13284E-03	0.14580E-03	-0.25826E-03	0.37628E-03	0.83480E-03
0.35698E-03	-0.60421E-04	0.10154E-03	-0.91863E-04	-0.57436E-04	-0.21186E-03
0.19534E-03	-0.31023E-04	0.88441E-03	-0.13384E-04	0.83765E-04	-0.10670E-03
-0.11960E-02	0.11088E-03	0.15676E-03	0.66072E-04	-0.20056E-03	0.59825E-04
-0.57436E-04	-0.21186E-03	0.10154E-03	-0.91863E-04	0.35698E-03	-0.60422E-04
0.37628E-03	0.83479E-03	0.14580E-03	-0.25826E-03	-0.29064E-04	-0.13284E-03
0.20056E-03	-0.59824E-04	-0.15677E-03	-0.66068E-04	0.11960E-02	-0.11088E-03
-0.83764E-04	0.10670E-03	-0.88441E-03	0.13390E-04	-0.19535E-03	0.31022E-04
-0.28524E-04	-0.47636E-04	0.66459E-05	-0.18900E-03	0.10360E-03	-0.87908E-04
0.14592E-03	-0.26219E-03	0.13299E-03	0.58539E-03	0.71358E-04	-0.44592E-03
0.59821E-04	-0.29723E-04	0.23876E-03	-0.57136E-04	-0.37480E-03	-0.63874E-04
0.15637E-02	-0.62641E-05	-0.35869E-03	-0.16623E-03	-0.41103E-03	-0.75482E-04
0.69983E-05	-0.59956E-04	-0.29188E-04	-0.48494E-04	-0.57258E-04	-0.21157E-03
-0.28352E-04	-0.13458E-03	0.72308E-04	-0.44178E-03	0.97603E-04	-0.15106E-03
0.50148E-04	0.72412E-05	-0.22667E-03	-0.10367E-05	0.51268E-03	-0.24145E-05
-0.51347E-03	-0.49103E-04	0.17296E-02	-0.18694E-03	-0.53110E-03	-0.10255E-03
-0.52829E-03	-0.10366E-03	-0.41845E-03	-0.75769E-04	-0.19572E-03	0.30980E-04
-0.20059E-03	0.60530E-04	-0.59692E-04	0.30668E-04	-0.50194E-04	-0.74061E-05
0.11007E-03	0.10305E-03	0.20068E-03	0.12991E-02	0.55968E-04	-0.26655E-03
0.53427E-05	0.37586E-03	0.20920E-05	-0.17650E-03	-0.75614E-05	0.41914E-04
0.17388E-02	-0.18564E-03	-0.34593E-03	-0.16815E-03	-0.87710E-03	0.99955E-05
0.15474E-03	0.63485E-04	-0.23219E-03	0.57119E-04	0.22671E-03	0.19751E-05
0.19857E-03	0.13012E-02	0.54240E-03	-0.64422E-02	0.23942E-03	0.59029E-02
0.14077E-03	-0.28827E-02	0.10520E-03	0.10026E-02	0.35522E-05	-0.17441E-03
-0.53165E-03	-0.48710E-04	0.15460E-02	-0.30965E-05	-0.86814E-04	0.11532E-03
-0.11961E-02	0.11863E-03	0.36433E-03	0.67142E-04	-0.52176E-03	-0.71086E-07
0.55875E-04	-0.27501E-03	0.24494E-03	0.59480E-02	0.20965E-03	-0.10186E-01
0.12640E-03	0.78095E-02	0.13146E-03	-0.29121E-02	0.22902E-05	0.37971E-03
0.52176E-03	0.72600E-07	-0.36432E-03	-0.67141E-04	0.11961E-02	-0.11863E-03
0.86815E-04	-0.11532E-03	-0.15460E-02	0.30934E-05	0.53165E-03	0.48707E-04
0.22886E-05	0.37971E-03	0.13145E-03	-0.29121E-02	0.12641E-03	0.78095E-02
0.20965E-03	-0.10186E-01	0.24494E-03	0.59480E-02	0.55873E-04	-0.27501E-03
-0.22671E-03	-0.19740E-05	0.23219E-03	-0.57121E-04	-0.15474E-03	-0.63489E-04
0.87711E-03	-0.99993E-05	0.34594E-03	0.16815E-03	-0.17388E-02	0.18564E-03
0.35521E-05	-0.17440E-03	0.10520E-03	0.10026E-02	0.14076E-03	-0.28826E-02
0.23943E-03	0.59029E-02	0.54240E-03	-0.64422E-02	0.19857E-03	0.13012E-02
0.50195E-04	0.74060E-05	0.59693E-04	-0.30668E-04	0.20059E-03	-0.60530E-04
0.19571E-03	-0.30981E-04	0.41845E-03	0.75768E-04	0.52830E-03	0.10365E-03
-0.75617E-05	0.41914E-04	0.20917E-05	-0.17649E-03	0.53410E-05	0.37587E-03
0.55967E-04	-0.26655E-03	0.20068E-03	0.12991E-02	0.11007E-03	0.10305E-03
0.53842E-04	-0.40144E-02	-0.52138E-04	0.14186E-02	-0.36285E-04	-0.60356E-03
-0.48750E-04	-0.12476E-02	-0.86093E-04	0.23584E-02	0.39007E-04	-0.23917E-02
0.18015E-02	0.20359E-04	-0.10623E-01	-0.11839E-03	0.13636E-01	0.25751E-03
-0.12864E-01	-0.22025E-03	0.72743E-02	0.18592E-03	-0.88698E-03	-0.12831E-04
-0.51742E-04	0.14685E-02	0.17562E-03	-0.28603E-02	0.99778E-04	0.17299E-03
0.70584E-04	0.11041E-02	0.96467E-04	-0.25227E-02	-0.83163E-04	0.24113E-02
-0.49669E-03	-0.14578E-04	0.78223E-02	0.37681E-03	-0.14820E-01	-0.35979E-03
0.12965E-01	0.44805E-03	-0.75466E-02	-0.21500E-03	0.88841E-03	0.30492E-04
-0.35407E-04	-0.61270E-03	0.97311E-04	0.17437E-03	0.60418E-04	-0.81463E-04
0.45707E-04	-0.70736E-03	0.66601E-04	0.10973E-02	-0.47248E-04	-0.12665E-02
0.24891E-03	-0.10903E-04	-0.11186E-02	0.21110E-03	0.46470E-02	-0.23704E-03

-0.68278E-02	0.25611E-03	0.35566E-02	-0.15772E-03	-0.47603E-03	0.16877E-04
-0.47244E-04	-0.12665E-02	0.66598E-04	0.10973E-02	0.45709E-04	-0.70736E-03
0.60417E-04	-0.81465E-03	0.97307E-04	0.17438E-03	-0.35403E-04	-0.61273E-03
0.47602E-03	-0.16876E-04	-0.35566E-02	0.15771E-03	0.68279E-02	-0.25610E-03
-0.46471E-02	0.23702E-03	0.11186E-02	-0.21109E-03	-0.24892E-03	0.10901E-04
-0.83166E-04	0.24112E-02	0.96475E-04	-0.25227E-02	0.70578E-04	0.11040E-02
0.99778E-04	0.17298E-03	0.17563E-03	-0.28602E-02	-0.51755E-04	0.14685E-02
-0.88839E-03	-0.30493E-04	0.75465E-02	0.21501E-03	-0.12965E-01	-0.44809E-03
0.14820E-01	0.35983E-03	-0.78223E-02	-0.37684E-03	0.49668E-03	0.14583E-04
0.39006E-04	-0.23917E-02	-0.86093E-04	0.23584E-02	-0.48745E-04	-0.12476E-02
-0.36288E-04	-0.60356E-03	-0.52142E-04	0.14186E-02	0.53846E-04	-0.40145E-02
0.88697E-03	0.12829E-04	-0.72743E-02	-0.18591E-03	0.12864E-01	0.22025E-03
-0.13636E-01	-0.25752E-03	0.10623E-01	0.11840E-03	-0.18016E-02	-0.20361E-04
-0.18028E-02	-0.19779E-04	0.47748E-03	0.15217E-04	-0.24414E-03	0.10830E-04
-0.46861E-03	0.16804E-04	0.86968E-03	0.31192E-04	-0.88778E-03	-0.13111E-04
0.73386E-05	-0.45393E-03	-0.37267E-04	0.40251E-02	0.90894E-04	-0.50270E-02
-0.75096E-04	0.47740E-02	0.67252E-04	-0.26919E-02	-0.42318E-05	0.32944E-03
0.10655E-01	0.12429E-03	-0.76806E-02	-0.38329E-03	0.10860E-02	-0.21340E-03
0.35074E-02	-0.16138E-03	-0.74150E-02	-0.22228E-03	0.73018E-02	0.18543E-03
-0.36931E-04	0.40371E-02	0.84255E-03	-0.28172E-01	-0.79047E-03	0.43334E-01
0.10262E-02	-0.39173E-01	-0.47915E-03	0.22508E-01	0.67687E-04	-0.26998E-02
-0.13809E-01	-0.25367E-03	0.14690E-01	0.37132E-03	-0.46154E-02	0.24767E-03
-0.67910E-02	0.26444E-03	0.12841E-01	0.45723E-03	-0.13018E-01	-0.22243E-03
0.90253E-04	-0.50858E-02	-0.78044E-03	0.43680E-01	0.14220E-02	-0.72704E-01
-0.12232E-02	0.70421E-01	0.10124E-02	-0.39507E-01	-0.74573E-04	0.48274E-02
0.13018E-01	0.22241E-03	-0.12841E-01	-0.45723E-03	0.67910E-02	-0.26442E-03
0.46154E-02	-0.24769E-03	-0.14690E-01	-0.37132E-03	0.13809E-01	0.25369E-03
-0.74562E-04	0.48273E-02	0.10123E-02	-0.39507E-01	-0.12232E-02	0.70421E-01
0.14220E-02	-0.72704E-01	-0.78048E-03	0.43680E-01	0.90261E-04	-0.50859E-02
-0.73016E-02	-0.16542E-03	0.74150E-02	0.22228E-03	-0.35074E-02	0.16137E-03
-0.10860E-02	0.21341E-03	0.76806E-02	0.38329E-03	-0.10655E-01	-0.12430E-03
0.67680E-04	-0.26997E-02	-0.47912E-03	0.22508E-01	0.10262E-02	-0.39173E-01
-0.79046E-03	0.43334E-01	0.84257E-03	-0.28172E-01	-0.36935E-04	0.40371E-02
0.88777E-03	0.13108E-04	-0.86969E-03	-0.31190E-04	0.46861E-03	-0.16803E-04
0.24414E-03	-0.10832E-04	-0.47749E-03	-0.15217E-04	0.18028E-02	0.19779E-04
-0.42307E-05	0.32944E-03	0.67245E-04	-0.26919E-02	-0.75091E-04	0.47741E-02
0.90890E-04	-0.50271E-02	-0.37268E-04	0.40251E-02	0.73387E-05	-0.45394E-03

APPENDIX C

This is a simplified version of the program in appendix J of the 1974 Final Report [1]. It is based on the theoretical formula for single wire scatterers of any length. The input data cards are unchanged.

```
      FUNCTION F(X)
      F=(1.+.926*X)/(2.+(1.792+3.104*X)*X)
      RETURN
      END
      FUNCTION G(X)
      G=1./(2.+(4.142+(3.492+6.670*X)*X)*X)
      RETURN
      END
      FUNCTION C(X)
      A=3.141593*X*X*.5
      C    =.5+F(X)*SIN(A)-G(X)*COS(A)
      RETURN
      END
      FUNCTION S(X)
      A=3.141593*X*X*.5
      S    =.5-F(X)*COS(A)-G(X)*SIN(A)
      RETURN
      END
      SUBROUTINE CTP(H,SH,E,R,SS,BK)
      COMPLEX SS,U,D
      U=(0.,1.)
      PI=3.141593
      HO=SH+H
      R1=R*R+SH*SH
      RO=SQRT(R1)
      ANG=SH/R
      ALP=ATAN(ANG)
      A=BK*RO/PI
      SA=SQRT(A)
      PO=2.*SA*SIN(ALP*.5)
      D=2.*C(PO)+SH/H-U*(2.*S(PO)+SH/H)
    5 AL1=(ALP+E)*.5
      AL2=(ALP-E)*.5
      P1=2.*SA*SIN(AL1)
      P2=2.*SA*SIN(AL2)
      X=BK*H*SIN(E)
      Y=BK*SH*SIN(E)
      SX=SIN(X)
      SY=SIN(Y)
      SI=SX/X
      SJ=SY/Y
      CX=COS(X)
      CY=COS(Y)
      IF(P2) 30,35,35
   30 P2=-P2
      SP=-S(P2)
      CP=-C(P2)
      GO TO 38
   35 SP=S(P2)
      CP=C(P2)
   38 SS=COS(E)/D*(SH/H*SJ*CX+(C(P1)+CP    )*SI*CY+(S(P1)-SP    )*SI*SY-
     1U*(SH*SJ*CX/H+(S(P1)+SP    )*SI*CY-(C(P1)-CP)*SI*SY))*BK*HO*SIN(E)
      RETURN
      END
      COMPLEX S1,SO
      DIMENSION FS(721),ER1(721),ER2(721)
   50 READ(1,10,END=500) H,SH,R,FRM
   10 FORMAT(4F10.2)
      WRITE(3,15) H,SH,R,FRM
   15 FORMAT('0H=',F6.2,' SH=',F5.2,' R=',F6.2,' FRM=',F7.2)
```

```
      READ(1,16) SR,HA,V,FO
   16 FORMAT(4F10.2)
      WRITE(3,17) SR,HA,V,FO
   17 FORMAT('0SR=',F6.2,' HA=',F8.1,' V=',F7.2,' FO=',F6.2)
      READ(1,20) D,AL1,AL2,A,H1
   20 FORMAT(5F10.2)
      WRITE(3,25) D,AL1,AL2,A,H1
   25 FORMAT('0D=',F7.2,' L1=',F7.2,' L2=',F7.2,' A=',F8.5,' H1=',F7.2)
      HO=H+SH
      READ(1,137) SPH,EPH,AINC
  137 FORMAT(3F10.2)
      WRITE(3,138) SPH,EPH,AINC
  138 FORMAT('0START PHI=',F7.2,' END PHI=',F7.2,' INCREMENT=',F7.2,
     1'   (DEGREE)')
      IF(AINC.LE.0.) GO TO 450
      SM=SR*1609.344
      HM=HA*.3048
      E=ATAN2(HM,SM)
      ALAM=300./(FRM*.3048)
      BK=2.*3.141593/ALAM
      GAM=.5772157
      OME=BK*D
      ET=H1/D
      FS =D*V/(1800.*SR*ALAM)
      A1=(1.+(AL1/D)**2)**.25
      A2=(1.+(AL2/D)**2)**.25
      Q1=SQRT(2./(3.141593*OME))
      Q3=SQRT(2.*OME)
      Q4=SQRT(2./3.141593)
      G1=BK*H1*E
      S  =SIN(G1)
      C1=BK*BK*HO*H1/OME
      C2=2./(BK*A)
      C3=ALOG(C2)
      PS1=ATAN2(D,AL1)
      PS2=ATAN2(D,AL2)
      PHI=SPH
      IQ=0
      WRITE(3,200)
  200 FORMAT(/12X,' INFINITE WIRE',15X,' FINITE WIRE'/3X,' PHI',1X,' ST
     1ENV',1X,' DY ENV',2X,' SCAL',7X,' ST ENV',1X,' DY ENV',2X,' SCAL')
  120 PH =PHI*.0174533
      SP=SIN(PH )
      CP=COS(PH)
      SL=ALOG(SP)
      C4=C3-GAM-SL
      B1=3.141593*.5/C4
      BO=ATAN(B1)
      Q2=SQRT(SP)
      AC=SQRT(1.-SP*SP)
      E1=H1*SP/D
      CALL CTP(H,SH,E,      R,SO,BK)
      CALL CTP(H,SH,E1,      R,S1,BK)
      SOR=REAL(SO)
      SOI=AIMAG(SO)
      S1R=REAL(S1)
      S1I=AIMAG(S1)
      ASO=ATAN2(SOI,SOR)
      AS1=ATAN2(S1I,S1R)
      SS=SQRT(S1R**2+S1I**2)/SQRT(SOR**2+SOI**2)
```

```
      FRE=1./(1.+(FS*CP/FO)**2)
      BMPI=360.*Q1*S*     SS *COS(BO)*Q2*AC/C4
      BMPD=BMPI*FRE
      ASI=OME*(1.+SQRT(1.+ET*ET))*SP+BO-3.*3.141593*.25-AS1+ASO
      SCAI=BMPD*COS(ASI)
      D1=(PS1-PH )*.5
      D2=(PH -PS2)*.5
      U1=Q3*A1*SIN(D1)
      U2=Q3*A2*SIN(D2)
      X1=Q4*ABS(U1)
      X2=Q4*ABS(U2)
      F1=F(X1)
      G1=G(X1)
      F2=F(X2)
      G2=G(X2)
      YP1=F1+G1
      YM1=F1-G1
      YP2=F2+G2
      YM2=F2-G2
      YS1=F1*F1+G1*G1
      YS2=F2*F2+G2*G2
      US1=U1*U1
      US2=U2*U2
      SU1=SIN(US1)
      CU1=COS(US1)
      SU2=SIN(US2)
      CU2=COS(US2)
      F3=1.+.5*YS1+YM1*SU1-YP1*CU1
      F4=1.+.5*YS2+YM2*SU2-YP2*CU2
      FS1=SQRT(.5*YS1)
      FS2=SQRT(.5*YS2)
      IF(D1.GT.0.) FS1=SQRT(F3)
      IF(D2.GT.0.) FS2=SQRT(F4)
      BMPF=FS1*FS2*BMPI
      BMPG=BMPF*FRE
      AA=2.
      IF(D1.LE.0.) AA=0.
      BB=2.
      IF(D2.LE.0.) BB=0.
      P1=YP1*SU1+YM1*CU1
      P2=AA+YM1*SU1-YP1*CU1
      P3=YP2*SU2+YM2*CU2
      P4=BB+YM2*SU2-YP2*CU2
      AF1=ATAN2(P1,P2)
      AF2=ATAN2(P3,P4)
      ASF=ASI-AF1-AF2
      SCAF=COS(ASF)*BMPG
      WRITE(3,100) PHI,BMPI,BMPD,SCAI,BMPF,BMPG,SCAF
  100 FORMAT(F7.1,3F8.3,5X,3F8.3)
      IQ=IQ+1
      ES(IQ)=PHI
      ER1(IQ)=SCAF
      PHI=PHI+AINC
      IF(PHI.LE.EPH.AND.PHI.GT.SPH) GO TO 120
      PUNCH 400,IQ,(ES(I),I=1,IQ)
      PUNCH 410,(ER1(I),I=1,IQ)
  400 FORMAT(I5,(10F7.2))
  410 FORMAT(10F8.3)
      GO TO 50
  450 WRITE(3,460)
```

```
460 FORMAT('0**ERROR** THE INCREMENT OF PHI IS NOT POSITIVE')
500 STOP
    END
 12.        4.        26.        109.
28.77     3000.      218.6       .35
205.       150.      250.      .00667      25.8
  1.        90.       2.
```

REFERENCES

1. B. J. Strait and H. Gruenberg, "Effects of Scattering by Obstacles in the Field of VOR/DVOR," Final Report No. FAA-RD-74-153, September 1974.

2. B. J. Strait and H. Gruenberg, "Effects of Scattering by Obstacles in the Field of VOR/DVOR," Interim Engineering Report No. 4, 1 August to 31 October 1974.

3. B. J. Strait and H. Gruenberg, "Effects of Scattering by Obstacles in the Field of VOR/DVOR," Interim Engineering Report No. 5, 1 November 1974 to 31 January 1975.

4. H. Gruenberg, "Effects of Scattering by Obstacles in the Field of VOR/DVOR," Interim Engineering Report No. 6, 1 February to 31 April 1975.

5. George Tyras, "Radiation and Propagation of Electromagnetic Waves," Academic Press, New York and London, 1969, p. 285.

6. George Tyras, "Radiation and Propagation of Electromagnetic Waves," Academic Press, New York and London, 1969, p. 106.

7. S. R. Anderson and H. F. Keary, VHF Omnirange Wave Reflections from Wires," Technical Report 126, Civil Aeronautics Administration, May 1952.